การประเมินสภาพผสมเข้ากันได้ระหว่างตัวยาต้นแบบและพอลิเมอร์ในฟิล์มที่เตรียมโดยการอัดรีดแบบหลอมร้อน

นางสาวญาดา วัฒนกิจยิ่งยง

วิทยานิพนธ์นี้เป็นส่วนหนึ่งของการศึกษาตามหลักสูตรปริญญาเภสัชศาสตรมหาบัณฑิต
สาขาวิชาเภสัชอุตสาหกรรม ภาควิชาวิทยาการเภสัชกรรมและเภสัชอุตสาหกรรม
คณะเภสัชศาสตร์ จุฬาลงกรณ์มหาวิทยาลัย
ปีการศึกษา 2557

EVALUATION OF MISCIBILITY BETWEEN MODEL DRUG AND POLYMER IN HOT MELT EXTRUDED FILMS

Miss Yada Vattanagijyingyong

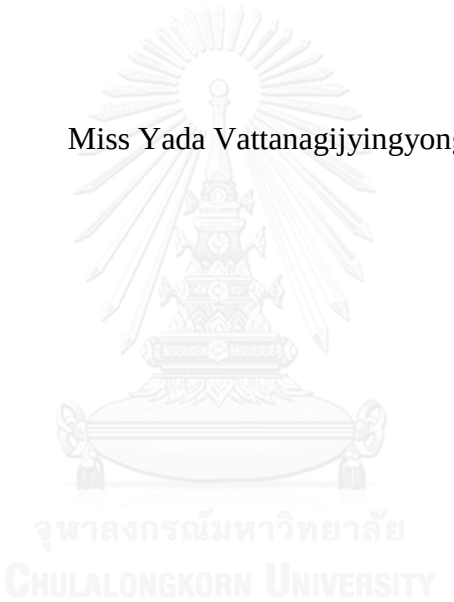

A Thesis Submitted in Partial Fulfillment of the Requirements
for the Degree of Master of Science in Pharmacy Program in Industrial Pharmacy
Department of Pharmaceutics and Industrial Pharmacy
Faculty of Pharmaceutical Sciences
Chulalongkorn University
Academic Year 2014

Thesis Title	EVALUATION OF MISCIBILITY BETWEEN MODEL DRUG AND POLYMER IN HOT MELT EXTRUDED FILMS
By	Miss Yada Vattanagijyingyong
Field of Study	Industrial Pharmacy
Thesis Advisor	Jittima Chatchawalsaisin, Ph.D.
Thesis Co-Advisor	Narueporn Sutanthavibul, Ph.D.

Accepted by the Faculty of Pharmaceutical Sciences, Chulalongkorn University in Partial Fulfillment of the Requirements for the Master's Degree

.....Dean of the Faculty of Pharmaceutical Sciences
(Assistant Professor Rungpetch Sakulbumrungsil, Ph.D.)

THESIS COMMITTEE

.....Chairman
(Associate Professor Parkpoom Tengamnuay, Ph.D.)
.....Thesis Advisor
(Jittima Chatchawalsaisin, Ph.D.)
.....Thesis Co-Advisor
(Narueporn Sutanthavibul, Ph.D.)
.....Examiner
(Associate Professor Pornchai Rojsitthisak, Ph.D.)
.....External Examiner
(Associate Professor Poj Kulvanich, Ph.D.)

ญาดา วัฒนกิจยิ่งยง : การประเมินสภาพผสมเข้ากันได้ระหว่างตัวยาต้นแบบและพอลิเมอร์ในฟิล์มที่เตรียมโดยการอัดรีดแบบหลอมร้อน (EVALUATION OF MISCIBILITY BETWEEN MODEL DRUG AND POLYMER IN HOT MELT EXTRUDED FILMS) อ.ที่ปรึกษาวิทยานิพนธ์หลัก: อ. ภญ. ดร.จิตติมา ชัชวาลย์สายสินธ์, อ.ที่ปรึกษาวิทยานิพนธ์ร่วม: อ. ภญ. ดร.นฤพร สุตัณฑวิบูลย์, 131 หน้า.

วัตถุประสงค์ของการศึกษานี้เพื่อตรวจสอบสภาพผสมเข้ากันได้ระหว่างตัวยาต้นแบบและพอลิเมอร์ในฟิล์มที่เตรียมโดยการอัดรีดแบบหลอมร้อน ตัวยาต้นแบบที่ใช้เป็นตัวยาที่มีแนวโน้มการตกผลึกที่ต่างกัน ได้แก่ เบนโซเคน อินโดเมธาซินและพาราเซตามอล และพอลิเมอร์ที่ใช้คือพอลิแลกไทด์ ซึ่งเป็นพอลิเมอร์กึ่งผลึก ทำนายสภาพผสมเข้ากันได้ระหว่างตัวยาและพอลิเมอร์โดยการคำนวณและพิจารณาจากพฤติกรรมเชิงความร้อนของตัวยาและพอลิเมอร์ ประเมินสภาพผสมเข้ากันได้ในผลิตภัณฑ์ที่ได้จากการอัดรีดโดยวิธีการเลี้ยวเบนรังสีเอกซ์และดิฟเฟอเรนเชียลสแกนนิงคาลอรีเมตรี รวมทั้งตรวจสอบอันตรกิริยาระหว่างตัวยาและพอลิเมอร์ด้วยอินฟราเรดสเปกโทรสโกปีชนิดฟูเรียร์ทรานสฟอร์ม การทำนายด้วยการคำนวณค่าพารามิเตอร์การละลายบ่งชี้ว่าเบนโซเคนและอินโดเมธาซินผสมเข้ากันได้กับพอลิแลกไทด์ แต่พาราเซตามอลผสมเข้ากันไม่ได้กับพอลิแลกไทด์ ซึ่งสอดคล้องกับพฤติกรรมเชิงความร้อนของส่วนผสมระหว่างตัวยากับพอลิเมอร์ พบว่าการทำนายดังกล่าวให้ผลในลักษณะเดียวกันกับสภาพผสมเข้ากันได้ระหว่างตัวยาและพอลิเมอร์ที่ตรวจพบในผลิตภัณฑ์ที่ได้จากการอัดรีดของอินโดเมธาซินและพาราเซตามอล แต่เบนโซเคนไม่สามารถทำการเตรียมเป็นผลิตภัณฑ์ได้เนื่องจากเสื่อมสลายที่อุณหภูมิของกระบวนการอัดรีด อินโดเมธาซินและพาราเซตามอลผสมเข้ากันได้กับพอลิแลกไทด์จนถึงอัตราส่วนระหว่างตัวยาและพอลิเมอร์ที่ 50:50 และ 10:90 ตามลำดับ พันธะไฮโดรเจนเป็นอันตรกิริยาหลักระหว่างตัวยาและพอลิเมอร์ในผลิตภัณฑ์ที่ได้จากการอัดรีดที่มีสภาพผสมเข้ากันได้ การศึกษานี้แสดงให้เห็นว่าอันตรกิริยาระหว่างตัวยาและพอลิเมอร์ขึ้นอยู่กับปริมาณตัวยา โดยที่ระดับปริมาณตัวยาต่ำอันตรกิริยาระหว่างตัวยาและพอลิเมอร์จะแข็งแรงกว่าอันตรกิริยาระหว่างโมเลกุลยา อย่างไรก็ตามไม่พบผลของตัวยาทำหน้าที่เป็นพลาสติไซเซอร์ในผลิตภัณฑ์ที่ได้จากการอัดรีด

ภาควิชา วิทยาการเภสัชกรรมและเภสัชอุตสาหกรรม

สาขาวิชา เภสัชอุตสาหกรรม

ปีการศึกษา 2557

ลายมือชื่อนิสิต .....

ลายมือชื่อ อ.ที่ปรึกษาหลัก .....

ลายมือชื่อ อ.ที่ปรึกษาร่วม .....

5476205733 : MAJOR INDUSTRIAL PHARMACY
KEYWORDS: MISCIBILITY / HOT MELT EXTRUSION / MOLECULAR DYNAMICS SIMULATION / THERMAL ANALYSIS / SOLUBILITY PARAMETER

YADA VATTANAGIJYINGYONG: EVALUATION OF MISCIBILITY BETWEEN MODEL DRUG AND POLYMER IN HOT MELT EXTRUDED FILMS. ADVISOR: JITTIMA CHATCHAWALSAISIN, Ph.D., CO-ADVISOR: NARUEPORN SUTANTHAVIBUL, Ph.D., 131 pp.

The aim of this study was to investigate miscibility between model drugs and polymer in the extruded films prepared by hot melt extrusion. The model drugs with different crystallization tendency were benzocaine (BZC), indomethacin (IND) and paracetamol (PAR) and the polymer was semi-crystalline polylactide. Drug-polymer miscibility was predicted by calculation and their thermal properties. The miscibility between drug and polymer in extrudates was evaluated by X-ray powder diffractometry (XRPD) and differential scanning calorimetry (DSC). Drug-polymer interaction was also investigated by Fourier transform infrared spectroscopy (FTIR). Prediction by calculating solubility parameters suggested that BZC and IND were miscible, while PAR was immiscible with polylactide. This corresponded to thermal behaviors of the drug-polymer blends. The prediction results of IND and PAR agreed with drug-polymer miscibility in the extrudate, while BZC degraded at the extrusion process temperature. IND and PAR was miscible with polylactide up to the drug to polymer ratio of 50:50 and 10:90, respectively. Hydrogen bonding was mainly responsible for drug-polymer interaction in the miscible extrudate. The study revealed that the drug-polymer interaction was dependent on the drug content, being stronger than drug-drug interaction at the relatively low drug content. However, a plasticizing effect of the drugs in the extrudates was not observed.

Department:	Pharmaceutics and Industrial Pharmacy	Student's Signature	.....
		Advisor's Signature	.....
Field of Study:	Industrial Pharmacy	Co-Advisor's Signature	.....
Academic Year:	2014		

ACKNOWLEDGEMENTS

I would like to sincerely thank my advisor and co-advisor, Jittima Chatchawalsaisin, Ph.D. and Narueporn Sutanthavibul, Ph.D., for supporting all parts of the thesis. I would like to thank the thesis committee, Associate Professor Parkpoom Tengamnuay, Ph.D., Associate Professor Pornchai Rojsitthisak, Ph.D. and Associate Professor Poj Kulvanich, Ph.D. for valuable comments and examination. I also wish to thank Chulalongkorn University Centenary Academic Development Project, Chulalongkorn University Drugs & Health Products Innovation Promotion Center and Process Development Center for Pharmaceutical and Herbal Products for the software packages and computer facilities. I am grateful to the National Metal and Materials Technology Center (MTEC) for ultra-centrifugal mill used in grinding the polymers and hot melt extrusion and Chiba University for ball mill. I am also grateful for Greater Pharma Co., Ltd. and Advance Pharmaceutical Manufacturing Co., Ltd. for the drugs in the experiments. I am thankful for the Ratchadaphiseksomphot Endowment Fund 2013 of Chulalongkorn University (CU-56-649-HR) for financial supporting. Furthermore, I would like to thank laboratory members and staffs in Department of Pharmaceutics and Industrial Pharmacy at Chulalongkorn University and Department of Pharmaceutical Technology at Chiba University for their friendships and the discussion about the work. Finally, I am very thankful to my family for their encouragement during the work period.

CONTENTS

Page

LIST OF TABLES

Page

Page

LIST OF FIGURES

Page

Page

Page

Page

Page

Page

LIST OF ABBREVIATIONS

3D	three dimensions
Å	Angstrom
$Å^3$	cubic Angstrom
ATBC	acetyl tributyl citrate
atm	standard atmospheric pressure
BZC	benzocaine
°C	celcius
°C/min	celcius per minute
CED	cohesive energy density
cm^{-1}	per centimeter
cm^3	cubic centimeter
COMPASS	condensed-phase optimized molecular potential for atomistic simulation studies
CPM	chlorpheniramine maleate
D	diameter
DBS	dibutyl sebacate
DLA	d-lactic acid
DSC	differential scanning calorimetry
ΔE_{mix}	energy of mixing
e	elongation or strain

E	Young's modulus
E_{coh}	cohesive energy
e.g.	exampli gratia (for example)
et al.	et alia (and other)
EC	ethyl cellulose
EX	extrudate
FTIR	Fourier transforms infrared spectroscopy
fs	femtosecond
ΔG_{mix}	Gibbs free energy of mixing
g(r)	atomic pair distribution function
g/cm^3	gram per cubic centimeter
GCM	group contribution method
GLU	glucose
GPa	giga Pascal
ΔH_v	heat of vaporization
ΔH_{mix}	enthalpy of mixing
HC	hydrocortisone
HPC	hydroxypropyl cellulose
HPMC	hydroxypropyl methyl cellulose
HSM	hot stage microscopy
i.e.	id est (that is)
IBU	ibuprofen

IND	indomethacin
IR	infrared
J	Joule
K	Kelvin
kcal/mol	kilocalorie per mole
kcal/mol/Å	kilocalorie per mole per Angstrom
kDa	kilodalton
L	length
L/D	length to diameter
LCP	lacipidine
LLA	l-lactic acid
M_w	molecular weight
MD	molecular dynamics
mg/ml	milligram per milliliter
min	minute
mm	millimeter
mm^2	square millimeter
MPa	mega Pascal
mol	mole
n	number of sample
N_P	repeating units of polymer
NMR	nuclear magnetic resonance

NPT	isothermal-isobaric ensemble (condition)
ns	nanosecond
NSAID	non-steroidal anti-inflammatory drug
NVT	canonical or isothermal-isovolume ensemble (condition)
OD/ID	outer diameter to inner diameter
PAR	paracetamol
PEO	polyethylene oxide
PLLA	poly l-lactide
PDLA	poly d-lactide
PDLLA	poly d,l-lactide
PM	physical mixture
ps	picosecond
PVA	polyvinyl alcohol
PVP	polyvinylpyrrolidone
PVP/VA	polyvinylpyrrolidone-co-vinylacetate
R	gas constant (8.314 J/mol.K)
RDF	radial distribution function
RM	raw material
ΔS_{mix}	entropy of mixing
SD	standard deviation
T	temperature
T_{de}	decomposition temperature

T_c	recrystallization temperature
T_g	glass transition temperature
T_m	melting temperature
T_{mo}	onset melting temperature
TEC	triethyl citrate
TGA	thermogravity analysis
THEO	theophylline
V	volume or molar volume
V_{ref}	reference volume
XRPD	X-ray powder diffractometry
χ_c	critical parameter
χ_{FH}	Flory-Huggins interaction parameter
σ	tensile strength or stress
ρ	density
$\Delta\delta$	difference of solubility parameter
δ	solubility parameter
ϕ	volume fraction

CHAPTER 1
INTRODUCTION

Solid dispersion is a common technology which is applied to improve dissolution of poorly soluble drug or to modify drug release. It is a system that the drug is dispersed in a solid polymeric matrix (1) and can be classified into several categories, i.e. solid solution, solid suspension and eutectic mixture, based on solid states of the components. Solid dispersion can overcome typical problems in pharmaceuticals. For example, dissolution of poorly soluble drug can be improved by conversion of a crystalline drug to amorphous drug or by molecular dispersion of the drug in the polymeric carrier. Drug release can be modified by changing the drug's micro-environment by dispersing the drug in a hydrophobic or swellable hydrophilic polymer (1-4). The dissolution behavior of drug must be consistent upon storage. However, the amorphous drug is thermodynamically unstable and tends to rearrange themselves to its crystalline state. The physical state of the drug in the miscible mixtures where the drug is molecularly dispersed is more desirable because there appears to be intermolecular interactions between drug and polymer which help to stabilize the drug (1). The products based on this technology are mostly in the form of tablet such as Kaletra® (Abbott Laboratories) which is lopinavir/ritonavir in a copovidone matrix (5), Norvir® (Abbott Laboratories) which is ritonavir in a copovidone matrix, Gris-PEG® (Pedinol Pharmacal) which is griseofulvin in a polyethylene glycol matrix, Cesamet® (Lilly) which is nabilone in a povidone matrix (6), Certican® tablets (Novatis) which is everolimus in a hydroxypropyl methylcellulose matrix. This technology is also applied to produce implants such as Zoladex® (AstraZeneca) which is goserelin acetate in a lactide/glycolide copolymer matrix, Implanon® (Organol) which is a etonogestrel in ethylene vinylacetate copolymer matrix; and devices such as NuvaRing® (Organon) which is etonogestrel, ethinyl estradiol in an ethylene vinylacetate copolymer matrix (7). In general, the polymers which are candidates for the carrier matrix must be safe and biocompatible (4, 8). For specific dosage forms such as films or rings, the polymers should also have an appropriate mechanical properties depending on their applications, i.e. low

tensile strength and high elongation for film coating (9). Thus, during the development, other excipients such as plasticizer or secondary polymer may be added to improve mechanical properties of polymer (10-12). Ratios of the polymer to plasticizer or secondary polymer and solid contents are attributed to products' mechanical properties. A high proportion of plasticizer or flexible secondary polymer often leads to an increase in elongation and decrease tensile strength of product (11-15). For example, hydroxypropyl methyl cellulose (HPMC) was mixed with shellac to increase elongation and decrease tensile strength of shellac film. An increase in elongation and a decrease in tensile strength depend on concentrations of HPMC in the shellac film (13). Also, cellulose films with high content of magnesium stearate was less flexible than the films with low content of magnesium stearate (9).

An important factor in developing solid dispersion is miscibility of the components in the system. Miscibility depends on viscosity of the polymer and existing intermolecular interaction, such as hydrogen bond, between the drug and the polymer (16-19). In this regard, there are some drugs which are well miscible with the polymer and have been reported as being a plasticizer for that polymer. For example, ibuprofen and chlopheniramine maleate (CPM) were miscible with Eudragit® RS and plasticized the polymer, resulting in a reduction of glass transition temperature (T_g) and an increase in flexibility of the beads coated with Eudragit® RS. The T_g, tensile strength and Young's modulus of the beads were changed upon increasing the drug proportion (20). CPM was also found to plasticize hydroxypropyl cellulose (HPC) film preparing by hot melt extrusion (21). Therefore, prediction and evaluation of drug-polymer miscibility is often useful in guiding successful solid dispersion formulation.

In this study, miscibility between model drugs and polymer were predicted by calculating solubility parameters, Flory-Huggins interaction parameters (χ_{FH}) and Gibbs free energy of mixing (ΔG_{mix}). It is also suggested by experimentally thermal study, e.g. differential scanning calorimetry (DSC) and hot stage microscopy (HSM). A relationship between the drug-polymer miscibility and mechanical properties, i.e. tensile strength and elongation were established. Intermolecular interaction between the drugs and polymer was explained by radial distribution function (RDF) and

Fourier transform infrared spectroscopy (FTIR). The use of calculated parameters and experimental values for pre-formulation of solid dispersions of the drugs (benzocaine, indomethacin, paracetamol), with different solubility parameters and crystallization tendency, and the polymer (polylactide) was demonstrated.

Objectives of the study

1. To estimate miscibility between model drugs and polymers by calculation and experimental methods.
2. To investigate a relationship between the drug-polymer miscibility and mechanical properties of hot melt extruded films.
3. To demonstrate the intermolecular interaction between model drugs and polymers by computer simulation.

CHAPTER 2
LITERATURE REVIEW

1. Solid dispersions

Generally, a solid dispersion in pharmaceuticals consists of two components including drug and polymer. The drug may be dispersed molecularly in polymeric carrier, or precipitated as a separate amorphous or crystalline depending on miscibility between drug and solid polymeric matrix. If the drug is well miscible with the polymer, molecular dispersion of the drug will occur and this molecular state tends to be stable over storage time. If the drug is immiscible with the polymer, it will be dispersed as a separate crystalline or amorphous which may be recrystallized during storage. For this reason, miscibility between the drug and polymer should be considered (1, 2).

Solid dispersion can be divided into five groups according to solid states of drug and polymeric carrier. These groups are eutectic mixture, solid solution, glass solution or glass suspension, amorphous precipitation, and combination among the former four groups. The states of the drug and carrier in each group of solid dispersions are shown in Table 1 (22-24).

Table 1 Classes of solid dispersions (22-24)

Class	I	II	III		IV	V
	Eutectic mixture	Solid solution	Glass solution	Glass suspension	Amorphous precipitation	Others
Phases	2	1	1	2	2	combination among the four groups
Drug	C	M	M	A/C	A	
Carrier	C	C	A	A	C	

A = amorphous, C = crystalline, M = molecularly dispersed.

Solid dispersions are generally prepared by melting and solvent methods (6, 22). By the melting method, the solid dispersion is prepared through heating a physical mixture between drug and polymer until it is melted. Then, the dispersion is cooled and solidified. For the solvent method, the solid dispersion is prepared by dissolving the drug and the polymer in common solvents which is followed by mixing and evaporating to remove the solvent (22). Among many techniques that are proceeded by melting and solvent methods, hot-melt extrusion and spray drying are widely used in commercial production (1). The solid dispersion preparing methods have various advantages and disadvantages which are shown in Table 2. Selection of the methods depends on the drug and polymer properties.

Table 2 Advantages and disadvantages of different solid dispersion preparing methods (22)

Preparing methods	**Advantages**	**Disadvantages**
Melting method	1. Simple and economical 2. Fine drug particles were trapped in polymer matrix during quenching the melt	1. Drug and polymer may be decomposed at a high temperature
Solvent method	1. Suitable for heat-sensitive drugs	1. High cost 2. Long processing time in solvent evaporation 3. Difficult to remove solvent completely 4. Less chemical stability of a drug in a matrix

2. Hot-melt extrusion

Hot-melt extrusion is a technique providing solvent-free solid dispersion. This technique is able to transfer the powdered mixture of drug-polymer through the die to make various shapes. The instrument used in a hot-melt extrusion process is called hot-melt extruder which is shown in Figure 1. It consists of feeding, conveying, mixing and cooling zones. A feeding port is assembled with the feeding zone. Temperatures of the conveying and mixing zones are controlled by a heater which is assembled as a barreled heater. In the conveying and mixing zone, there is also a screw which can be oriented in various configurations depending on types of the extruder and application. Rotation of the screw is controlled by a motor. The conveying zone is an area that a powdered mixture is converted to fluid-like substance by heated screw and transferred to mixing zone by screw rotation. Mixing between the drug and the polymer will occur in the mixing zone during fluid-like state of the polymer. In the cooling zone, there is a die which may be attached with downstream processing, e.g. cutters, rollers and injection molds (1, 7, 24-26).

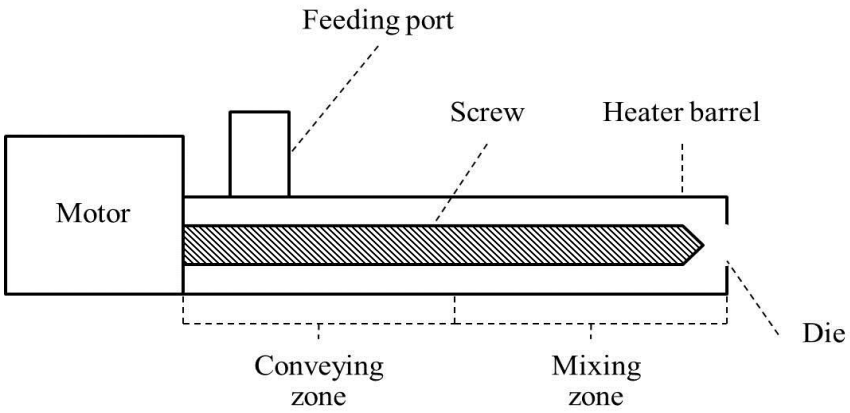

Figure 1 Side view of screw extruder (modified from (1))

The extruders can be classified into various types according to the number of screws and their rotation, i.e. single screw extruder, twin (co-rotating or counter-rotating) screw extruder and multi screw extruder (7, 27). Less number of screws like single screw extruder consumes long time for mixing because of its insufficient shear force. As a result, homogenous mixing is difficult to occur, especially when a drug is mixed with a high viscosity polymer. In the case of twin screw extruder, it has higher

shear force than the single screw extruder and mixing will occur near a feeding port. Therefore, the twin screw extruder requires short time of mixing and homogenous mixing can be easily obtained, comparing with the single screw extruder (7, 26). Direction of screw rotation also affects transferring and mixing of the mixture. It has been reported that a co-rotating screw extruder has higher degree of mixing than a counter-rotating screw extruder due to a maximum velocity of co-rotating screw at the screw tip. This allows the mixture to move easily from one position to the other position. While, in a counter-rotating screw, the maximum velocity occurred in the intermeshing zone; hence, it gives higher pressure during mixing (28). For this reason, the co-rotating twins screw extruder is often employed in pharmaceutical product development (7).

The screw configuration is important to conveying and mixing functions of the extruder. Configuration design depends on required properties of the compounds and the product because it can affect particle size and shape of the dispersed drug. Screw elements can be classified into two types according to their function as conveying and mixing elements. The mixing element is subdivided into two groups as 1) dispersive mixing element, i.e. kneading element, which gives high shear force to reduce particle size, and 2) distributive mixing element, i.e. combing element, which makes the mixture moving faster than the dispersive mixing element due to higher axial velocity and less shear planar effects (29, 30). Nakamichi et al. found that the kneading element of twin screw extruder highly influenced on converting crystalline to amorphous nifedipine during producing a solid dispersion of NP and hydroxypropylmethyl cellulose phthalate (31).

There are some simple calculations applied for screw configuration selection. First is the length to diameter (L/D) ratio. L is the length of barrel and D is the outside diameter of screw. This ratio affects residence time of the mixture in the barrel of extruder from which it will be useful information for formulation of heat-labile and shear-sensitive substances. The extruder with a L/D ratio less than 40 is preferred to be used in pharmaceutical applications; and if the drug is heat-sensitive, the L/D ratio of extruder should be shorter than 20. Second is the flight depth and free volume in the barrel. It is described in terms of the outer diameter to inner

diameter of screw (OD/ID) ratio. It affects conveying and mixing operation as well as the residence time in the barrel (30). Processing parameters in hot-melt extrusion are feeding rate, screw speed and processing temperature (26, 30). The feeding rate and screw speed directly affect residence time and shear stress which has an impact on the physicochemical stability of products (26). In addition, all these processing parameters are important for scaling up to a commercial batch.

The properties of drug and polymer that should be concerned for hot-melt extrusion technique are thermal sensitivity (22), solid-fluid or fluid-like state transformation, melting behavior and solidification of drug-polymer fluid mixture (1).

3. Miscibility prediction and evaluation by thermal analysis

The factors influencing miscibility are viscosity of polymeric carrier and intermolecular interaction such as hydrogen bond between drug and polymer (24). Miscibility study often provides useful information for solid dispersion formulation. It also reduces trials and errors during the formulation development from long time consumption (1, 18, 19). Basically, miscibility of components in a solid dispersion can be predicted by thermal analysis and calculation of difference solubility parameters (16, 18).

Differential scanning calorimetry (DSC) through heat-cool-heat cycle and hot stage microscopy (HSM) are the techniques which are widely used in the thermal analysis for miscibility study. This technique provides information of thermal properties, such as onset of melting temperature (T_{mo}) and melting temperature (T_m) from heating step, and glass transition temperature (T_g) form reheating step of heat-cool-heat cycle. Hot stage microscopy (HSM) is a method to monitor melting behaviors of a mixture. The thermal properties of the mixture may be varied, depending on drugs and carriers, and the group of solid dispersions which are shown in Table 1 (16, 18).

Forster et al. reported that the miscible mixture such as the mixture of indomethacin (IND; T_g = 43.7°C, T_{mo} = 159.4°C) and polyvinylpyrrolidone-co-

vinylacetate (PVP/VA; T_g = 106.2°C) at the ratio of 1:1 had a single T_g at 67.2°C which exhibited between the original T_gs of these two components. T_{mo} of IND in the mixtures was decreased to 134.0°C. Likewise the mixture of lacipidine (LCP; T_g = 48.0°C, T_{mo} = 182.1°C) and PVP/VA in the ratio of 1:1 had a single T_g at 73.3°C. T_{mo} of LCP was also decreased to 178.7°C.

The partially miscible mixture such as the mixture of LCP and polyvinylpyrrolidone K30 (PVP K30; T_g = 164.2°C) at a ratio of 1:4 had two separating T_gs at 89.8°C and 159.9°C. Both T_gs were changed from the components' T_g and the second T_g was close to the T_g of polymer. T_{mo} of LCP in LCP:PVP K30 was found at 179.6°C, demonstrating small decrease of T_{mo} of LCP in the mixture.

The immiscible mixture such as the mixture of LCP and sucrose (T_g = 70.7°C, T_{mo} = 189.3°C) at the ratio of 1:1 had two separated T_gs at 49.5°C and 70.7°C. Both T_gs were not changed from T_g of LCP and that of sucrose. T_{mo} of LCP in the mixture was 183.3°C, showing a slight increase from its T_{mo} (16).

Gupta et al. also reported the use of T_g and T_{mo} of the mixture for miscibility prediction between drug and polymer. The immiscible mixture such as the mixture between IND (T_g = 43°C, T_{mo} = 159.7°C) and glucose (GLU; T_g = 30.6°C, T_{mo} = 148.5°C) at all ratios showed no change of T_{mo} of IND and GLU. While, the miscible mixture such as the mixture of IND and polyethylene oxide (PEO; Tg = -53.3°C, T_{mo} = 61.0°C) showed no T_{mo} of IND in the mixture at the ratio of 10:90 and 25:75 and depression of the drug's T_{mo} at the ratio of 50:50 and 75:25 due to the drug dissolving in the molten polymer (18).

All the results of T_g and T_{mo} were confirmed by melting behaviors observed by HSM. Under HSM, IND was melted before its T_{mo} when mixed with PVP/VA at the ratio of 1:1, also with PEO at all studied ratios (16). IND was not melted before its T_{mo} and was not dissolved in the molten polymer when mixed with citric acid or GLU (18).

In addition, an appearance of solid dispersions can suggest miscibility of the mixtures. If the mixtures are miscible, the products are transparent. If the mixtures

are immiscible, the products are turbid or opaque. Here, a T_g of the product can be determined by DSC during heating step and compared with that of the physical mixtures obtained during reheating step. Moreover, there are some supportive tools to help investigating characteristics of solid dispersion, such as its crystallinity by X-ray powder diffractometry (XRPD), intermolecular interaction by Fourier transform infrared (FTIR) and nuclear magnetic resonance (NMR) spectroscopy, also drug release by dissolution test (1, 16).

After extrusion, Forster et al. reported that the extrudates of IND: PVP/VA (1:1) and LCP:PVP/VA (1:1) were transparent and brittle. These extrudates were considered to be in the group of glass solution because of theirs appearance and single T_g at 64.5°C and 75.6°C, respectively, when observed by DSC. XRPD was used to confirm an amorphous state of the drugs. It showed similar trend between predicted values of drug-polymer mixtures and determined values of solid dispersions (16). Prediction of miscibility is therefore useful to screen potential miscible compounds at an early stage of formulation development to save cost and time.

4. Miscibility prediction by solubility parameters

Hildebrand solubility parameter is obtained from square root of cohesive energy density (CED). The CED is cohesive energy (E_{coh}) per unit of volume (V) as shown in equation (1). The cohesive energy (E_{coh}) is an internal energy per mole of material when all intermolecular forces were eliminated. This energy can be easily calculated from heat of vaporization for liquid as the following equation (1) (32, 33).

$$\delta = \sqrt{CED} = \sqrt{\frac{E_{coh}}{V}} = \sqrt{\frac{\Delta H_v - RT}{V}} \qquad (1)$$

Where, (ΔH_v) is heat of vaporization; R is a gas constant and T is temperature (33). The unit of solubility parameter is in $[J/cm^3]^{0.5}$ or $MPa^{0.5}$ (34).

Hansen solubility parameter is an extension of Hildebrand solubility parameter which is divided into partial solubility parameters from three difference types of force

which are dispersive force (δ_d) or van der Waals force, polar force (δ_p) and hydrogen-bonding force (δ_h) as shown equation (2), where δ_t is total solubility parameter.

$$\delta_t = \sqrt{\delta_d^2 + \delta_p^2 + \delta_h^2} \qquad (2)$$

Due to that heat sensitive substances and solids such as polymer cannot vaporize, E_{coh} of these substances cannot be obtained directly from the experiment. Instead, it can be calculated from small fragments which contribute in a chemical structure of the substance. This calculation is called group contribution method (GCM). The method estimates the E_{coh} of a substance by set of group contribution as described in equation (3).

$$E_{coh} \approx \frac{F^2}{V\,(298\ K)} \qquad (3)$$

Where, F is molar attraction constant and V is molar volume at room temperature (25°C) (32, 33, 35).

Hoftyzer/Van Krevelen and Hoy's GCM approaches are widely used because of theirs simplification. However, there are some limitations for large and complex molecules, such as highly containing hydrogen bonding (i.e. directional interactions) molecules and electrostatic interactions (i.e. long ranged interactions) containing molecules (18, 36), long-chain polymers and enantiomers which cannot be separated between the different isomers (37). The partial solubility parameters equations according to Hoftyzer/Van Krevelen approach are shown as equation (4).

$$\delta_d = \frac{\sum F_{di}}{V}; \qquad \delta_p = \frac{\sqrt{\sum F_{pi}^2}}{V}; \qquad \delta_h = \sqrt{\frac{\sum E_{hi}}{V}} \qquad (4)$$

Where, F_{di} is molar attraction constant of dispersion component; F_{pi} is molar attraction constant for polar component; E_{hi} is hydrogen bonding energy per structural group which has been stated by Hansen (32, 33).

Calculation using Hoy approach is different from Hoftyzer/Van Krevelen approach in that Hoy's approach consists of four additive molar functions, a number

of auxiliary equations, and the final expressions for δ_t and for partial solubility parameter as shown in Table 3 (33).

Table 3 Terms and equations in Hoy approach

Formula	**Low-molecular liquids (solvents)**	**Amorphous polymers**
Additive molar functions	$F_t = \sum N_i F_{t,i}$ $F_p = \sum N_i F_{p,i}$ $V = \sum N_i V_i$ $\Delta_T = \sum N_i \Delta_{T,i}$	$F_t = \sum N_i F_{t,i}$ $F_p = \sum N_i F_{p,i}$ $V = \sum N_i V_i$ $\Delta_T^{(P)} = \sum N_i \Delta_{T,i}^{(P)}$
Auxiliary equations	$\text{Log } \alpha = 3.39 \log (T_b/T_{cr}) - 0.1585 - \log V$ T_b = boiling temperature T_{cr} = critical temperature $T_b/T_{cr} = 0.57 + \Delta_T - (\Delta_T)^2$ (Lyderson equation)	$\alpha(P) = 777\ \Delta_T^{(P)}/V$ $n = 0.5/\ \Delta_T^{(P)}$
Expressions for δ (F_i must be combined with a Base value (B) for liquids and $B/\bar{n}$ for polymers)	$\delta_t = (F_i + B)/V$ $B = 277$ $\delta_p = \delta_t \left(\frac{1}{\alpha}\frac{F_p}{F_t + B}\right)^{\frac{1}{2}}$ $\delta_h = \delta_t \left[\frac{(\alpha - 1)}{\alpha}\right]^{\frac{1}{2}}$ $\delta_d = \left(\delta_t^2 - \delta_p^2 - \delta_h^2\right)^{\frac{1}{2}}$	$\delta_t = (F_i + B/\bar{n})/V$ $\delta_p = \delta_t \left(\frac{1}{\alpha^{(P)}}\frac{F_p}{F_t + B/\bar{n}}\right)^{\frac{1}{2}}$ $\delta_h = \delta_t \left[\frac{(\alpha^{(P)} - 1)}{\alpha^{(P)}}\right]^{\frac{1}{2}}$ $\delta_d = \left(\delta_t^2 - \delta_p^2 - \delta_h^2\right)^{\frac{1}{2}}$

F_t is molar attraction function. Δ_T is Lydersen correction for non-ideality in low-molecular liquids' equation. $\Delta_T^{(P)}$ in the polymers' equation has been derived by Hoy (33).

Molecular dynamics (MD) simulation is another method to calculate the solubility parameters from cohesive energy density (CED) which is related to partial

solubility parameters as dispersion solubility parameter (δ_d) and electrostatic solubility parameter (δ_e) by equation (5).

$$\delta_t = \sqrt{CED} = \sqrt{\delta_d^2 + \delta_e^2} \qquad (5)$$

This method gives more accurate value of solubility parameter for the complex molecules than GCM (18).

The value of $\sqrt{\delta_d^2 + \delta_e^2}$ from MD simulation is equivalent to $\sqrt{\delta_d^2 + \delta_p^2 + \delta_h^2}$ in Hansen solubility parameter. Therefore, δ_e^2 includes the terms of δ_p^2 and δ_h^2.

If the solubility parameters of two components have minor difference, the components are highly potential to be miscible (16, 17, 19). Greenhalgh et al. reported a criterion which was widely used for prediction of miscibility based on the difference in the solubility parameters of components ($\Delta\delta$) (16-18). If $\Delta\delta$ is below 7.0 $MPa^{0.5}$, the components are likely to be miscible. If $\Delta\delta$ is more than 10.0 $MPa^{0.5}$, the components are likely to be immiscible. For example, the miscible mixture of ibuprofen (IBU) and Lutrol F86 showed $\Delta\delta$ of 1.9 $MPa^{0.5}$. The immiscible mixture of IBU and maltose showed $\Delta\delta$ of 18.0 $MPa^{0.5}$ of (17). The $\Delta\delta$ value out of the range of the mentioned criteria showed some degree of immiscible between the drug and the polymer in liquid state as found in the mixture of phenobarbital and sorbitol with $\Delta\delta$ of 8.7 $MPa^{0.5}$ by Timko and Lordi (17, 38).

Forster et al. extended the classification of miscibility based on results of $\Delta\delta$ and thermal behaviors of drugs and polymers from their experiments. They proposed that the components with $\Delta\delta$ value below 2.0 $MPa^{0.5}$ are likely to be completely miscible and those with $\Delta\delta$ value above 10.0 $MPa^{0.5}$ tend to be immiscible. In addition, the $\Delta\delta$ value in a range of 5.0 to 10.0 $MPa^{0.5}$ indicates partially miscible.

Forster et al. showed that $\Delta\delta$ of indomethacin (IND) and polyvinylpyrrolidone-co-vinylacetate (PVP/VA) was 0.8 $MPa^{0.5}$ and 1.3 $MPa^{0.5}$ based on Hoftyzer/Van Krevelen and Hoy methods, respectively, indicating that the drug and polymer were miscible. The $\Delta\delta$ of lacidipine (LCP) and sucrose was 15.9 $MPa^{0.5}$

and 13.7 $MPa^{0.5}$ based on Hoftyzer/Van Krevelen and Hoy methods, respectively, indicating immiscibility of the drug and polymer. The $\Delta\delta$ of IND and polyvinyl alcohol (PVA) was 9.4 $MPa^{0.5}$ and 8.4 $MPa^{0.5}$ based on Hoftyzer/Van Krevelen and Hoy methods, respectively, indicating borderline miscibility. The predicted values were confirmed by the experimental results obtained from DSC which also showed that the mixtures of IND:PVP/VA (1:1 and 4:1) were miscible, and the mixtures of LCP:sucrose (1:4, 1:1 and 4:1) were immiscible. The mixture of IND:PVA had a single T_g due to miscibility between IND and amorphous PVA but it showed T_m of crystalline PVA at 187°C which was immiscible with the molten IND. These results agreed with the miscibility results of IND and amorphous PVA observed through HSM (16).

Gupta et al. reported that the $\Delta\delta$ of IND and polyethylene oxide (PEO) was 0.4 $MPa^{0.5}$ and 1.9 $MPa^{0.5}$, based on Hoftyzer/Van Krevelen and Hoy methods, respectively. The values corresponded with a result of molecular dynamic (MD) simulation of 1.7 $MPa^{0.5}$, suggesting miscibility of the components. While, the $\Delta\delta$ of IND and glucose was 15.7 $MPa^{0.5}$ and 15.9 $MPa^{0.5}$, based on Hoftyzer/Van Krevelen and Hoy methods, respectively, also 10.9 $MPa^{0.5}$ from MD simulation, suggesting immiscibility. Prediction of solubility parameters agreed with DSC results which showed that IND and PEO were miscible and IND and GLU were immiscible (18).

Besides solubility parameters, Flory-Huggins interaction parameter (χ_{FH}) which can be also calculated from cohesive energy density (CED) is another method to predict miscibility of the blends (1, 19, 39-41).

5. Miscibility prediction by Flory-Huggins interaction parameter and Gibbs free energy of mixing

Flory-Huggins lattice-based theory is widely used in miscibility prediction for binary mixture, i.e. regular solutions (solute-solvent), polymer solutions (polymer-solvent) and polymer blends (polymer-polymer). It is based on the assumption of thermodynamics that in a mixture (as shown in Figure 2), the energy will change

without changing the volume of system due to random moving of molecules. The random moving and changing of energy are described in thermodynamic terms as entropy of mixing (ΔS_{mix}) and Gibbs free energy of mixing (ΔG_{mix}). The ΔS_{mix} in lattice-based theory of the binary mixture between A and B can be written as entropy of mixing per lattice site ($\Delta \bar{S}_{mix}$) in equation (6).

$$\Delta \bar{S}_{mix} = - k \left[\left(\frac{\phi_A}{N_A} \right) \ln \phi_A + \left(\frac{\phi_B}{N_B} \right) \ln \phi_B \right] \qquad (6)$$

Where, ϕ is a volume fraction. As a result of no volume changing, $\phi_B = 1 - \phi_A$. k is Boltzmann constant. N is the number of lattice sites occupied per mole that will be replaced by repeating unit of polymers and 1 for solvents or other solutes in regular solution (42, 43).

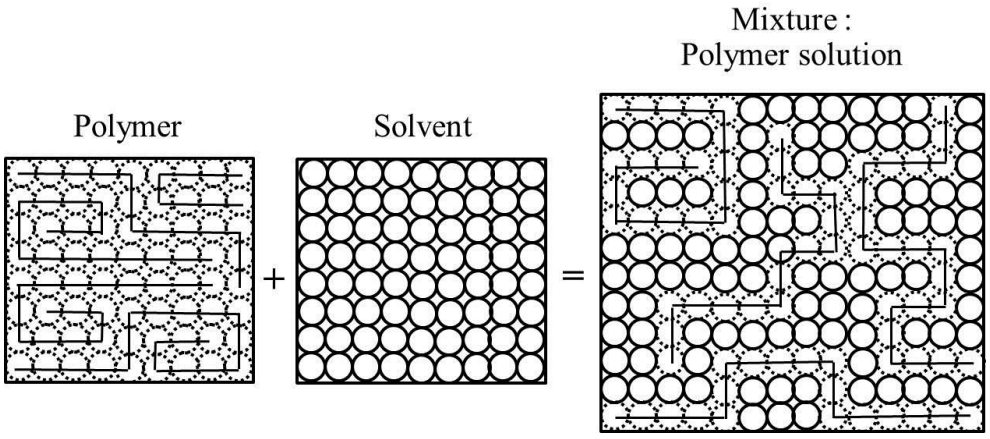

Figure 2 Lattice model of polymer solution; ○ is a lattice site which is defined as molecular volume (modified from (42)).

The assumption of the Flory-Huggins theory is that in the mixture of A and B, each lattice site is replaced by a molecule or monomer randomly, and by ignoring the polymer chain connectivity, the mixture behaves like regular solutions.

In addition, there are many interactions in the binary mixture between A and B. The Flory-Huggins interaction parameters are calculated based on the energy of the mixtures as the followings:

The energy in the mixture (E) is written into three pairwise interaction energies as u_{AA}, u_{AB} and u_{BB}. When focusing on an A molecule, E of A (E_A) is described in the equation (7).

$$E_A = u_{AA}\phi_A + u_{AB}\phi_B \qquad (7)$$

When focusing on a B molecule, E of B (E_B) is described the same as for the A molecule, which is equation (8).

$$E_B = u_{AB}\phi_A + u_{BB}\phi_B \qquad (8)$$

Each lattice site has neighboring molecules which is represented as *z*. *z* is a coordination number of lattice, e.g. $z = 4$ for square lattice and $z = 6$ for cubic lattice. Therefore, all pairwise interaction energies can be written in equation (9) and *n* is the total number of sites in the mixture.

$$E = \frac{zn}{2}\left[E_A\phi_A + E_B\phi_B\right] \qquad (9)$$

The initial energies (E_0) of A and B before mixing are calculated by equation (10).

$$E_{0A} = \frac{zn}{2}u_{AA}\phi_A \; ; \quad E_{0B} = \frac{zn}{2}u_{BB}\phi_B \qquad (10)$$

During mixing, the average energy per lattice site is obtained by equation (11).

$$\Delta\bar{E}_{mix} = \frac{E - E_0}{n} = \frac{z}{2}\phi_A\phi_B\,(2u_{AB} - u_{AA} - u_{BB}) \qquad (11)$$

The Flory-Huggins interaction parameter (χ_{FH}) is defined as interaction energies in the mixture by equation (12), where T is temperature in Kelvin (K).

$$\chi_{FH} \equiv \frac{z}{2}\frac{(2u_{AB} - u_{AA} - u_{BB})}{kT} \qquad (12)$$

As a result, the energy of mixing per lattice site ($\Delta\bar{E}_{mix}$) can be written in term of χ_{FH} following equation (13) (42).

$$\Delta\bar{E}_{mix} = \chi_{FH}\,\phi_A\phi_B\,kT \qquad (13)$$

Under a constant pressure condition, ΔE_{mix} is approximate to enthalpy of mixing (ΔH_{mix}). Therefore, it can be written as equation (14).

$$\Delta E_{mix} = \Delta H_{mix} = \frac{kT\chi_{FH}\phi_A\phi_B}{V_{ref}} = \frac{RT\,\chi_{FH}\phi_A\phi_B}{V_{ref}} \qquad (14)$$

Where, R is gas constant in molar parameters. V_{ref} is replaced by molecular or molar volume of a segment, i.e. monomer (37, 44) which is normally a value of the smallest volume in the blend (45).

The relation of ΔG_{mix}, ΔH_{mix} and ΔS_{mix} is written as equation (15).

$$\Delta G_{mix} = \Delta H_{mix} - T\Delta S_{mix} \qquad (15)$$

$T\Delta S_{mix}$ is always positive. From this equation, the mixture will be miscible when ΔG_{mix} is less than zero ($\Delta G_{mix} < 0$) (32, 42-44, 46) and enthalpy of mixing is less than entropy term ($\Delta H_{mix} < T\Delta S_{mix}$) (43). ΔG_{mix} can be written in term of χ_{FH} in equation (16).

$$\Delta G_{mix} = RT\left[\phi_A \ln \phi_A + \left(\frac{\phi_B}{m}\right)\ln \phi_B + \phi_A\phi_B\chi_{FH}\right] \qquad (16)$$

Where, m is a ratio of volume per mole of polymer chain (defined as B) to drug (defined as A), or molar volume which was calculated from equation (17).

$$m = \frac{\frac{M_{wB}}{\rho_B}}{\frac{M_{wA}}{\rho_A}} \qquad (17)$$

Where, M_{wA} and M_{wB} are molecular weight of A and B. ρ_A and ρ_B are density of A and B (44, 46).

ΔE_{mix} can be obtained from MD simulation of binary mixture between A and B, calculated by equation (18) (47).

$$\Delta E_{mix} = \phi_A(CED)_A + \phi_B(CED)_B - (CED)_{mix} \qquad (18)$$

MD simulation with NVT ensemble, i.e. a constant volume condition is preferred to calculate ΔE_{mix} due to that constant volume is required under assumption of this theory.

The relationship between ΔH_{mix} and E_{coh} is shown in equation (19). V is molar volume at room temperature (25°C) (32).

$$\Delta H_{mix} = V \left[\left(\frac{E_{coh,\,A}}{V_A} \right)^{1/2} - \left(\frac{E_{coh,\,B}}{V_B} \right)^{1/2} \right]^2 \phi_A \phi_B \qquad (19)$$

Thus,

$$\Delta H_{mix} = V_{ref} (\delta_A - \delta_B)^2 \phi_A \phi_B \qquad (20)$$

As a result, χ_{FH} can be written in term of solubility parameters (δ) following equation (21) (1, 32).

$$\chi_{FH} = \frac{V_{ref} (\delta_A - \delta_B)^2}{RT} \qquad (21)$$

However, the concentration of each component has an influence on miscibility. χ_{FH} is simply calculated from solubility parameters but it does not take the concentration of each component into account. For this reason, alternatively, χ_{FH} can be calculated from ΔE_{mix} by MD simulation following equation (22). The mixtures tend to be miscible when calculated χ_{FH} is less than critical parameters (χ_c) (39, 47, 48).

$$\chi_{FH} = \frac{\Delta E_{mix} V_{ref}}{RT \, \phi_A \, \phi_B} \qquad (22)$$

Flory-Huggins lattice-based theory is used for miscibility prediction in the binary systems such as drug-polymer and plasticizer-polymer. The drug-polymer binary system is analogue with polymer-solvent binary system (37, 49, 50). An amorphous drug is considered to be solvent in Flory-Huggins theory (50).

For example, Maus et al. reported miscibility of Eudragit®RS and water-soluble plasticizer, i.e. triethyl citrate (TEC), or water-insoluble plasticizers, i.e. acetyl tributyl citrate (ATBC) and dibutyl sebacate (DBS), or plasticizing effect drug,

i.e. ibuprofen (IBU), or non-plasticizing effect drug, i.e. theophylline (THEO) in solid dispersions by hot-melt extrusion technique. χ_{FH} values of Eudragit®RS-TEC, Eudragit®RS-ATBC, Eudragit®RS-DBS and Eudragit®RS-amorphous IBU blends were less than the critical value at 1.132. As a result, these four mixtures were predicted to be miscible. However, χ_{FH} values of Eudragit®RS-crystalline IBU, Eudragit®RS-crystalline THEO and Eudragit®RS-amorphous THEO blends were higher than the critical value. These three mixtures were predicted to be less miscible. All the predictions agreed with the results from solid dispersion characterization. The miscible mixtures appeared to be transparent, while the immiscible mixtures were opaque (19). Huynh et al. also reported about miscibility between docetaxel and excipient in emulsions. The excipients were tricaprylin, tricaproin, tributyrin, vitamin E and β-caryophyllene. χ_{FH} values based on ΔE_{mix} which was calculated by MD simulation was used to estimate the solubility of the drug in the excipients. The simulated solubility was approximately 2-6% different from experimental solubility, i.e. simulated solubility of docetaxel in tributyrin (114.4 mg/ml) was 6% different from experimental solubility (108 mg/ml) and simulated solubility of docetaxel in vitamin E (76.2 mg/ml) was 1.6% different from experimental solubility (75.0 mg/ml) (41).

6. MD simulation

MD simulation is mesoscale simulation, explaining various phenomenon, which cannot be visually seen, through thermodynamics such an energy, temperature and pressure (51, 52). It is based on atoms in a system moving under Newton's second law of motion that force (F) is acting on an atom (mass of atom; m) and that atom will move from one position to another position (moving distance; r) with acceleration (a) following equation (23), where t is time (52, 53).

$$F = ma = m\frac{\partial^2 r}{\partial t^2} \qquad (23)$$

The force can be calculated from derivative of potential energy (E) in equation (24) (54, 55).

$$F = -\frac{\partial E}{\partial r} \qquad (24)$$

Thus,

$$m\frac{\partial^2 r}{\partial t^2} = F = -\frac{\partial E}{\partial r} \qquad (25)$$

Potential energy is the energy assigned by forcefield. It is obtained from bonded interaction, i.e. bond stretching (E_b), bond bending (E_θ) and torsion angle rotation (E_ϕ), and from non-bonded interaction, i.e. van der Waals or Lennard-Jones interaction (E_{VdW}) and electrostatic or coulombic interaction (E_Q) (37, 54). The summation of the total potential energy is shown in equation (26) (56).

$$E_{total} = E_{bonded} + E_{non\text{-}bonded} + E_{others} \qquad (26)$$

Potential energy of bond stretching, bond bending and torsion angle rotation is involved with length of bond (r), angle of bond (θ) and angle of torsion (ϕ) as shown in Figure 3 (52).

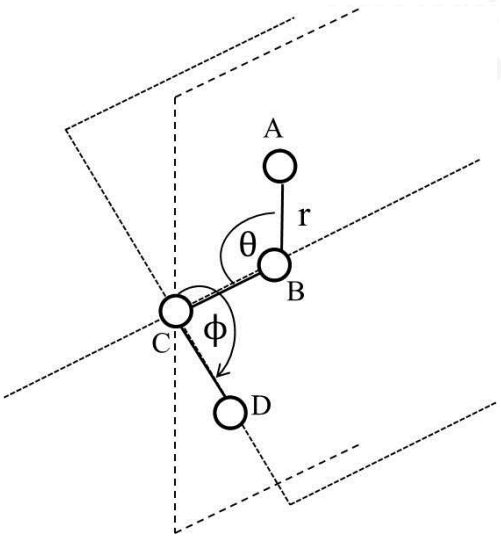

$$E_b = \frac{1}{2} K_{AB}\left(r_{AB} - r_{e,AB}\right)^2$$

$$E_\theta = \frac{1}{2} K_{ABC}\left(\theta_{ABC} - \theta_{e,\,ABC}\right)^2$$

$$E_\phi = \frac{E_0}{2}\left(1 - \cos\left(n\left(\phi - \phi_e\right)\right)\right)$$

K = force constant

r_e = bond length at equilibrium

θ_e = angle at equilibrium

ϕ_e = torsional angle of equilibrium value

n = periodicity parameter

Figure 3 Potential energy of bonded interations

Potential energy of van der Waals and electrostatic interactions is involved with distance of atoms (r) and charges of atoms (Q) in Figure 4 (55).

$$E_Q(r) = \frac{Q_1 Q_2}{4\pi\epsilon_0 r}$$

$$E_{VdW}(r) = 4\varepsilon \left[\left(\frac{\sigma}{r}\right)^{12} - \left(\frac{\sigma}{r}\right)^{6}\right]$$

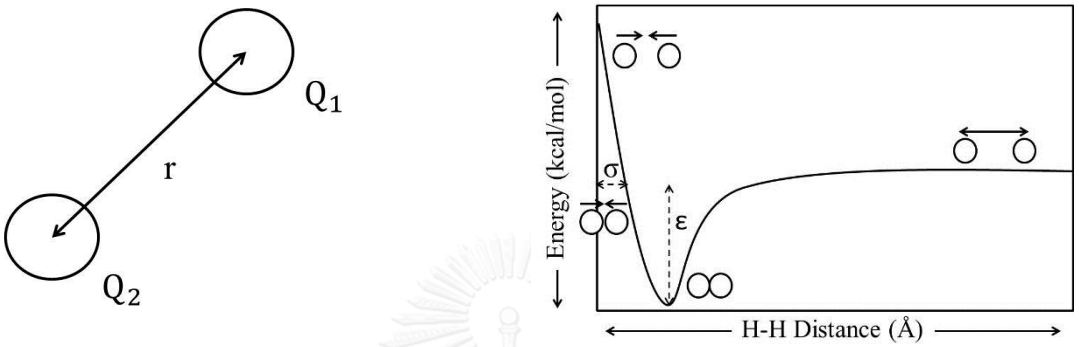

Figure 4 Potential energy of non-bonded interactions

There are many sets of forcefield, e.g. AMBER (57), COMPASS (58) and GROMOS (57) which are widely used in MD simulation. COMPASS forcefield is generally used in simulation of organic compounds (39, 40, 47, 59).

In MD simulation, the sample (atoms or molecules) is placed in a simulation box. The atoms at the edge of the box is acted by force which is different from the force near the center of the box and those atoms can accidentally disappeared by passing through the box wall, while they are moving during a simulation. As a result, those atoms are not counted in the calculation; hence, undesirable loss of density can be occurred. For this reason, periodic boundary condition is used in MD simulation. This condition can eliminate the wall effect by copying a simulation box as shown as Figure 5 (52).

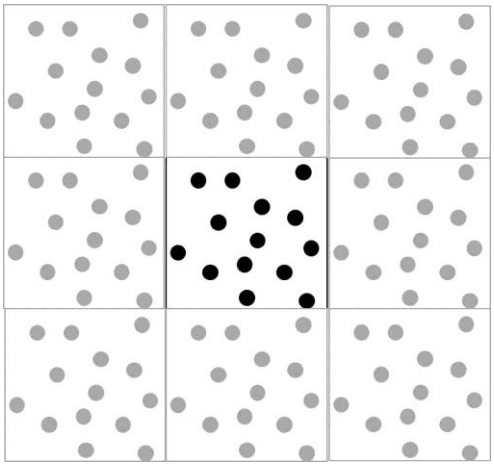

Figure 5 Periodic boundary condition: the box in black is a simulation box. The boxes in grey are periodic boundary boxes (modified from (52)).

Radial distribution function (RDF) is a function for analyzing an arrangement of atoms in the system (Figure 6).

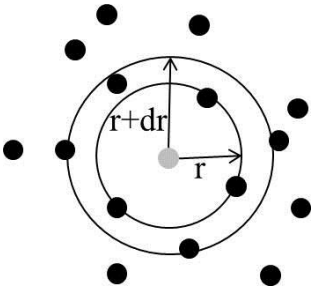

Figure 6 Distribution of atoms (modified from (52))

The method proceeds by establishing the reference atom (grey atom) and counting the other atoms (black atoms) in the distance between r and r+dr. RDF is defined as equation (27). N is the number of atoms (black atoms) (52).

$$g(r)dr = \frac{1}{N} \sum_{i=1}^{N} g_i(r)dr \qquad (27)$$

7. Mechanical properties

Mechanical properties indicate behavior of a material under the force. The simple test to evaluate mechanical properties is a tension test (Figure 7) which gives results in terms of stress (σ) and strain (e) as shown in equation (28). Stress is called tensile stress or tensile strength which is about the acting load or force (P) on an area (cross-sectional area; A) of the material. The unit of stress is load or force per unit area (N/m^2) or Pascal (Pa). Strain or elongation (e) is a dimensionless measure of stretching which can be calculated from axial deflection or extension length (ΔL) and initial length (L_0) (60, 61).

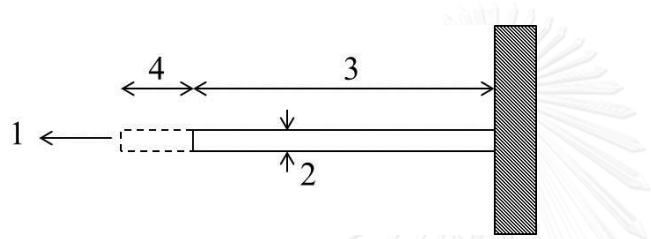

Figure 7 Tension test: Load or force (1), cross-sectional area (2), initial length (3) and axial deflection (4) (modified from (61))

$$\sigma = \frac{P}{A}\ ; \qquad e = \frac{\Delta L}{L_0} \qquad (28)$$

By following Hooke's law, during elastic deformation, the relationship between P and ΔL is linear (Figure 8 (a)); and it can be written as equation (29).

$$P = k(\Delta L) \qquad (29)$$

Where, k is a constant of proportionality called stiffness that can represent resistance of the material from deformation by force. The unit of stiffness is load per unit length (N/m).

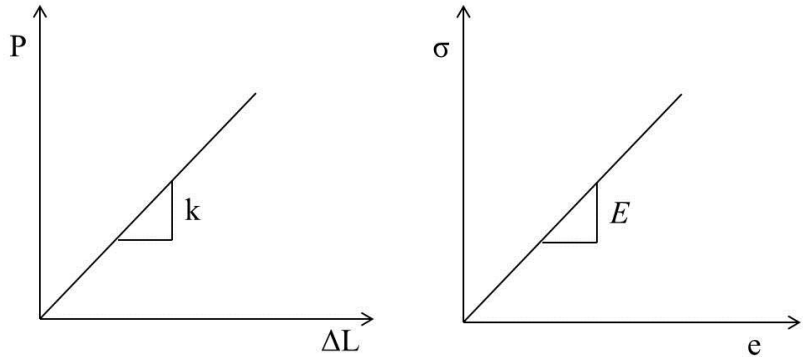

(a) (b)

Figure 8 Load-deflection curve (a) and stress-strain curve (b) during elastic deformation under Hooke's law

In fact, k is not enough to represent the resistance of material because k does not depend on types of the material alone. Shape of the sample in the tension test also affects k. For this reason, the normalized values such as stress and strain are used to calculate for evaluating the resistance to deformation by force through equation (30) and the relationship of stress and strain is shown in Figure 8 (b).

$$E = \frac{\sigma}{e} \qquad (30)$$

Where, *E* is a constant of proportionality called Young's modulus or modulus of elasticity. The unit of *E* is Pascal (Pa) as same as stress (61).

A plasticizer or secondary flexible polymer may be added to mix with the polymer to improve mechanical properties by reducing σ and *E*, and increasing elongation (e) of the polymer due to effect on T_g and interaction with molecules of the polymer (13, 21). For example, mixing hydroxypropyl methyl cellulose (HPMC) or carbomer with shellac resulted in a decrease in σ and *E*, and an increase in e of the shellac film. When the proportion of the secondary polymer was increased, T_g was decreased. Mixing ethyl cellulose (EC) with shellac resulted in slightly decreasing of σ and *E* at a low percentage of EC. When increasing the proportion of EC, σ and *E* were increased. The strain (e) was significantly decreased as increasing the percentage of EC. In addition, there was no reduction of T_g (13).

Some drugs were reported to be a plasticizer for a polymer, indicated by a decrease in σ and *E*, and an increase in strain (e). For example, mixing chlorpheniramine maleate (CPM) or hydrocortisone (HC) with hydroxypropyl cellulose (HPC) can reduce σ and *E*, and increase e of the HPC extrudate. Reduction of T_g was found in the extrudate of the drug-HPC (21).

A change of T_g was involved in miscibility of the components as mentioned in *section 3*. It is therefore, possible that the change of mechanical properties can be explained by miscibility between the polymer and secondary polymer or plasticizer or drug.

8. Model drugs and polymer

In the present study, miscibility of a polymer, i.e. polylactide with two stereoisomers and three model drugs which have different solubility parameters and thermal properties such as melting temperature (T_m), structures and recrystallization examined by heat-cool-heat cycle of DSC (62) was studied. The solubility parameters of benzocaine and indomethacin were similar to the solubility parameter of polylactide (16, 18, 39, 63), while the solubility parameter of paracetamol was largely different from that of polylactide (39, 64). The recrystallization of benzocaine and paracetamol occurred during cooling step and reheating step of heat-cool-heat cycle, respectively, while indomethacin was not recrystallized (62).

8.1 Polylactide

Polylactide is a biodegradable polymer. It can be eroded by hydrolysis at ester linkage to obtain lactic acid which is broken into carbon dioxide and water that will be eliminated by respiration and urination. Therefore, this polymer is non-toxic and biocompatible (65, 66).

Also, it is a thermoplastic polymer which can be processed by solvent or melting methods (67, 68). It is mostly hydrophobic molecules because of ester linkage between lactic acid monomer. Focusing on a repeating unit, lactic acid, it is a

chiral molecule; hence, this polymer can be existing in two stereoisomers as L and D form (Figure 9).

L form is naturally occurred by bacterial fermentation of D-glucose which is derived from foods. Poly l-lactide (PLLA) and poly d-lactide (PDLA) are semicrystalline polymers. Poly d,l-lactide (PDLLA) is from racemic mixture between l-lactide and d-lactide and it is generally amorphous (67, 69). A glass transition temperature (T_g) and a melting temperature (T_m) of the polymer varies in the range of 55-72°C and of 130-230°C, respectively; and its solid states, e.g. amorphous or semi-crystalline, depending on the ratio of L or D configuration in the polymer chain (68).

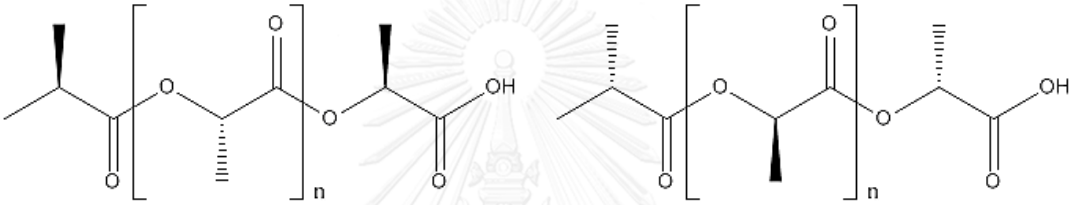

(A) (B)

Figure 9 Structures of polylactide: poly l-lactide (A) and poly d-lactide (B)

Polylactide has a wide range of molecular weight (10,000 to 756,000 kDa) (65). The molecular weight affects degree of crystallinity of polylactide in a way that high molecular weight is high crystallinity. The degree of crystallinity affects mechanical strength of polylactide. The strength of the polymer becomes high when crystallinity is high (66, 67). A rate of biodegradation is also affected by crystallinity and strength of the polymer. If it is high crystallinity, biodegradation is slow. PDLLA is less mechanical strength and high extension than PLLA due to its amorphous form; therefore, PDLLA has a higher rate of biodegradation than PLLA (66).

The structure of polylactide which plays role for hydrogen bonding is oxygen (O) of carbonyl (C=O) in ester group (70).

Polylactide and polylactide copolymers are widely used for medical devices such as surgical mesh, i.e. TIGR® Matrix (71), resorbable sutures, e.g. Caprosyn™ (which is composed of glycolide, caprolactone, trimethylene carbonate and lactide

copolymer) (72) or Polysorb^{TM} (which is composed of glycolide and lactide copolymer coated with caprolactone and glycolide copolymer) (73), orthopedic implants, e.g. polylactide and polyglycolic acid copolymer (65), polylactide and hydroxyapatite composites (74). In drug delivery systems, they are applied to formulations of implant, e.g. tinidazole in PLLA matrix for periodontitis (75), vaginal ring, e.g. tenofovir with PDLA and polyethylene vinyl acetate (76), microparticles, e.g. rifampicin-PLLA microparticles for inhalation (77) and polylactide-co-glycolide nanoparticles containing BZC (78).

8.2 Benzocaine

Benzocaine (BZC) or 4-ethylaminobenzoate is a small molecule drug which is a local anesthetic drug. Its structure contains ester and amine groups, as shown in Figure 10, which normally form interactions with other molecules. The amine group may be either hydrogen donor by hydrogen (H) or acceptor by nitrogen (N). The ester group has two oxygen (O) which can be hydrogen acceptors. An aromatic ring may interact with the other ring by dispersive forces, e.g. stacking or weak hydrogen bonding (79, 80). Recrystallization of BZC was found in cooling step of heat-cool-heat cycle by DSC (62).

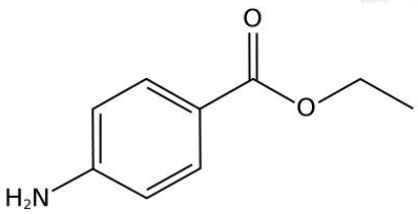

Figure 10 Structure of benzocaine

8.3 Indomethacin

Indomethacin (IND) is a non-steroidal anti-inflammatory drug (NSAID). The structure contains various fragments, e.g. indole, chlorobenzyl, carbonyl, methoxy and carboxylic groups, as illustrated in Figure 11. The possible positions for establishing hydrogen bonds with other molecules are carbonyl (C=O; O5) and hydroxyl (OH; H1) of carboxylic group and carbonyl (C=O; O3) which is between

indole and chlorobenzyl groups. H1 of carboxylic group is a hydrogen donor while O3 and O5 are hydrogen acceptors. O5 has more influence than O3 in hydrogen bonding (81). No recrystallization of IND was found when evaluated with heat-cool-heat cycle by DSC (62).

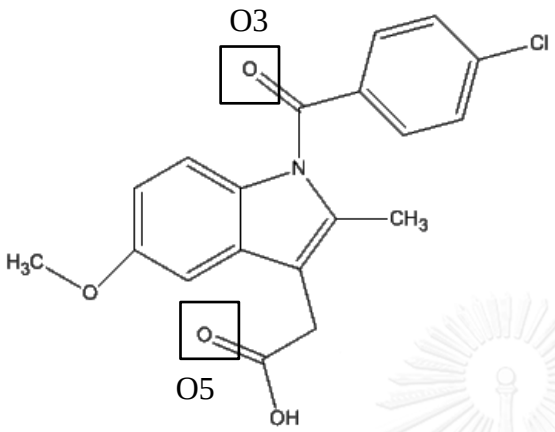

Figure 11 Structure of indomethacin

8.4 Paracetamol

Paracetamol (PAR) or acetaminophen is a small molecule drug which uses for analgesics and antipyretics. The structure, as shown in Figure 12, has high potential to hydrogen bonding with other molecules at C=O and NH of amide group and hydroxyl (OH) group. Oxygen (O) of C=O in amide and O in OH groups are hydrogen acceptors. Hydrogen (H) of NH in amide and H in OH groups are hydrogen donors (82). It was found recrystallization occurred in reheating step of heat-cool-heat cycle by DSC (62).

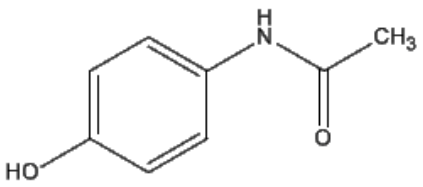

Figure 12 Structure of paracetamol

CHAPTER 3
MATERIALS AND METHODS

1. Miscibility prediction by calculation

In the present study, Hansen solubility parameter (δ), Flory-Huggins interaction parameter (χ_{FH}) and Gibbs free energy of mixing (ΔG_{mix}) were calculated for miscibility prediction. The solubility parameter was calculated by group contribution method (GCM) and by molecular dynamic (MD) simulation.

1.1 Models of model drugs and polymers

Three dimensional models (3D models) of benzocaine (BZC), indomethacin (IND), paracetamol (PAR), a unit of l-lactic acid (LLA) and d-lactic acid (DLA) were obtained from PubChem Substance (83), which are illustrated in Figure 13. Poly l-lactide (PLLA) and poly d-lactide (PDLA) chains were built from LLA and DLA repeat units by Visualizer of Material Studio software package version 5.5 (Accelrys, San Diego, CA, United State of America) as shown in Figure 14 and 15, respectively.

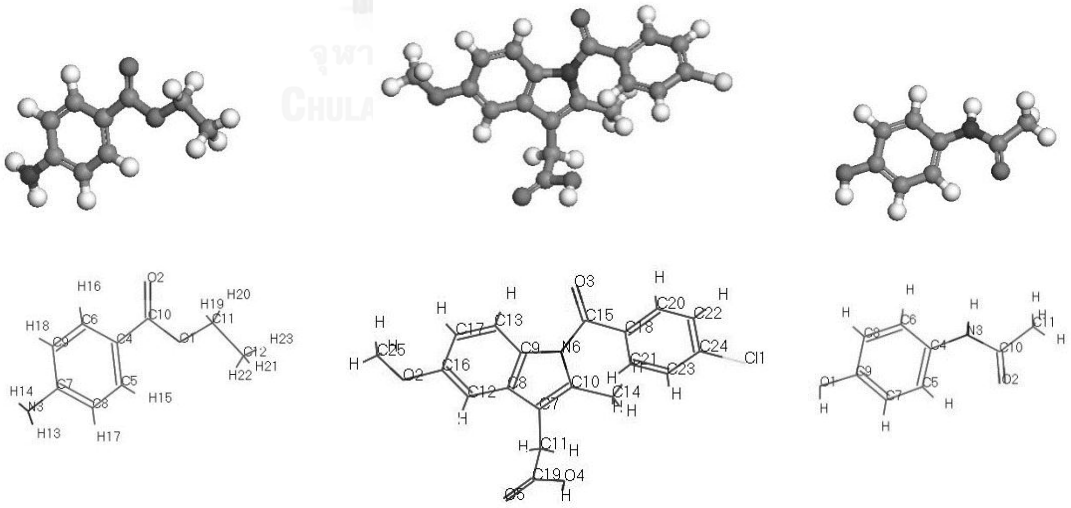

(A) (B) (C)

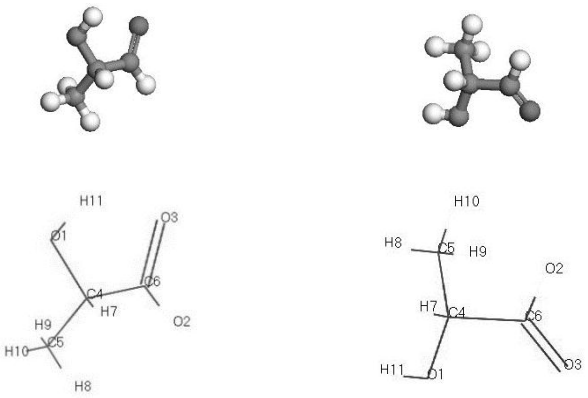

(D) LLA (E) DLA

Figure 13 3D models of drugs and a repeating unit of polymer: BZC (A), IND (B), PAR (C), LLA (D) and DLA (E)

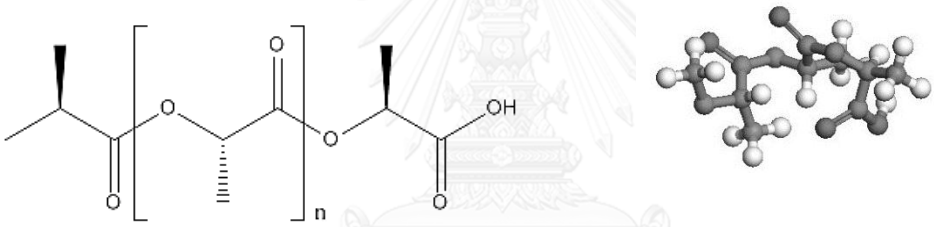

(A) (B)

Figure 14 PLLA with three repeating units: chemical structure (A) and 3D model (B)

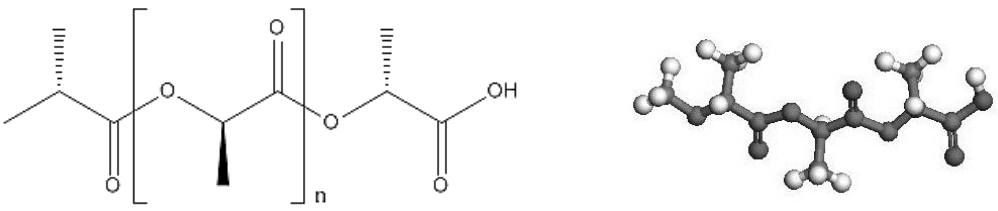

(A) (B)

Figure 15 PDLA with three repeating units: chemical structure (A) and 3D model (B)

1.2 Group contribution methods

Calculation of Hansen solubility parameters of BZC, IND, PAR, PLLA and PDLA were based on Hoftyzer/Van Krevelen and Hoy's group contribution (GCM) approaches. Basically, structures of the studied molecules were divided into fragments. The fragments were used to calculate Hansen solubility parameter using the Hansen Solubility Parameters in Practice (HSPiP) package version 3.1 (Digital River, Minnetonka, MN, United State of America). For PLLA and PDLA, the structure of a repeating unit of the polymer was used in the GCM calculation. The difference between solubility parameters of the model drug and the polymer was then calculated.

1.3 Molecular dynamics simulation

Prior to molecular dynamics (MD) simulations, a minimum number of configurations and repeating unit of polymer required to ensure consistent results of calculation in MD simulation were examined through three different configurations of one model drug (i.e. BZC) and varied number of repeating units of polymers (i.e. PLLA and PDLA). The methods are described in *sections 1.3.1 and 1.3.2*, respectively. Once, the required number of repeating units was established. The number of configurations required for MD simulation of blends was also examined through three different configurations of the blend between BZC and PLLA, as described in *section 1.3.3.*

1.3.1 Determination of the number of configurations required for MD simulation

3D models of BZC were obtained from the Pubchem Substance Database as mentioned in the *section 1.1*. A 30x30x30 $Å^3$ simulation box with a periodic boundary condition, containing bulk amorphous BZC of 81 molecules was created by Amorphous cell module at a temperature of 298 K. Atomic charges and interactions between atoms were assigned with COMPASS forcefield (58). Atom-based summation was used for van der Waals interaction with cut off distance 8.5 Å, spline width of 0 Å and buffer width of 0.5 Å. Cell multipole summation was used for electrostatic interaction.

Three different configurations of BZC which possessed low energy were selected and used for geometry optimization. Geometry optimization was carried out by Forcite Plus module of the Materials Studio software package version 5.5 using SMART algorithm at a convergence tolerance for energy of 0.001 kcal/mol and force of 0.5 kcal/mol/Å. This algorithm was started with steepest descent, then conjugate gradient, and ended with Newton method. Atom-based summation was used for van der Waals terms with a cut off distance of 12.5 Å, spline width of 1 Å and buffer width of 0.5 Å. Ewald summation was used for electrostatic terms with accuracy of 0.001 kcal/mol and buffer width of 0.5 Å.

MD simulation was then carried out using Forcite Plus module for density correction under NPT ensemble at 298 K and 0.0001 GPa (1 atm) until the density was equilibrated and fluctuated around average value. The temperature was controlled by Nose thermostat with q ratio at 1.0; and the pressure was controlled by Berendsen barostat with decay constant of 0.1 ps. Run time was 1,000 ps. A time step of 1.0 fs was used. Van der Waals and electrostatic terms were calculated using atom-based and Ewald summation, respectively, as described for geometry optimization. Trajectories were also saved every 1 ps and the last 400 ps were used for calculating density.

After that, the MD simulation was carried out under NVT ensemble at 298 K until the energy was equilibrated which was around 500 ps. The temperature control, time step, summation methods and trajectories saving were the same as described for simulation under NPT ensemble. The last 400 ps, i.e. from 100 to 500 ps were used for calculating cohesive energy densities (CED) and solubility parameters.

A small variation in calculated solubility parameters of three different configurations suggested that MD simulation of each single component was adequately carried out with one configuration.

1.3.2 Determination of the number of repeating units of polymer required for MD simulation

PLLA and PDLA with 5, 10, 20, 25, 35, 40, 50, 55 or 60 repeating units (n) were built by Visualizer of Material Studio. A 30x30x30 $Å^3$ simulation box with a periodic boundary condition, containing bulk amorphous PLLA and PDLA as described in Table 4 was created by Amorphous cell module at a temperature of 298 K, the details of which are described for creating the simulation box of BZC in the *section 1.3.1*.

Geometry optimization and density correction were proceeded as mentioned in the *section 1.3.1* except for run time of NPT for density correction which was varied from 2,000 to 3,500 ps, depending on the chain length of polymers. After that, NVT simulation was carried out for CED and solubility parameters calculation as described in the *section 1.3.1*. A minimum chain length of PLLA and PDLA which gave a relatively constant solubility parameter was chosen for MD simulation of each polymer and of the blends between model drugs and the polymers in the *section 1.3.3 and 1.3.5*.

Table 4 The number of polymer chains in a simulation box

Chain length (n, repeating units) of polymer	M_w of a polymer chain	PLLA			PDLA		
		Number of polymer chains	Number of atoms	Density (g/cm^3)	Number of polymer chain	Number of atoms	Density (g/cm^3)
5	378.33	35	1,680	1.20	35	1,680	1.21
10	738.65	18	1,674	1.19	18	1,674	1.20
20	1,459.27	9	1,647	1.17	9	1,647	1.19
25	1,747.53	8	1,752	1.13	8	1,752	1.17
35	2,468.16	6	1,854	1.19	6	1,854	1.18
40	2,828.47	5	1,770	1.17	5	1,770	1.20
50	3,621.16	4	1,812	1.18	4	1,812	1.16
55	3,909.42	4	1,956	1.19	4	1,956	1.17
60	4,269.73	4	2,136	1.18	3	1,629	1.18

1.3.3 Determination of the number of configurations of drug-polymer blend required for MD simulation

In this study, only PLLA was used as a model polymer. A 30x30x30 $Å^3$ simulation box with a periodic boundary condition, containing the blends of BZC and PLLA with repeating units designated from the result in *section 1.3.2* at various ratios as shown in Table 2 was created by Amorphous cell module at a temperature of 298 K. As for creating simulation boxes described earlier, atomic charges and interactions between atoms were assigned with COMPASS forcefield. Atom-based summation was used for van der Waals interaction with a cut off distance 8.5 Å, spline width of 0

Å and buffer width of 0.5 Å. Cell multipole summation was used for electrostatic interaction.

Geometry optimization and density correction were carried out using three different configurations of BZC and PLLA blend as described in the *section 1.3.1* except for run time of NPT for density correction which was 2,400 ps. After that, NVT simulation was carried out for 2,000 ps to calculate CED under the condition that described in the *section 1.3.1*. Flory-Huggins interaction parameter (χ_{FH}) and Gibbs free energy of mixing (ΔG_{mix}) were also calculated from CED, the equations of which are described further in the *section 1.3.5*. Plots between χ_{FH} or ΔG_{mix} and drug to polymer ratios were used to suggest a minimum number of starting configurations required for simulation. Reproducible results allowed MD simulation of blends to be carried out with one configuration.

1.3.4 MD simulation of amorphous drugs and polymers

3D models of model drugs, i.e. BZC, IND and PAR, were obtained from the Pubchem Substance Database as mentioned in the *section 1.1*. A 30x30x30 $Å^3$ simulation box with a periodic boundary condition, containing bulk amorphous BZC of 81 molecules, IND of 38 molecules and PAR of 88 molecules, was created by Amorphous cell module at a temperature of 298 K, the details of which are described for creating the simulation box of BZC in the *section 1.3.1*.

Geometry optimization and density correction were proceeded as described in the *section 1.3.1* except for run time of NPT for density correction which was varied, i.e. 1,000 ps for BZC, 1,600 ps for IND and 1,200 ps for PAR. After that, NVT simulation was carried out for CED and solubility parameters calculation as described in the *section 1.3.1*. For polymers, CED and the solubility parameter of chosen number of repeating units from the *section 1.3.2* were used. The difference between solubility parameters of model drugs and polymers was calculated.

1.3.5 MD simulation of drug and polymer blends

A 30x30x30 $Å^3$ simulation boxes with a periodic boundary condition, containing model drugs and polymer blends at various ratios as shown in Table 5,

were created by Amorphous cell module at a temperature of 298 K. The minimum number of blend's configuration required for simulation was determined in the *section 1.3.3.* As for creating the simulation box, the details of method are described in the *section 1.3.1*.

Table 5 Number of drug molecules and polymer chains which were used in MD simulation in a simulation box

Ratio	**Number of drug molecules : polymer chains**					
Drug:Polymer	**BZC**		**IND**		**PAR**	
	PLLA	**PDLA**	**PLLA**	**PDLA**	**PLLA**	**PDLA**
5:95	5:9	5:6	2:8	2:5	5:8	5:6
10:90	8:7	10:6	4:7	5:6	9:7	11:6
20:80	16:6	19:5	9:7	9:5	20:7	21:5
30:70	27:6	33:5	13:6	12:4	30:6	36:5
50:50	42:4	46:3	20:4	21:3	46:4	50:3

Geometry optimization and density correction were proceeded as described in the *section 1.3.1* except for run time of NPT for density correction which was varied from 2,400 to 3,000 ps depending on chain length of the polymers and size of model drugs. After that, the NVT simulation was carried out under the condition as described in the *section 1.3.1* except for run time of NVT which was 2,000 ps and the last 400 ps of NVT was used for calculating CED and to analyze radial distribution function (RDF) in the *section 3.4*

Calculation of Flory-Huggins interaction parameter.

CEDs were used to calculate energy of mixing (ΔE_{mix}) through the following equation:

$$\Delta E_{mix} = \phi_P(CED)_P + \phi_D(CED)_D - (CED)_{mix}$$

Where, ϕ_P and ϕ_D are volume fractions of the polymer and the drug, respectively. $(CED)_P$, $(CED)_D$ and $(CED)_{mix}$ are CED of the polymer, the drug and the blend, respectively. The CED of the polymer and the drug were obtained from the *section 1.3.4* and the CED of blends was obtained from the *section 1.3.5* (47).

ΔE_{mix} was then used to calculate Flory-Huggins interaction parameter (χ_{FH}) through the following equation:

$$\chi_{FH} = \frac{\Delta E_{mix} V_{ref}}{RT \phi_P \phi_D}$$

Where, V_{ref} is a reference volume (smallest volume of the blend system) which is obtained from molecular weight of a repeat unit divided by simulated density of polymer. ϕ_P and ϕ_D are volume fractions of the polymer and the drug which are calculated from the number of molecules and molar volume. R is a gas constant which is 8.314472 (J/mol.K). T is temperature (K) (39).

The value of χ_{FH} was determined by critical parameter (χ_c) which was obtained from equation:

$$\chi_c = \frac{1}{2}\left(1+\frac{1}{\sqrt{N_P}}\right)^2$$

Where, N_P is repeating units of the polymer (34, 42, 49, 50, 84).

It has been postulated that if χ_{FH} is less than χ_c, the drug and polymer tends to be miscible (37, 39-41).

The χ_{FH} was used to calculate Gibbs free energy of mixing (ΔG_{mix}) through the following equation:

$$\Delta G_{mix} = RT\left[\phi_D \ln \phi_D + \left(\frac{\phi_P}{m}\right)\ln \phi_P + \phi_D \phi_P \chi_{FH}\right]$$

Where, ϕ_P and ϕ_D are volume fractions of the polymer and the drug. R is gas constant which is 8.314472 (J/mol.K). T is temperature (K) (44, 46). m is a ratio of volume per mole of the polymer and the drug, which can be calculated from equation:

$$m = \frac{\frac{M_{wP}}{\rho_P}}{\frac{M_{wD}}{\rho_D}}$$

Where, M_{wP} and M_{wD} are molecular weights of the polymer and the drug. ρ_P and ρ_D are densities of the polymer and the drug which were corrected by MD simulation in the *section 1.3.4* (46).

If ΔG_{mix} is negative, the drug and the polymer tend to be miscible (39, 41, 46).

1.4 Radial distribution function analysis

Hydrogen bonding between the model drugs and the polymers (PLLA and PLDA) in the blends was evaluated by radial distribution function (RDF) analysis based on the results of MD simulation. The trajectories of last 400 ps of NVT simulation were analyzed with cut off distance of 12.5 Å and interval of 0.02 Å.

2. Miscibility prediction by experiments

Materials

BZC (≥ 99% purity) was purchased from Sigma-Aldrich (Missouri, United State of America). Polylactide (Naturework®PLA2003D, 0.19% of residue lactide, 4.4% of d-isomer) was purchased from BC Polymer Marketing Co., Ltd. (Bangkok, Thailand). The polymer was rich in L-form; therefore it was referred to as poly l-lactide (PLLA) in the study. IND (99.8% purity) manufactured by CSPC Ouyi Pharmaceutical Co., Ltd. (Hebei, China) was given by Greater Pharma, Co., Ltd. (Bangkok, Thailand). PAR (100.4% purity) manufactured by Changshu Huagang Pharmaceuticals Co., Ltd. (Jiangsu, China) was given by Advance Pharmaceutical Manufacturing Co., Ltd (Pranakorn Sri Ayutthaya, Thailand). PLLA was cooled in

liquid nitrogen for 5-10 min before grinding in a ultra-centrifugal mill (Model ZM200, Retsch, Germany) which was assembled with 0.5 mm sieve before use.

2.1 Thermogravimetric analysis

Decomposition temperature (T_{de}) of model drugs and PLLA were determined by thermogravimetric analysis **(**TGA; Model SDTA851e, Mettler Toledo, Columbus, United State of America). A sample was heated from 25 to 300°C at the rate of 10°C/min with nitrogen gas purge at 30 ml/min. The T_{de} was used to designate the temperature used in hot melt extrusion.

2.2 Differential scanning calorimetry

The melting temperature (T_m) and decomposition temperature (T_{de}) of model drugs and PLLA were determined by differential scanning calorimetry (DSC; Model PB822e, Mettler Toledo, Columbus, United State of America). The sample was heated from 25 to 300°C at the rate of 10°C/min with nitrogen gas purge at 30 ml/min. The measured T_m and $T_{de,}$ determined by DSC together with the T_{de} determined by TGA, were used to designate the maximum temperatures employed in hot melt extrusion and other DSC experiments.

The glass transitions temperature (T_g) and melting temperature (T_m) of drugs, PLLA and the mixtures between the drug and polymer at various ratios as shown in Table 6 were determined by DSC using heat-cool-heat cycle. The experiment was started by heating 6-7 mg of the samples in a 40 µl standard aluminium pan from 25°C to about 10°C above a higher T_m of the components in the mixture, i.e. 165°C, 175°C and 185°C for BZC, IND and PAR mixtures, respectively, at the rate of 10°C/min to melt the sample and holding at this temperature for 2 min, followed by cooling the molten material to -60°C at the rate of 20°C/min, and ended with reheating the samples to 10°C above the higher T_m of the components again at the rate of 10°C/min. The T_m and T_g were detected during heating and reheating step, respectively. The theoretical T_g of the mixtures were obtained from the Gordon-Taylor equation (85), as following equation:

$$T_g = \frac{w_P T_{gP} + K w_D T_{gD}}{w_P + K w_D} \quad ; \quad K = \frac{\rho_P T_{gP}}{\rho_D T_{gD}}$$

Where, w_P and w_D are weight fractions of the polymer and model drug, respectively. T_{gP} and T_{gD} are T_gs of polymer and model drug, respectively. ρ_P and ρ_D are true densities of polymer and model drug, respectively, which were measured by gas pycnometer (Model Ultrapycnometer 1000, Quantachrome, Florida, United State of America). The experimental T_gs were compared with the theoretical T_gs.

Table 6 Weight ratios of drug and PLLA in the experiments.

Drug	**PLLA**
5	95
10	90
20	80
30	70
50	50

2.3 Hot stage microscopy

Thermal behaviors of BZC, IND, PAR, PLLA and drug:polymer mixtures at the ratios as shown in Table 6 were examined on a hot stage (Model FP82HT, Mettler Toledo, Columbus, United State of America) which was connected to a light microscope (Model Eclipse E200, Nikon, Tokyo, Japan) and an objective lens x10, together with a camera (Model EOS, Canon, Tokyo, Japan). An amount of samples was placed on a glass slide, covered with a cover slide and then fixed on the hot stage. The sample was heated from 30°C to a temperature at about 10-15°C above the higher T_m of the components, comparing between two T_ms of the components, i.e. 165°C, 175°C and 185°C for BZC, IND and PAR mixtures, respectively, at heating rate of 10°C/min.

3. Miscibility evaluation between drug and polymer in extrudates

Hot melt extrusion

The model drugs (except BZC) and PLLA at the same drug to polymer ratios as tabulated in the *section 2.2* (Table 6) were gently mixed in a beaker for 5 min. The mixture was melt extruded by twin-screw extruder (Model HAAKE Minilab II, Thermo Scientific, Karlsruhe, Germany), at 160°C, approximately 10°C above T_m of PLLA to ensure that PLLA was melted completely. A screw speed was kept constant at 60 rpm. After extrusion, an extruded film, which was called an extrudate in this study, was cooled at an ambient temperature and kept at -20°C. An appearance of the extrudate was visually observed. Before characterization, the extrudate was cut into small pieces or ground by a ball mill (Model MM400, Retsch, Germany) in a cold room at 4°C. Only for mechanical properties, an intact extrudate was tested.

3.1 X-ray powder diffractometry

The extrudate was ground and placed on a sample holder. Crystallinity of the extrudate was investigated by X-ray powder diffractometer (XRPD; Model Miniflex II, Rigaku, Tokyo, Japan) with Cu-Kα radiation from 5 to 40° 2θ at a scanning rate of 4°/min. XRPD patterns of the extrudates were compared with that of the model drugs, polymer and the physical mixtures.

3.2 Differential scanning calorimetry

The extrudate was cut into small pieces. T_g and T_m of the extrudate were determined by DSC under nitrogen gas purge at 30 ml/min. The experiment was carried out by heating the sample from 0 to 200°C at a heating rate of 10°C/min.

3.3 Fourier transform infrared spectroscopy

Drug-polymer interaction in the extrudate was examined by FTIR with Smart iTR universal ATR sampling accessory (Model Nicolet iS10, Thermo Scientific, Wisconsin, United State of America). A powdered sample was placed on the window of ATR sampling accessory before scanning in the region of 4,000-650 cm^{-1}. IR

spectra of the extrudates were compared with that of the model drugs, polymer and the physical mixtures.

4. Mechanical properties of extrudates

An intact extrudate of approximately 4-5 mm width and the about 3-4 cm length was used for mechanical property study. The mechanical properties, i.e. tensile strength (σ), elongation (e) and Young's modulus (*E*), of the extrudate were examined by Universal Testing Machine (Model EZ-S 500 N, Shimadzu, Osaka, Japan) attached with a load cell of 500 N. A distance of grip separation was 10 mm. The pulling rate was 10 mm/s. The result of each blended ratio was average from 5 samples.

Tensile strength or stress (σ) is calculated from a maximum force (P_{max}) and sectional area (A). The sectional area was calculated from width x length (mm^2). A percentage of elongation or strain (e) is calculated from the length at start (L_0) and extended length (ΔL) at rupture of extrudates. Young's modulus (*E*) was obtained from the slope of stress-strain curve (61). These values were calculated by following equations:

$$\sigma = \frac{P_{max}}{A} ; \qquad e = \frac{\Delta L}{L_0} \times 100 ; \qquad E = \frac{\sigma}{e}$$

CHAPTER 4
RESULTS AND DISCUSSIONS

1. Miscibility prediction by calculation

Difference in the solubility parameters of the drug and the polymers and values of Flory-Huggins interaction parameter and Gibbs free energy of mixing were applied to predict drug-polymer miscibility in this study. The solubility parameters were calculated from group contribution method (GCM) which estimated cohesive energy, and from MD simulation which calculated cohesive energy as described *in the section 1.1*. The parameters of Flory-Huggins lattice-based theory could be also calculated from cohesive energy provided by MD simulation *in the section 1.2*.

The minimum number of configurations of the pure component and the blends which was required to provide a reproducible result of solubility parameter was proved to be one configuration. Therefore, the configuration with the lowest energy was taken into molecular dynamics (MD) simulation. The minimum repeating units (chain length) of polymers were 25 units for PLLA and 35 units for PDLA. These results are shown in Table A-16 and Figure 41-43 of Appendix.

1.1 Miscibility prediction by solubility parameter

Table 7 Solubility parameters

Methods	**Type of δ**	**δ_{BZC}**	**δ_{IND}**	**δ_{PAR}**	**δ_{PLLA}**	**δ_{PDLA}**
				$MPa^{0.5}$		
Hoftyzer/ Van Krevelen	**δ_t**	**20.7**	**21.4**	**24.6**	**17.4**	**17.4**
	δ_d	17.7	19.0	18.7	12.5	12.5
	δ_p	3.4	4.9	7.5	6.9	6.9
	δ_h	10.2	8.5	14.1	9.9	9.9
Hoy	**δ_t**	**23.3**	**21.5**	**26.8**	**21.3**	**21.3**
	δ_d	15.3	16.5	16.4	14.3	14.3
	δ_p	12.4	10.3	14.9	13.0	13.0
	δ_h	12.4	9.2	15.1	8.8	8.8
MD simulation	**δ_t**	**22.6**	**23.2**	**29.0**	**17.4**	**18.2**
	δ_d	20.2	20.5	20.8	15.6	16.8
	δ_e	10.2	10.8	20.1	7.6	7.0

δ_t = total solubility parameter, δ_d = dispersive solubility parameter, δ_p = polar solubility parameter, δ_h = hydrogen bonding solubility parameter, δ_e = electrostatic solubility parameter and $\delta_e^2 = \delta_p^2 + \delta_h^2$

1 mega Pascal (MPa) is equivalent to 1 Joule per cubic centimeter (J/cm^3) (34). The unit of δ are simply expressed in $MPa^{0.5}$, instead of $(J/cm^3)^{0.5}$ obtained from the software.

δ_t values of BZC were varied in a range of 20.7 to 23.3 $MPa^{0.5}$, depending on calculation methods. The values resulted from Hoy's GCM method and MD simulation were similar to the reported value of 23.6 $MPa^{0.5}$, which was calculated based on Fedors' GCM method (63).

δ_t values of IND were varied in a range of 21.4 to 23.2 $MPa^{0.5}$. The values from both GCM methods were slightly different. They were similar to the reported value of 21.9 $MPa^{0.5}$ which was calculated based on Hoy's GCM method by Gupta et al. (18) and Forster et al. (16). While, the value resulted from MD simulation was similar to the reported value of 23.3 $MPa^{0.5}$ calculated based on Hoftyzer/Van Krevelen's GCM approach and the reported value of 23.9 $MPa^{0.5}$ obtained from MD simulation by Gupta et al. (18). All values were similar to the value reported by Forster et al. which was 22.3 $MPa^{0.5}$, calculated based on GCM using Hoftyzer/Van Krevelen approach (16).

δ_t values of PAR were varied in a range of 24.6 to 29.0 $MPa^{0.5}$. The value resulted from Hoy's GCM method and MD simulation were close to the reported value of 27.5 $MPa^{0.5}$, calculated based on Hoftyzer/Van Krevelen's GCM method by Edgar et al. (64).

δ_t values of PLLA and PDLA were varied in a range of 17.4 to 21.3 $MPa^{0.5}$. The δ_t value resulted from Hoftyzer/Van Krevelen's GCM method and that of PLLA resulted from MD simulation were same. They were equivalent to the reported value of 17.4 $MPa^{0.5}$ for PLLA, obtained from MD simulation by Arenaza et al. (39).

In fact, the δ_t values of both stereoisomers, PLLA and PDLA, resulted from both GCM methods were the same. While, from MD simulation, the δ_t of PLLA was lower than that of PLDA because the δ_d of PLLA was considerably lower than that of PDLA, while the δ_e of PLLA was slightly higher than that of PDLA. This is basically due to that by the GCM approaches, no information of stereoisomers was included in the calculation. While, in the MD simulation, the configurations of different stereoisomers of polymer were taken into calculation. The lower δ_t of PLLA may be caused by the lower δ_d of PLLA in relative to that of PDLA, which could not be

counteracted by a slightly higher δ_e value of PLLA in calculation. It must be noted that the δ_t was decreased as increasing the repeating units up to 25 repeating units for PLLA and up to 35 repeating units for PDLA where the δ_t values were stable as shown in Figure 41 of Appendix. These results showed that the molecular weight or the polymer chain length could contribute to the calculated values to a certain extent. In other words, beyond a certain number of repeating units, increasing molecular weight or the polymer chain length would not affect the solubility parameter.

Overall, the values of δ_t obtained from the Hoy method were greater than those calculated using Hoftyzer/Van Krevelen method. The difference might be arisen from the δ_p, which was greater in all cases.

The two GCM approaches and MD simulation gave a similar trend of results. The δ_t values of BZC were similar to the δ_t values of IND and they were smaller than those of PAR. The results also showed that the δ_t values of BZC and IND were close to the δ_t values of the polymers. While, the δ_t value of PAR was largely different from the δ_t values of the polymers.

Table 8 Difference of solubility parameters

Methods	**$\Delta\delta_t$ ($MPa^{0.5}$)**					
	BZC-PLLA	**BZC-PDLA**	**IND-PLLA**	**IND-PDLA**	**PAR-PLLA**	**PAR-PDLA**
GCM						
Hoftyzer/ Van Krevelen	3.3	3.3	4.0	4.0	7.2	7.2
Hoy	2.0	2.0	0.2	0.2	5.5	5.5
MD simulation	5.2	4.4	5.8	5.0	11.6	10.8

The difference of solubility parameter ($\Delta\delta_t$) between the model drugs and the polymer are shown in Table 8. Greenhalgh et al.'s suggested that the $\Delta\delta_t$ below 7.0 $MPa^{0.5}$ indicates miscible mixture and the $\Delta\delta_t$ above 10.0 $MPa^{0.5}$ indicates immiscible mixtures (17). The results showed the values of $\Delta\delta_{BZC:polymer}$ and $\Delta\delta_{IND:polymer}$

obtained from both GCM methods and MD simulation were below 7.0 $MPa^{0.5}$. This suggests that BZC and IND were miscible with the polymers. The values of $\Delta\delta_{PAR:polymer}$ obtained from MD simulation were above 10.0 $MPa^{0.5}$. This suggested that PAR was likely to be immiscible with the polymers. Moreover, the $\Delta\delta_{PAR:polymer}$ was 7.2 $MPa^{0.5}$ based on Hoftyzer/Van Krevelen, suggesting some degree of immiscible between the drug and polymer following the discussion in Greenhalgh et al.'s study (17).

Alternatively, Forster et al. have proposed three groups of miscibility level based on $\Delta\delta$ values. The $\Delta\delta$ value below 2.0 $MPa^{0.5}$ indicates a miscible mixture and that above 10.0 $MPa^{0.5}$ indicates an immiscible mixtures. The $\Delta\delta$ value lying between 5.0 to 10.0 $MPa^{0.5}$ indicates a partially miscible mixture (16). According to their criteria, BZC and IND were most likely to be miscible; while PAR was partially miscible with the polymers according to the results of Hoy's GCM method. In addition, BZC and IND tended to be partially miscible; while PAR was immiscible with the polymers based on the results of MD simulation. Foster et al.'s criteria also indicated that PAR was partially miscible with the polymers but could not be applied to clearly classify the values of $\Delta\delta_{BZC:polymer}$ and $\Delta\delta_{IND:polymer}$ obtained from Hoftyzer/Van Krevelen method.

Overall results suggested that BZC and IND are more likely to be miscible with the polymers than PAR.

Greenhalgh et al.'s criteria could effectively applied to classify miscibility of the drug and the polymer due to that the criteria was established and generalized based on the results of numerous studies which were shown in their discussion (17). While, Forster et al.'s criteria could not clearly justify miscibility for the present calculated results because the criteria was developed based on the results of two drugs, i.e. indomethacin and lacipidine with some polymers; therefore, it was more specific for their study (16).

1.2 Evaluation of miscibility between model drugs and polymer by Flory-Huggins interaction parameters and Gibbs free energy of mixing

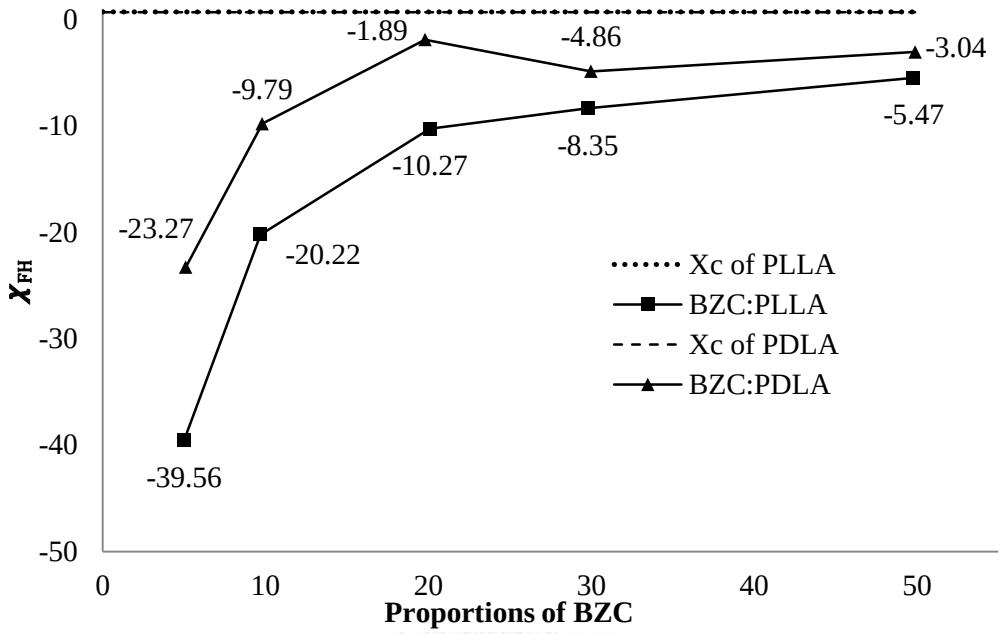

Figure 16 Relationship between Flory-Huggins interaction parameter and proportions of BZC in the blends of BZC:PLLA, (n=3), and BZC:PDLA, (n=1).

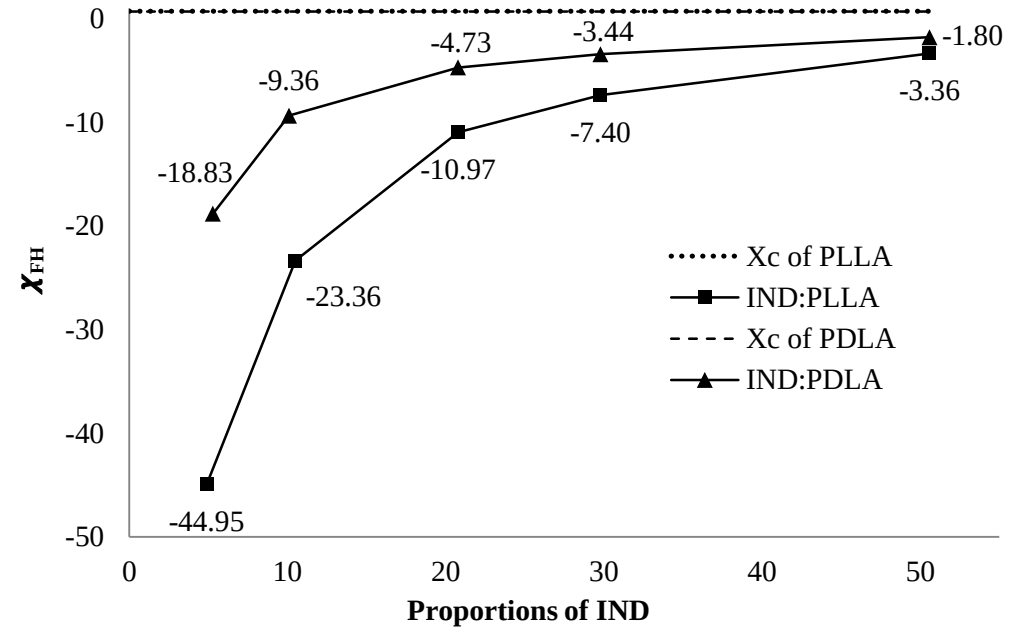

Figure 17 Relationship between Flory-Huggins interaction parameter and proportions of IND in the blends of IND:PLLA and IND:PDLA, (n=1).

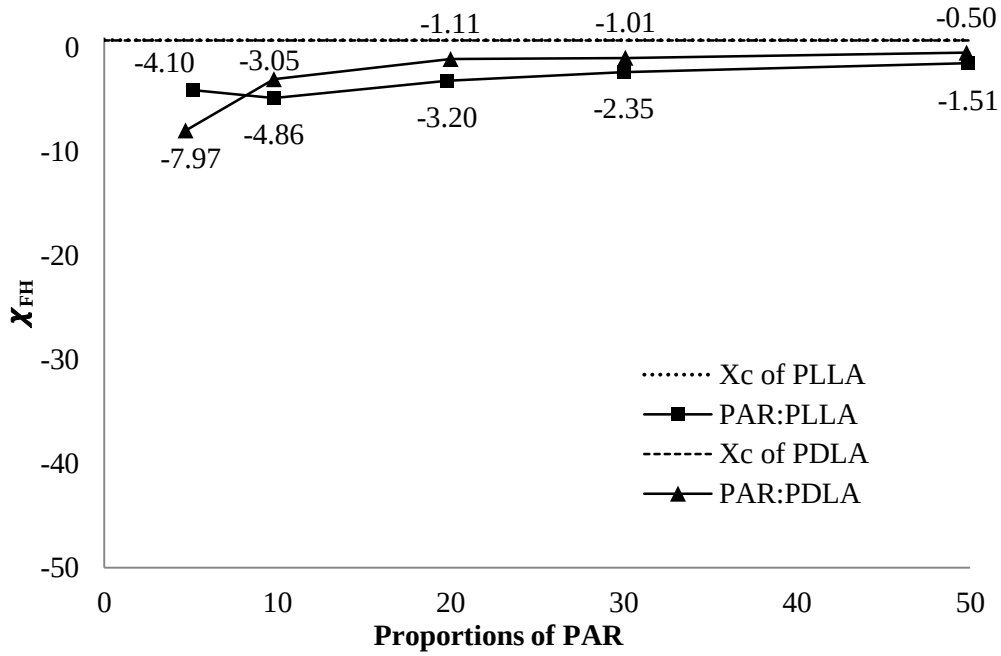

Figure 18 Relationship between Flory-Huggins interaction parameter and proportions of PAR in the blends of PAR:PLLA and PAR:PDLA, (n=1).

The plot between Flory-Huggins interaction parameter (χ_{FH}) and proportions of the drug in the blends of drug:PLLA and drug:PDLA exhibited in similar patterns. The value of χ_{FH} was increased as increasing the drug to polymer ratios. The χ_{FH} values of drug:PDLA blends were mostly higher than those of drug:PLLA blends, except for that of PAR:polymers at the ratio of 5:95; and there appeared to be smaller difference between two polymers' configurations at the relatively higher drug content.

The χ_{FH} values of PAR:polymers were higher than that of BZC:polymers and of IND:polymers at all drug:polymer ratios.

Critical parameters (χ_c) were 0.72 and 0.68 for PLLA and PDLA, respectively. All the χ_{FH} values of BZC:polymers, IND:polymers and PAR:polymers at the ratio of 5:95, 10:90, 20:80, 30:70 and 50:50 was less than the χ_c. As a result, the blends were predicted to be miscible (37, 39-41) up to the studied drug:polymer ratio of 50:50. At the higher drug:polymer ratio than the 50:50 ratio, it is possible that the χ_{FH} values would be further increased beyond the χ_c, suggesting immiscibility.

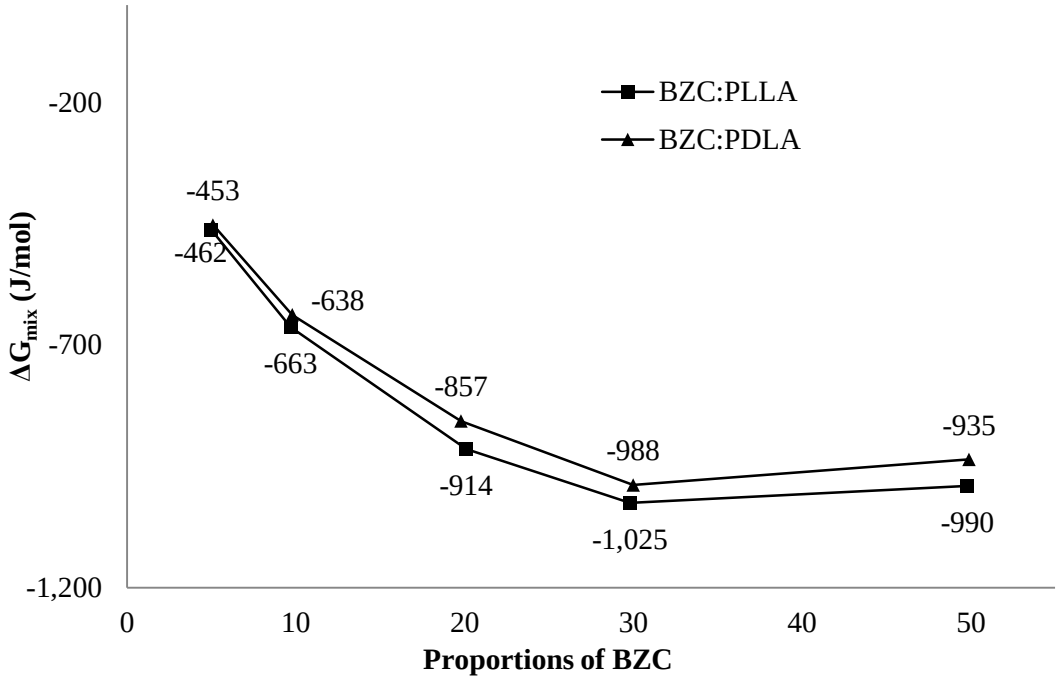

Figure 19 Retationship between Gibbs free energy of mixing and proportions of BZC in the blends of BZC:PLLA, (n=3), and BZC:PDLA, (n=1).

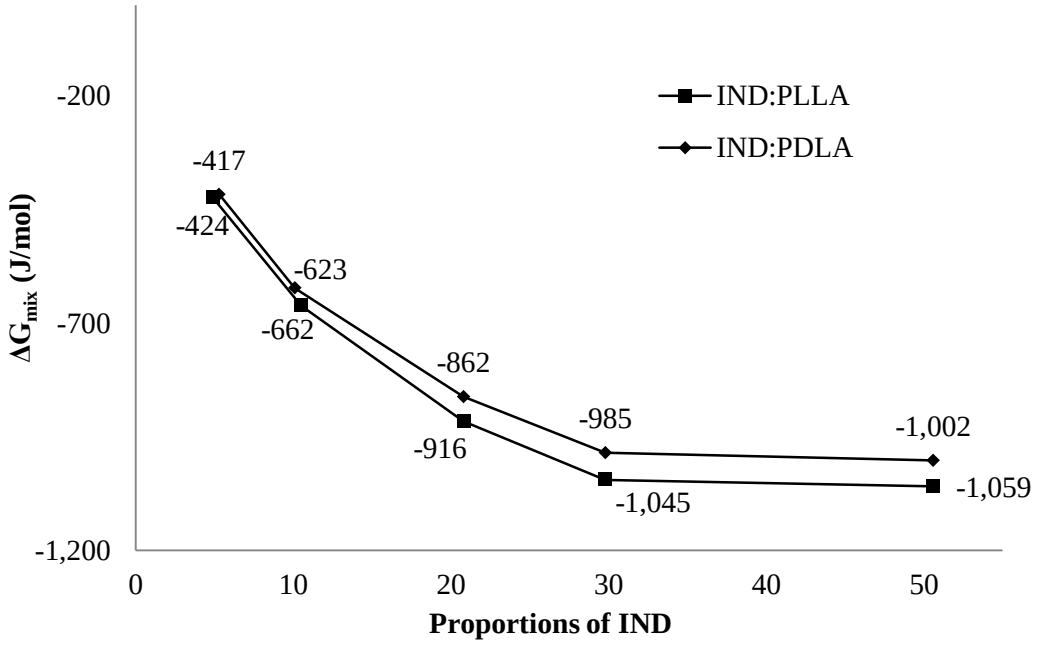

Figure 20 Retationship between Gibbs free energy of mixing and proportions of IND in the blends of IND:PLLA and IND:PDLA, (n=1).

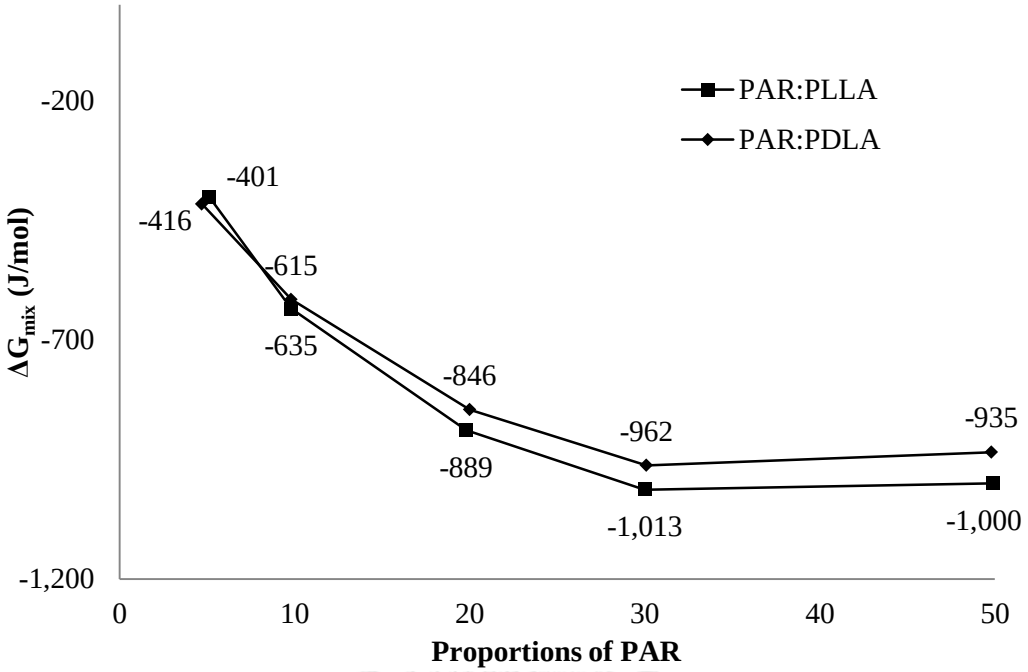

Figure 21 Retationship between Gibbs free energy of mixing and proportions of PAR in the blends of PAR:PLLA and PAR:PDLA, (n=1).

Gibbs free energy of mixing (ΔG_{mix}) of IND:polymers were decreased as increasing the drug content up to 50:50. While, the ΔG_{mix} values of BZC:polymers and PAR:polymers were decreased as increasing the drug content up to 30:70 and then slightly increased again at the drug to polymer ratio of 50:50. The ΔG_{mix} values of drug:PDLA blends were higher than those of drug:PLLA blends

However, all ΔG_{mix} values of BZC:polymers, IND:polymers and PAR:polymers at the ratio of 5:95, 10:90, 20:80, 30:70 and 50:50 were negative (39, 41, 46). Therefore, the blends were predicted to be miscible up to the drug:polymer ratio of 50:50. The trend of the plots between ΔG_{mix} values and the drug proportions was similar to the plot of the miscible mixture between IND and polyvinylpyrrolidone (PVP) which was calculated from MD simulation (86).

According to the above MD simulation results, the blends of BZC:polymers, IND:polymers and PAR:polymers at the ratio of 5:95, 10:90, 20:80, 30:70 and 50:50 were predicted to be miscible by χ_{FH} and ΔG_{mix} calculation.

The results of the χ_{FH} values agreed with the miscibility results of the $\Delta\delta$ values obtained from MD simulation (also from both GCM approaches) for BZC:polymer and IND:polymer blends, classified by Greenhalgh et al.'s criteria (17). For PAR:polymer blends, the relatively high $\Delta\delta$ values (> 10.0 $MPa^{0.5}$) from MD simulation were clearly classified as immiscibility. Although the χ_{FH} values of these blends were lower than the χ_c value, indicating miscibility, they were markedly high comparing with the the χ_{FH} values of BZC:polymer and IND:polymer blends.

1.3 Radial distribution function analysis

Drug-polymer miscibility is involved with drug-polymer interactions, while drug-polymer immiscibility is governed by drug-drug or polymer-polymer interactions. One of influencing interactions is hydrogen bonding which can be explained by MD simulation using radial distribution function.

The radial distribution function or a pair correlation function of MD simulation module helps to determine how hydrogen acceptor and donor atoms are radially packed around each other at the defined distance. The strength of hydrogen bonding can be determined by distance of the atom pair. The distance (d_{H---A}) of strong, moderate and weak hydrogen bonding were 1.2-1.5 Å, 1.5-2.2 Å and more than 2.2 Å, respectively (87). Van der Waal interaction cannot be identified because it was weak and non-directional interaction (88). The results of RDF are shown in Figure 44-56 in Appendix

In this study, atom pairing in the distance of 1.2-1.5 of strong hydrogen bonding was not found. The atoms were found to be radially packed in the distance of 1.5-2.2 Å of moderate hydrogen bonding and in the distance more than 2.2 Å of weak hydrogen bonding.

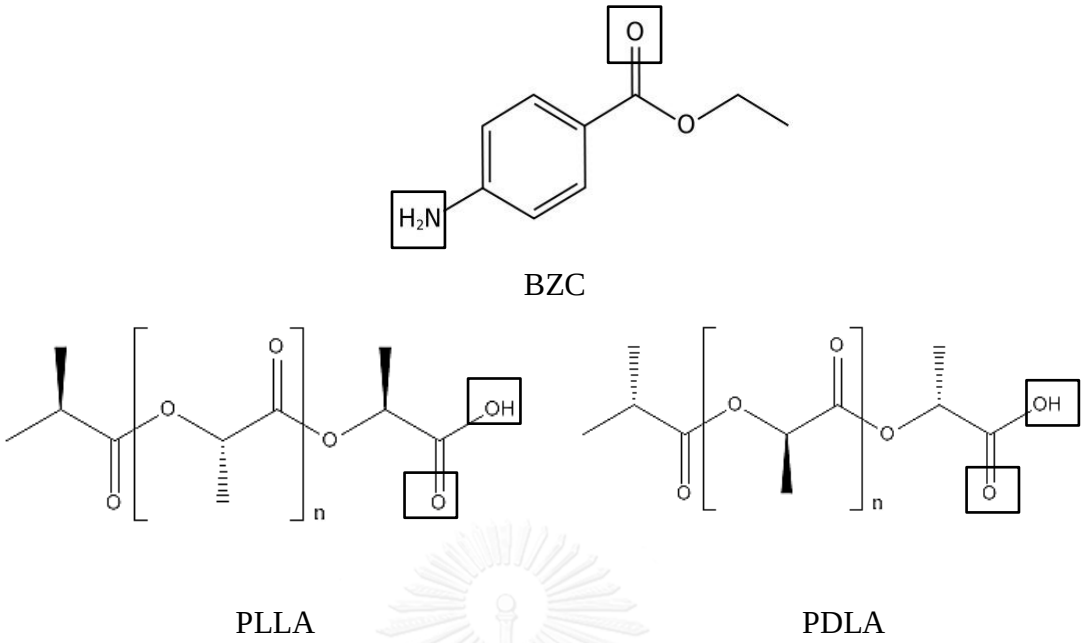

BZC

PLLA PDLA

Figure 22 Structures of drug and polymer in BZC:PLLA and BZC:PDLA blends for RDF analysis

Within the distance of 1.5-2.2 Å, the main drug-polymer interaction was the interaction between C=O in the ester group of BZC and the OH group of polymer (Figure 44, 45 (A) and 47 in Appendix). Its peak height or atom density in this shell was decreased as increasing the drug content. There was also interaction between N in amine group of BZC and OH group of polymers for BZC:PLLA. The peak height was increased as increasing the drug proportions. The interaction of polymer-polymer was C=O in ester group and OH group and the main interaction of drug-drug was C=O in ester group and H in amine group (Figure 45 (B), 46 and 48 in Appendix). The polymer-polymer interaction was found at all ratios of the blends and was stable as increasing the drug proportions. The drug-drug interaction was found in the blends at low drug proportions (5:95, 10:90) for BZC:PLLA and all ratios for BZC:PDLA.

It is noted that the main results discussed here were obtained during simulation time of 1600-2000 ps. The drug-polymer interaction was greater than drug-drug and polymer-polymer interactions in BZC:PLLA (except for the ratio of 10:90) (Figure 44 and 46 in Appendix) and in BZC:PDLA (except for the ratio of 30:70) (Figure 47 and 48 in Appendix). The drug-polymer interaction was not found at some ratios of BZC:PLLA and BZC:PDLA probably due to instability of the interaction over

simulation time. This can be demonstrated by Figure 45 in Appendix where the drug-polymer interaction in the BZC:PLLA blend at the ratio of 10:90 was found to be higher than drug-drug and polymer-polymer interactions during simulation time of 400-800 ps.

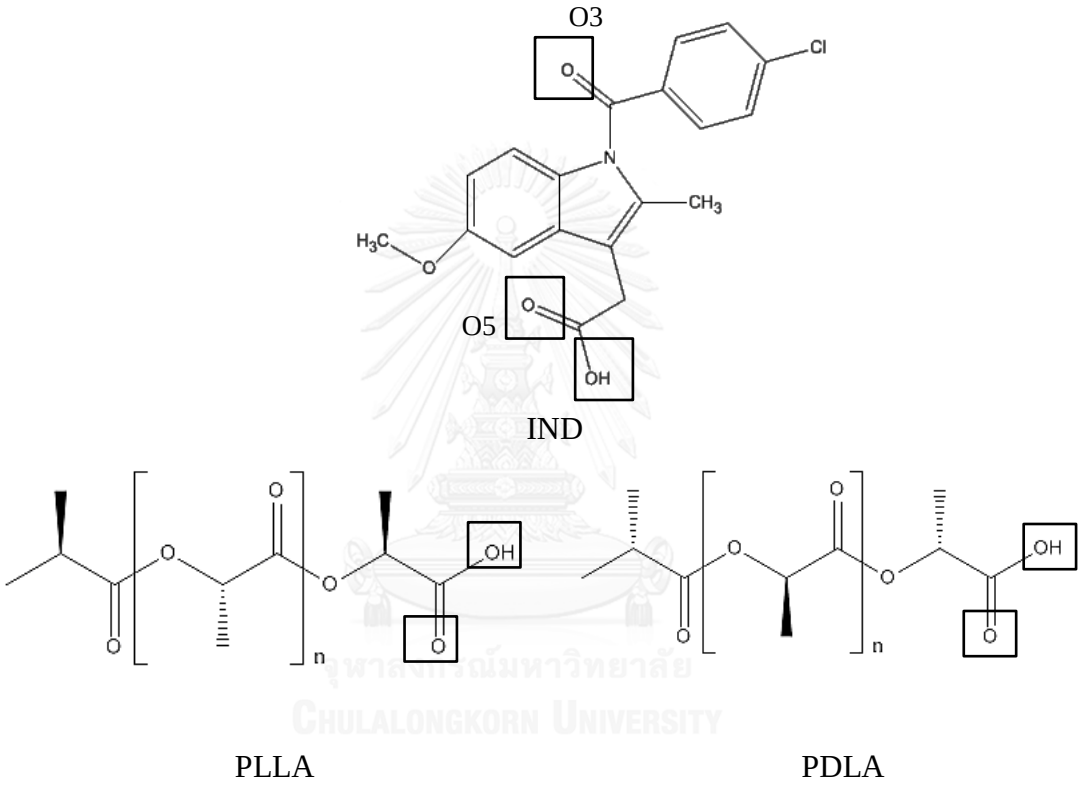

PLLA PDLA

Figure 23 Structures of drug and polymer in IND:PLLA and IND:PDLA blends for RDF analysis

Within the distance of 1.5-2.2 Å, the main drug-polymer interaction was the interaction between OH in the carboxylic group of IND and C=O in the ester group of polymers in both IND:PLLA and IND:PDLA blends (Figure 49 and 51 in Appendix). The height of this peak was decreased as increasing the drug content. There was also the interaction between C=O (between indole and chlorobenzyl groups (O3)) of IND and OH of polymers. In IND:PLLA blends, the peak height was decreased as increasing the drug proportions, like the first interaction. In IND:PDLA blends, this interaction was found in the blends with high drug content and was not stable as

increasing the drug proportions. The polymer-polymer interaction was found to be the same as described for BZC:polymers blends. The drug-drug interaction between OH in the carboxylic group and C=O (between indole and chlorobenzyl groups (O3) or in the carboxylic group (O5)) was found (Figure 50 and 52 in Appendix). In IND:PLLA blends, its peak height was increased as increasing the drug:polymer from 20:80 to 50:50. However, in IND:PDLA blends, the peak height was decreased as increasing the drug:polymer from 20:80 to 50:50. While, the drug-drug interaction within the distance of 1.5-2.2 Å was not detected in the blends of IND:PLLA and IND:PDLA at the ratios of 5:95 and 10:90.

In summary, the peak height or density of drug-polymer interaction in the IND:PLLA blends was higher than drug-drug and polymer-polymer interactions at the ratio of 5:95, 10:90 and 20:80. The peak height of drug-polymer interaction was similar to the peak height of homo-molecule interaction in the blend at the ratio of 30:70, and was lower than homo-molecule interaction in the blend at the ratio of 50:50. While, the drug-polymer interaction in IND:PDLA blends was greater than the drug-drug and polymer-polymer interactions at the ratio of 5:95, 10:90, 30:70 and 50:50. However, at one ratio of 20:80, the O3 and OH of carboxylic group in IND interaction was markedly increased. The results of IND:PDLA blends showed no relationship between the drug content and g(r) of the interactions. This was probably due to the main interaction in IND:PDLA may not be hydrogen bonding interaction or the hydrogen bonding interaction in this blends was unstable over the simulation time.

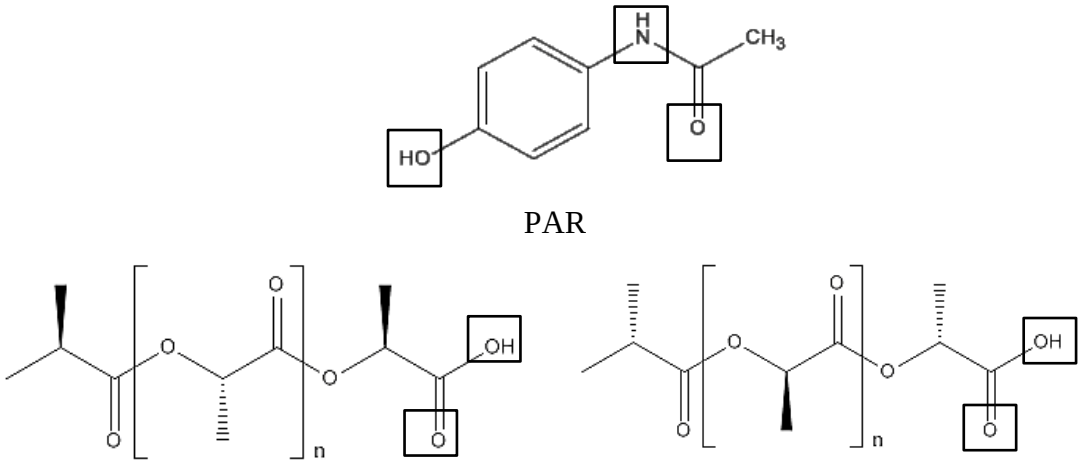

PAR

PLLA PDLA

Figure 24 Structures of drug and polymer in PAR:PLLA and PAR:PDLA blends for RDF analysis

Within the distance of 1.5-2.2 Å, the main drug-polymer interaction was the OH group of PAR and C=O in the ester group of polymers in both PAR:PLLA and PAR:PDLA blends (Figure 53 and 55 in Appendix). Its peak height was stable as increasing the drug proportions. There was also the interaction between C=O in the amide group of PAR and OH group of the polymers which was found as one of the main drug-polymer interactions in PAR:PLLA blends which was affected by the drug content; its peak height was decreased as increasing the drug to polymer ratios. In PAR:PDLA blends, the peak height of this interaction did not correspond with the drug content. The polymer-polymer interaction was found same as described for BZC:polymers blends. The drug-drug interaction between C=O in the amide group and H in the amide group or the OH group was found at all ratios of PAR:PLLA and PAR:PDLA blends except for PAR:PLLA blend at the ratio of 5:95 (Figure 54 and 56 in Appendix). The peak height was slightly decreased as increasing the drug content in PAR:PLLA blends. While, it was obviously decreased as increasing the drug content in PAR:PDLA blends at the ratios from 5:95 up to 20:80.

Accordingly, in PAR:PLLA blends, the drug-polymer interaction was greater than the interaction between drug-drug and polymer-polymer themselves at the PAR:PLLA ratio of 5:95. The drug-polymer interaction was slightly higher than

drug-drug interaction at the ratio of 10:90, 20:80 and 30:70 and was similar to drug-drug interaction at the ratio of 50:50. While, in PAR:PDLA blends, the interaction was different from that occurred in PAR:PLLA blends. The drug-drug interaction was greater than the interaction between drug-polymer interaction in the blend with low drug contents (5:95) and the drug-polymer interaction was greater than drug-drug interaction in the blends with high drug contents (10:90 up to 50:50). Likewise the results of IND:PDLA blends, the results of PAR:PDLA blends showed no relationship between the drug content and g(r) of interaction which could explain miscibility in the blends, in terms of drug-polymer interaction.

2. Miscibility prediction by experiments

2.1 Thermal properties of model drugs and polymer

Table 9 Thermal properties of model drugs and polymer determined by heat-cool-heat cycle of DSC and by TGA

Lists	**$T_{m,1}$ (°C)**	**T_c (°C)**	**T_g (°C)**	**T_{de}[b] (°C)**	**T_{de}[b] from TGA; start, maximum weight lost (%) (°C)**
PLLA	151.7±0.55[c]	-	59.3±0.26[c]	-	-
BZC	89.9	48.0[d]	-	286	137, 280 (50%)
IND	161.8	-	45.5	-	223, 293 (12%)
PAR	169.6	80.6[e]	23.8	-	224, 294 (11%)

[a]determined during heating of heat-cool-heat cycle, [b]observed during heating from 25-300°C, [c]n=3, [d]detected during cooling of heat-cool-heat cycle, [e]determined during reheating of heat-cool-heat cycle. $T_{m,1}$ is a melting temperature which was obtained during heating of heat-cool-heat cycle. T_c is a recrystallization temperature, excluding recrystallization of PLLA. T_g is a glass transition temperature. T_{de} is a degradation temperature.

The thermal behaviors of the model drugs agreed with those reported by Baird et al. (62) The reported T_gs of BZC, IND and PAR were -31°C, 45°C and 24°C, respectively. T_g of BZC was not detected by heat-cool-heat cycle at the heating rate 10°C/min and cooling rate 20°C/min in this study. T_ms of BZC, IND and PAR were similar to reported T_m which were 89°C, 161°C and 170°C, respectively. Recrystallization of BZC was detected at 48.0°C during cooling of heat-cool-heat cycle, while recrystallization of PAR was detected at 80.6°C during reheating of heat-cool-heat cycle. Recrystallization of IND was not detected. The recrystallization behaviors of the model drugs agreed with those reported by Baird et al. (62).

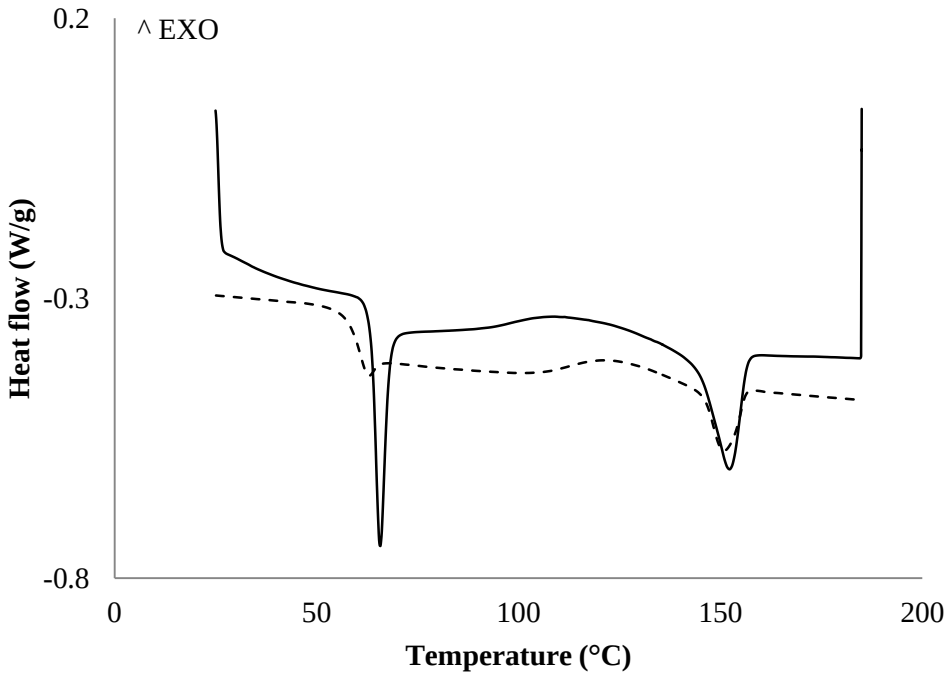

Figure 25 DSC thermogram of PLLA during heating (black line) and reheating (dash line) of heat-cool-heat cycle of PAR:PLLA mixture by DSC

Commercially available polylactide used in the experiment consisted of poly l-lactide (PLLA) approximate 96% and poly d-lactide (PDLA) 4.4%. Change of baseline around 59-66°C (midpoint = 64.4°C) during heating step (blank line in Figure 10) and around 56-61°C (midpoint = 59.2°C) during reheating step (dash line in Figure 10) indicating T_g of PLLA that agreed with the reported value at 59°C

during reheating step of heat-cool-heat cycle in Pipatpanukul's study (89) and 58°C in Tabi et al.'s study (90). A broad exothermic peak was detected at 111.6°C before sharp endothermic peak at 152.3°C during heating step. Also, a broad exothermic peak was detected at 123.4°C before sharp endothermic peak at 151.2°C during reheating step. This broad exothermic peak is attributed to PLLA recrystallization which agreed with the reported value at 117.8°C in Tabi et al.'s study (90) and at 106°C in Lasprilla et al.'s study (91). Also, the following sharp endothermic peak was T_m of PLLA which was confirmed by the reported value at 149.2°C in Tabi et al.'s study (90) and 130-230°C in Henton et al.'s work (68).

The average T_m of PLLA at 151.7°C was used to designate a processing temperature of hot melt extrusion. Degradation of the polymer could not be detected within the observed range of 25-300°C. However, it was reported that it started to degrade by the temperature above 200°C and the maximum degradation occurred at 360°C (92). Due to that BZC started to degrade at 137°C which was lower than T_m of PLLA, the mixture of BZC:PLLA could not be extruded at the temperature above T_m of PLLA. Thus, the BZC:PLLA blend was excluded from the experiment of hot melt extrusion with processing temperature at 160°C.

The experiments which could predict miscibility between drug and polymer were hot stage microscopy (HSM) and differential scanning calorimetry (DSC) using heat-cool-heat cycle as described *in the section 2.1 and 2.2*. These methods examined melting behavior and thermal properties such as T_g and T_m using the physical mixtures of drug and polymer as samples.

2.2 Hot stage microscopy

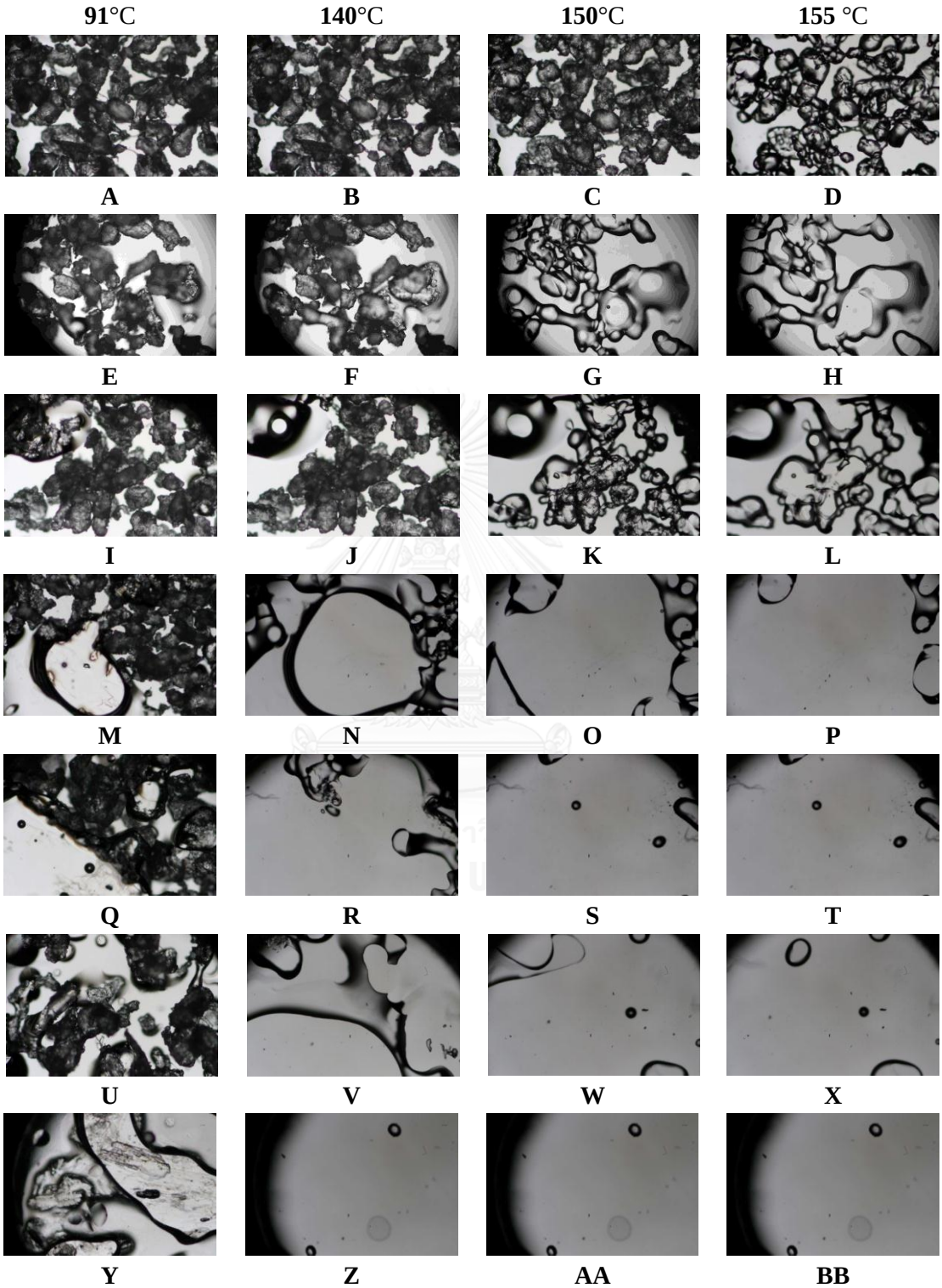

Figure 26 Hot-stage photomicrographs of BZC:PLLA blends at varied ratios: 0:100 (A-D), 5:95 (E-H), 10:90 (I-L), 20:80 (M-P), 30:70 (Q-T), 50:50 (U-X) and 100:0 (Y-BB).

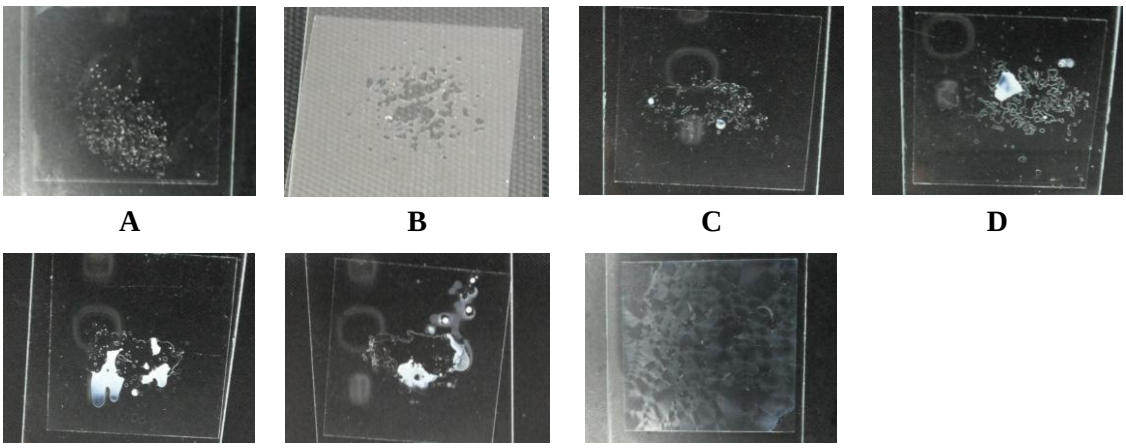

Figure 27 Photos of BZC:PLLA blends at various ratios which were cooled for 1 hour at an ambient temperature after tested by hot stage microscopy: 0:100 (A), 5:95 (B), 10:90 (C), 20:80 (D), 30:70 (E), 50:50 (F) and 100:0 (G).

The melting event of PLLA started to melt at above 150°C (Figure 26 (D)), while that of BZC occurred approximate 91°C (Figure 26 (Y)). In BZC:PLLA physical blends, when the drug content was increased, melting temperature of PLLA was decreased (Figure 26 (G, K, N, R, U)). Dissolving of PLLA in melted BZC was observed at all ratios of BZC:PLLA blends. As a result, BZC was miscible with PLLA at all studied ratios in the molten state. After testing by HSM, the samples were cooled at an ambient temperature. White portions on the glass slide was detected at all ratios of BZC:PLLA blends (Figure 27). This could be phase separation of BZC occurring at the ambient temperature.

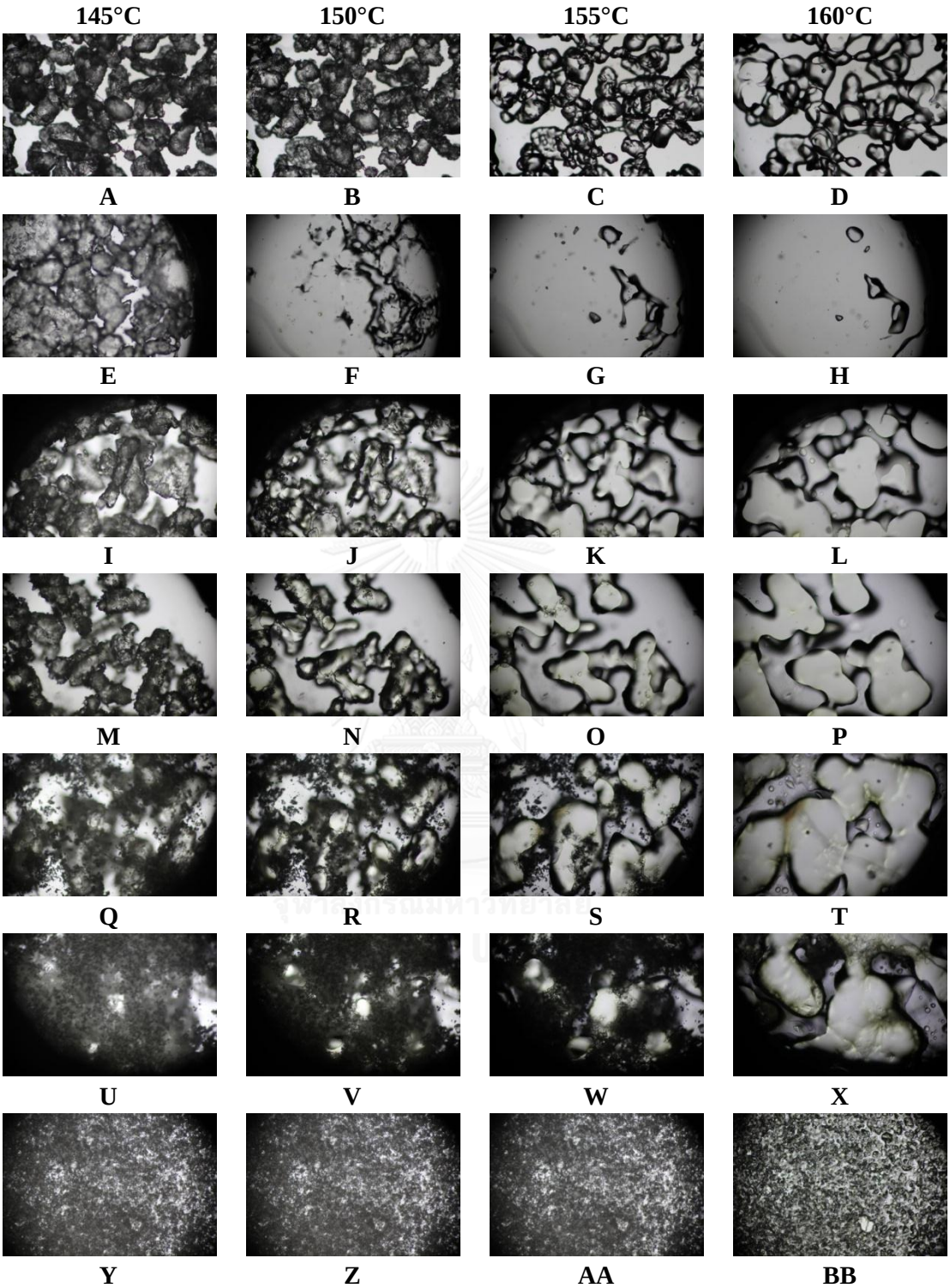

Figure 28 Hot-stage photomicrographs of IND:PLLA blends at varied ratios: 0:100 (A-D), 5:95 (E-H), 10:90 (I-L), 20:80 (M-P), 30:70 (Q-T), 50:50 (U-X) and 100:0 (Y-BB).

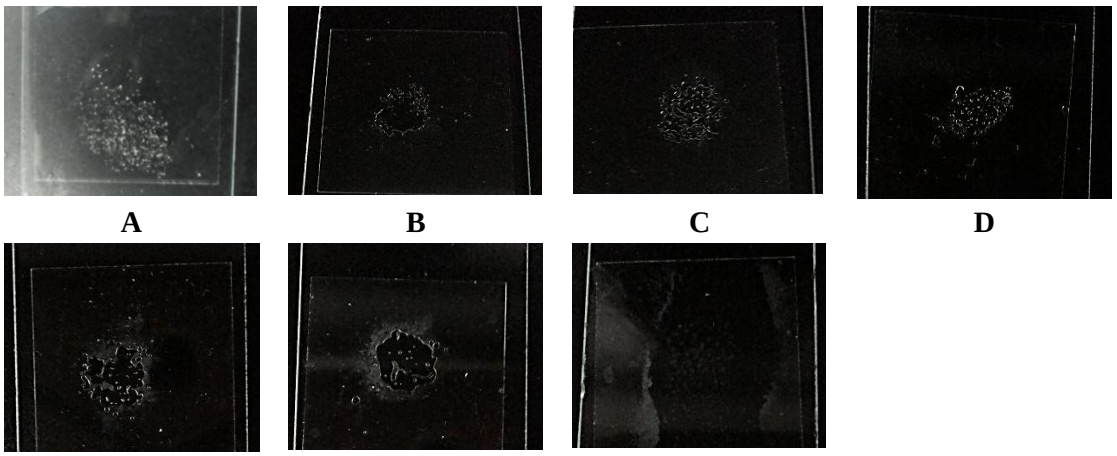

A **B** **C** **D**

E **F** **G**

Figure 29 Photos of IND:PLLA blends at various ratios which were cooled for 1 hour at an ambient temperature after tested by hot stage microscopy: 0:100 (A), 5:95 (B), 10:90 (C), 20:80 (D), 30:70 (E), 50:50 (F) and 100:0 (G)

The melting event of PLLA was also observed at above 150°C (Figure 28 (C)), while IND began to melt at approximate 160°C (Figure 28 (BB)). Due to that PLLA was melted earlier, in IND:PLLA blends, when the PLLA ratio was increased, T_m of IND was decreased (Figure 28 (F, K, O, T, X)). Dissolving of IND in the molten PLLA was detected at all ratios of IND:PLLA blends. As a result, IND was predicted to be miscible with the molten PLLA at all studied ratios. Also, after testing by HSM, the samples were cooled at an ambient temperature and no white part on the glass slide was observed (Figure 29).

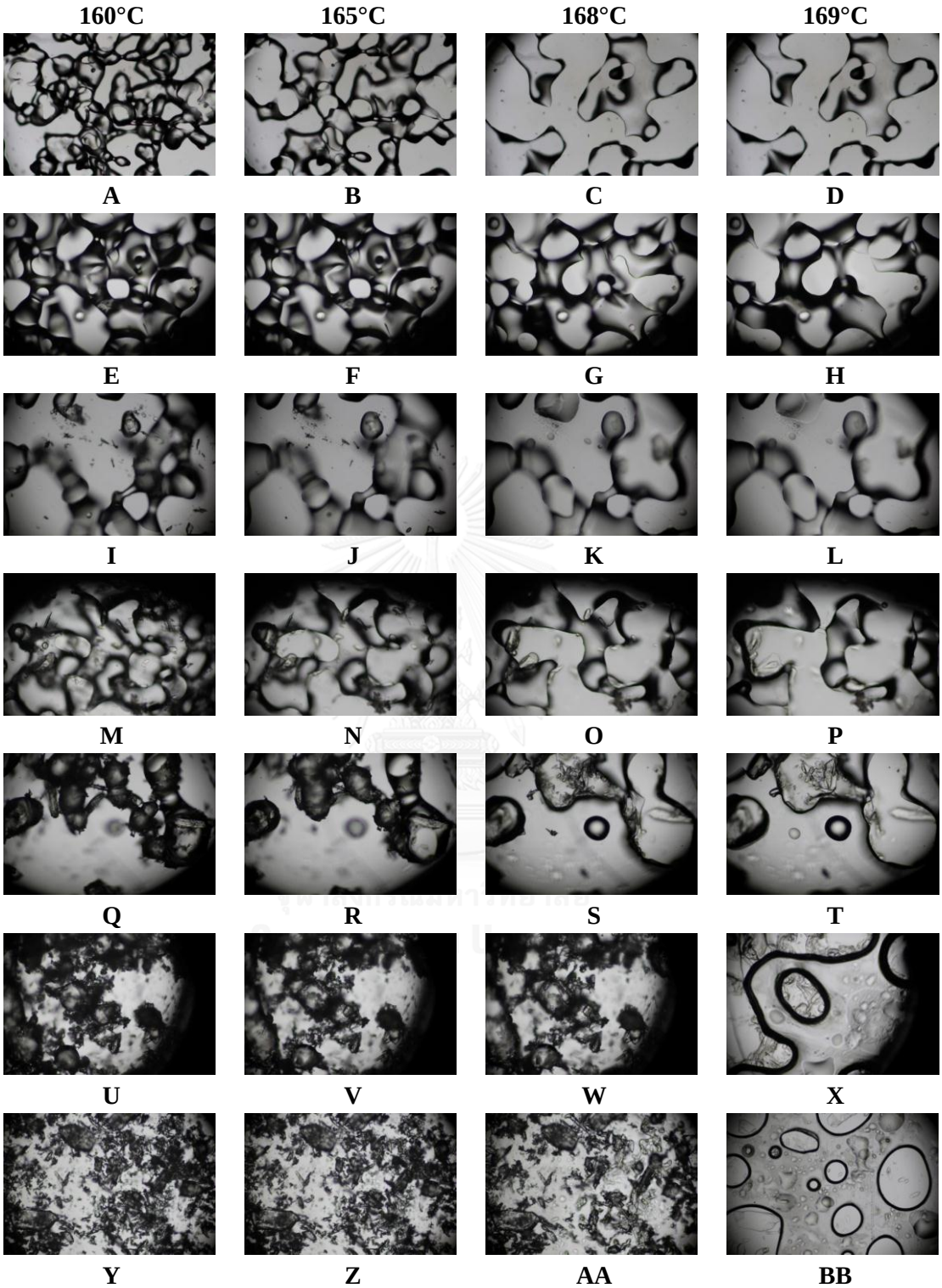

Figure 30 Hot-stage photomicrographs of PAR:PLLA blends at varied ratios: 0:100 (A-D), 5:95 (E-H), 10:90 (I-L), 20:80 (M-P), 30:70 (Q-T), 50:50 (U-X) and 100:0 (Y-BB).

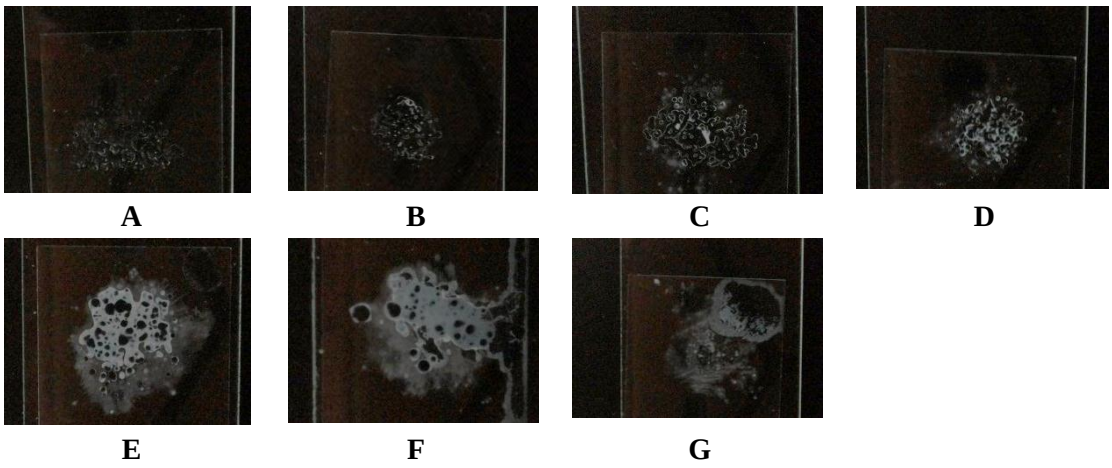

Figure 31 Photos of PAR:PLLA blends at various ratios which were cooled for 1 hour at an ambient temperature after tested by hot stage microscopy: 0:100 (A), 5:95 (B), 10:90 (C), 20:80 (D), 30:70 (E), 50:50 (F) and 100:0 (G)

The melting event of PLLA started below 160°C (Figure 30 (A)), while PAR began to melt approximate 168°C (Figure 30 (AA)) and was completely melted at 169°C (Figure 30 (BB)). In PAR:PLLA blends, at the ratio less than 20:80, when the PLLA ratio was increased, T_m of PAR was decreased (Figure 30 (E, J)). Dissolving of PAR in melted PLLA was observed at all ratios of PAR:PLLA blends. However, complete dissolving of PAR in the molten PLLA was detected in the PAR:PLLA blends at the ratios of 5:95 and 10:90 (Figure 30 (E, J)). PAR was partially dissolved in the molten PLLA in PAR:PLLA blends at the ratio of 20:80, 30:70 and 50:50 (Figure 30 (O, S, W)). As a result, PAR was miscible with molten PLLA in the blends at the ratio of 5:95 and 10:90, and partially miscible with molten PLLA in the blends at the ratio of 20:80, 30:70 and 50:50. After testing by HSM, the samples were cooled at an ambient temperature and white part on the glass slide was observed at all ratios of PAR:PLLA blends, indicating phase separation of PAR (Figure 31).

2.3 Differential scanning calorimetry

Table 10 Thermal properties of BZC:PLLA physical blends by DSC

Ratio of BZC:PLLA	T_g (°C)	Theoretical T_g (°C)	$T_{m,1}$ (°C)	$T_{m,3}$ (°C)	T_c (°C)
0:100	59.3±0.26[a]	59.3	151.7±0.55[a]	150.8±0.32[a]	-
5:95	51.0	50.5	92.6, 149.4	146.1	-
10:90	32.6	42.6	92.4, 141.0	134.5	-
20:80	27.6	28.8	90.0, 138.3	132.0	-
30:70	23.9	17.1	90.4, 136.4	129.3	-
50:50	-4.0	-1.3	90.0, *	79.0, 104.4	48.2[b]
100:0	-31.0[d]	-31.0	89.9	90.7	48.0[c]

[a]n=3, [b]detected during cooling of heat-cool-heat cycle, [c]determined during reheating of heat-cool-heat cycle, [d]from literature (62). *cannot be determined. $T_{m,1}$ is a melting temperature during heating of heat-cool-heat cycle. $T_{m,3}$ is a melting temperature during reheating of heat-cool-heat cycle. T_c excluded recrystallization of PLLA.

DSC thermograms of BZC:PLLA physical blends were shown in Figure 57 and 58 of Appendix. T_g, $T_{m,1}$ and $T_{m,3}$ of PLLA was detected at 59.3°C, 151.7°C and at 150.8°C, respectively. T_g of BZC could not be detected in this study due to recrystallization at 48.0°C during cooling step of heat-cool-heat cycle. Its T_g was reported at -31°C (62). $T_{m,1}$ and $T_{m,3}$ of BZC was found at 89.9°C and at 90.7°C, respectively. $T_{m,1}$ of PLLA was decreased as BZC content in the blends was increased. The $T_{m,1}$ of PLLA in BZC:PLLA blend at the ratio of 50:50 was not detected because PLLA began to melt after drug melting immediately.

Single T_gs and $T_{m,3}$s were detected between the values of BZC and PLLA for the BZC:PLLA blends at the ratio of 5:95, 10:90, 20:80 and 30:70. Although, in the blend at the ratio of 50:50, a single T_g was detected, two separated $T_{m,3}$s were also detected. This was attributed to the rubbery state of the system above the blend's T_g allowed recrystallization of BZC at 48.2°C. The single T_g and $T_{m,3}$ were generally decreased when the drug content was increased. Theoretical T_gs of the blends which were calculated by Gordon-Taylor equation were similar to T_gs measured by DSC.

Table 11 Thermal properties of IND:PLLA physical blends by DSC

Ratio of IND:PLLA	**T_g (°C)**	**Theoretical T_g (°C)**	**$T_{m,1}$ (°C)**	**$T_{m,3}$ (°C)**	**T_c (°C)**
0:100	59.3±0.26[a]	59.3	151.7±0.55[a]	150.8±0.32[a]	-
5:95	57.8	58.3	148.9	149.7	-
10:90	56.0	57.5	147	147.9	-
20:80	53.4	55.9	144.5, 160.5	-	-
30:70	51.9	54.5	144.8, 160.6	-	-
50:50	48.6	51.7	144.5, 160.9	-	-
100:0	45.5	45.5	161.8	-	-

[a]n=3. $T_{m,1}$ is a melting temperature during heating of heat-cool-heat cycle. $T_{m,3}$ is a melting temperature during reheating step of heat-cool-heat cycle. T_c excluded recrystallization of PLLA.

DSC thermograms of IND:PLLA physical blends were shown in Figure 59 and 60 of Appendix. T_g and $T_{m,1}$ of IND was detected at 45.5°C and 161.8°C, respectively. $T_{m,3}$ was not found due to that crystallization from amorphous did not occur (62). In IND:PLLA blends at the ratio of 20:80, 30:70 and 50:50, $T_{m,1}$s of PLLA and IND were lower than their own $T_{m,1}$. While, for IND:PLLA blends at the

ratio of 5:95 and 10:90, $T_{m,1}$ was detected as a single T_m which was decreased when the drug content was increased. As a result, the drug completely dissolved in the molten PLLA at the low drug to PLLA ratios.

The single T_g was detected between the T_g of IND and that of PLLA for IND:PLLA blends at the ratio of 5:95, 10:90, 20:80, 30:70 and 50:50. The single $T_{m,3}$ was also detected between the values of IND and PLLA for IND:PLLA blends at the ratio of 5:95 and 10:90, while absence of $T_{m,3}$ was found for IND:PLLA blends at the ratio of 20:80, 30:70 and 50:50. These results showed inhibition of PLLA from recrystallization by IND. The single T_g and $T_{m,3}$ was decreased when the drug content was increased. The T_g of blends observed from DSC was slightly lower than theoretical T_gs calculated by Gordon-Taylor equation. The negative deviation of T_g from theoretical T_g indicates that the drug-drug or polymer-polymer interaction is stronger than drug-polymer interaction (93).

Table 12 Thermal properties of PAR:PLLA physical blends by DSC

Ratio of PAR:PLLA	**T_g (°C)**	**Theoretical T_g (°C)**	**$T_{m,1}$ (°C)**	**$T_{m,3}$ (°C)**	**T_c (°C)**
0:100	59.3±0.26[a]	59.3	151.7±0.55[a]	150.8±0.32[a]	-
5:95	54.3	55.5	151.0, 170.3	148.0	-
10:90	49.0	51.9	149.2, 170.6	144.7, 153.4	114.2[b]
20:80	45.3	45.9	149.0, 170.3	144.6, 152.8	111.3[b]
30:70	22.3, 43.7	41.1	147.4, 170.0	143.9, 156.6	103.3[b]
50:50	24.5, 44.5	34.0	148.9, 170.0	145.4, 157.1	100.3[b]
100:0	23.8	23.8	169.6	158.4[c]	80.6[b]

[a]n=3, [b]determined during reheating of heat-cool-heat cycle and [c]polymorphic form conversion (from form I to form II). $T_{m,1}$ is a melting temperature during heating of heat-cool-heat cycle.

$T_{m,3}$ is a melting temperature during reheating of heat-cool-heat cycle. T_c excluded recrystallization of PLLA.

DSC thermograms of PAR:PLLA physical blends were shown in Figure 61 and 62 of Appendix. T_g, $T_{m,1}$ and $T_{m,3}$ of PAR were detected at 23.8°C, 169.6°C and at 158.4°C, respectively. The $T_{m,1}$ and $T_{m,3}$ were different due to conversion of crystalline form I (monoclinic) to form II (orthorhombic) (94). For PAR:PLLA blends at the ratios of 5:95, 10:90, 20:80, 30:70 and 50:50, $T_{m,1}$ of PLLA was lower than its $T_{m,1}$, but that of PAR was not changed.

The single T_g and $T_{m,3}$ were detected in PAR:PLLA blends at the ratio of 5:95 and the $T_{m,3}$ of this blend was lower than $T_{m,3}$s of PLLA and PAR. As a result, PAR was completely dissolved in the molten PLLA and the drug-polymer interaction was sufficient to inhibit recrystallization of PAR. After increasing the ratio of PAR:PLLA blends to 10:90 and 20:80, the single T_g was also found, while $T_{m,3}$ was found as two separated $T_{m,3}$s. In PAR:PLLA blends at the ratios of 30:70 and 50:50, two separated T_gs and $T_{m,3}$s were found. Overall, the single T_g was decreased as increasing the drug content and it was slightly lower than theoretical T_gs calculated by Gordon-Taylor equation. As above mentioned, the negative deviation of T_g from theoretical T_g indicates that the drug-drug or polymer-polymer interaction is stronger than drug-polymer interaction (93). The two separated $T_{m,3}$s were detected due to recrystallization of PAR during reheating step. The lower $T_{m,3}$ was lower than $T_{m,3}$ of PLLA and PAR. The higher $T_{m,3}$ was in the position between PLLA and PAR, and was increased as increasing the drug content. As a result, there was some PAR dissolved into PLLA and the rest remained crystalline. The T_c of PAR in the blends was decreased to T_c of PAR (pure PAR) as increasing the drug to polymer ratio.

The melting behaviors observed by HSM and the single T_gs of BZC:PLLA and IND:PLLA blends determined by DSC indicated miscibility between these drugs and PLLA. Reduction of T_m and absence of T_c in the case of BZC blends observed in the DSC results also suggested miscibility between the drug and PLLA.

The melting behaviors observed by HSM and the T_g, T_m and T_c values determined by DSC suggested that PAR was miscible with PLLA with a limited drug

content, i.e. low drug to polymer ratio (5:95) and partially (or likely to be immiscible) miscible with the PLLA with high drug content (10:90, 20:80, 30:70 and 50:50).

The miscibility of BZC:PLLA and IND:PLLA blends predicted by experimental results corresponded to the calculation results based on both approaches of GCM and MD simulation. The results demonstrated that BZC and IND were more likely to be miscible with the polymer. While, PAR tended to be partially miscible or immiscible with PLLA

The miscibility at all studied ratios of BZC:PLLA and IND:PLLA blends, and at the 5:95 ratio of PAR:PLLA blend predicted by thermal analysis also corresponded to the predictive results of χ_{FH} and ΔG_{mix}.

3. Miscibility evaluation between drug and polymer in extrudates

The miscibility between drug and polymer in an extrudate was evaluated through several properties, i.e. appearance, crystallinity and thermal properties (glass transition temperature (T_g) and melting temperature (T_m) as discussed *in the section 3.1-3.3*.

3.1 Hot melt extrusion

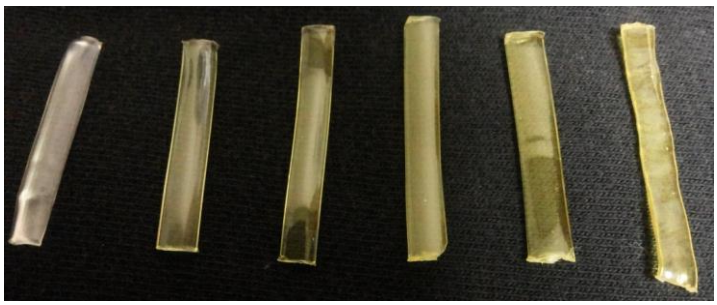

0 5 10 20 30 50

Proportions of IND

Figure 32 IND:PLLA extrudates at the ratios of 0:100, 5:95, 10:90, 20:80, 30:70 and 50:50

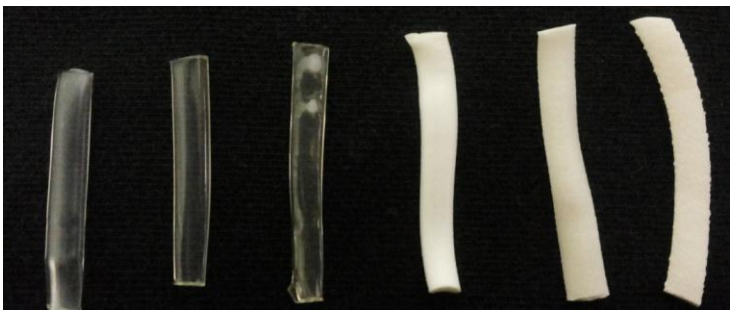

0 5 10 20 30 50

Proportions of PAR

Figure 33 PAR:PLLA extrudates at the ratios of 0:100, 5:95, 10:90, 20:80, 30:70 and 50:50

The extrudates (EX) of polymer and drug:polymer blends are shown in Figure 32 and 33. PLLA EX, IND:PLLA EX at the ratios of 5:95, 10:90, 20:80, 30:70 and 50:50 (Figure 32), and PAR:PLLA EX at the ratios of 5:95 and 10:90 (Figure 33) were transparent. PAR:PLLA EX at the ratios of 20:80, 30:70 and 50:50 were opaque. In fact, the PAR:PLLA EX at the ratio of 20:80 was transparent after extrusion but it turned to be opaque after cooling in an ambient temperature for 1-2 min.

3.2 X-ray powder diffractometry

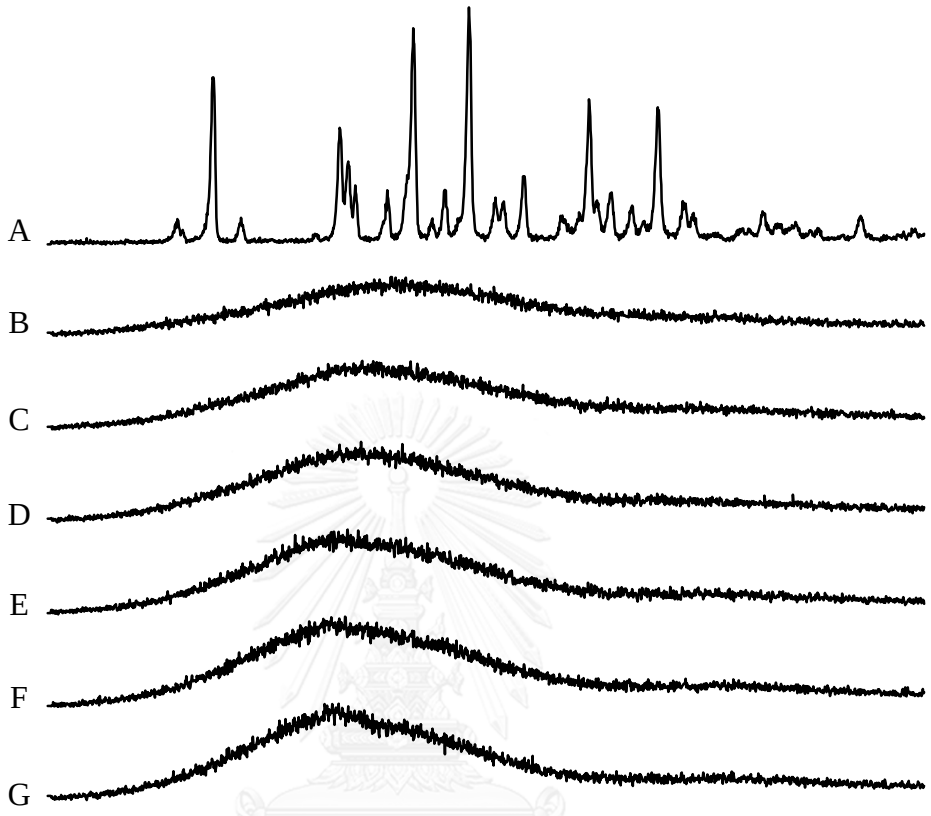

Figure 34 Crystallinity of IND:PLLA extrudates examined by XRPD. IND RM (A), IND:PLLA EX 50:50 (B), IND:PLLA EX 30:70 (C), IND:PLLA EX 20:80 (D), IND:PLLA EX 10:90 (E), IND:PLLA EX 5:95 (F) and PLLA EX (G).

An X-ray pattern of PLLA raw material (PLLA RM) has a peak at 16.7° due to its semi-crystalline form (Figure 63 (G) in Appendix) (90). X-ray patterns of indomethacin and PLLA physical mixture (IND:PLLA PM) at the ratios of 5:95, 10:90, 20:80, 30:70 and 50:50 (Figure 63 (B-F) in Appendix) were the same as the diffraction pattern of IND raw material (IND RM) of crystalline γ form (Figure 63 (A) in Appendix and Figure 34 (A)) (95). After extrusion, X-ray patterns of PLLA extrudate (PLLA EX) and that of blends' extrudate (IND:PLLA EX) at the ratios of 5:95, 10:90, 20:80, 30:70 and 50:50 showed halo pattern, indicating amorphous character in Figure 34 (B-G). The halo pattern was a result of dispersion of IND in

PLLA at molecular level rather than dispersion of amorphous IND. This was confirmed with the transparent of IND:PLLA EX at all ratios.

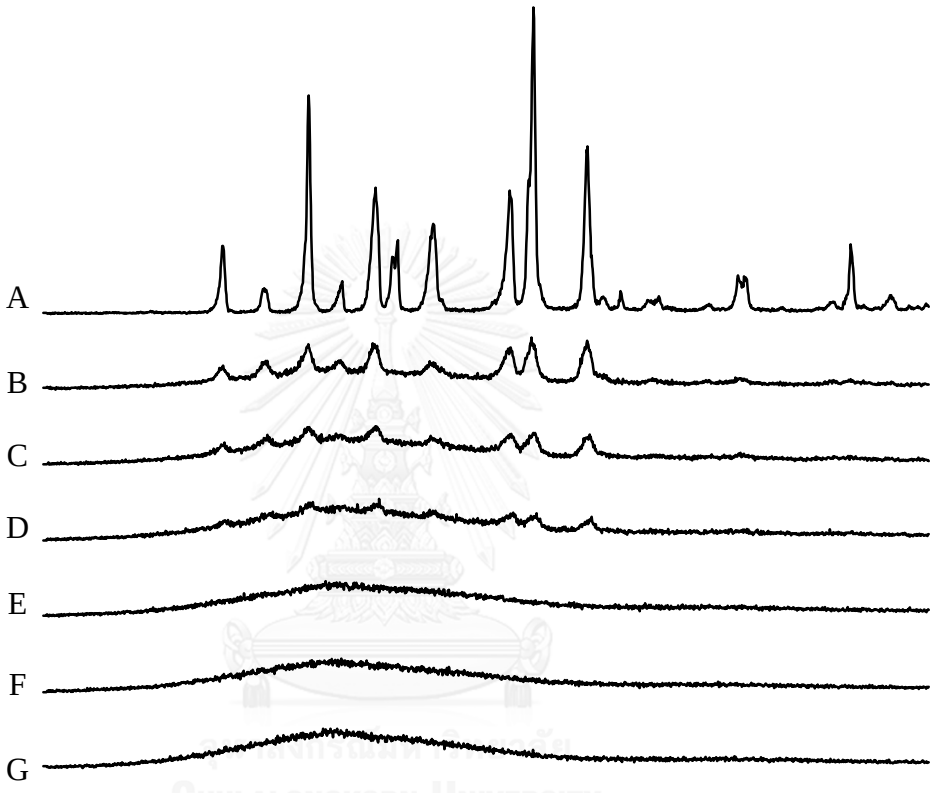

Figure 35 Crystallinity of PAR:PLLA extrudates examined by XRPD: PAR RM (A), PAR:PLLA EX 50:50 (B), PAR:PLLA EX 30:70 (C), PAR:PLLA EX 20:80 (D), PAR:PLLA EX 10:90 (E), PAR:PLLA EX 5:95 (F) and PLLA EX (G).

X-ray patterns of paracetamol and PLLA physical mixtures (PAR:PLLA PM) at the ratio of 5:95, 10:90 20:80, 30:70 and 50:50 as shown in Figure 64 (B-F) in Appendix are the same as the diffraction of paracetamol raw material (PAR RM) of crystalline form I (Figure 64 (A) in Appendix and Figure 35 (A)) (96). After extrusion, the X-ray patterns of paracetamol and PLLA blends' extrudate (PAR:PLLA EX) at the ratios of 5:95 and 10:90 were halo indicating amorphous state (Figure 35 (E, F)). These extrudates were transparent and thus, PAR was molecularly dispersed in the polymer. While, those of PAR:PLLA EX at the ratios of 20:80, 30:70 and

50:50 (Figure 35 (B, C, D)) were the same as diffraction patterns of PAR:PLLA PM, indicating the drug remained crystalline form resulting in opaque extrudates. The intensity of the diffraction peaks in these extrudates was increased when the drug content increased.

3.3 Differential scanning calorimetry

Table 13 Thermal properties of IND:PLLA extrudates determined by DSC

Ratio of IND:PLLA	**T_g (°C)**	**T_m (°C)**
0:100	60.9 / 58.4[a]	155.8 / 154.8[a]
5:95	59.4	153.8
10:90	58.5	151.9
20:80	52.4	146.6
30:70	50.6	142.1, 153.0
50:50	41.3	153.0, 158.7

[a]n=2

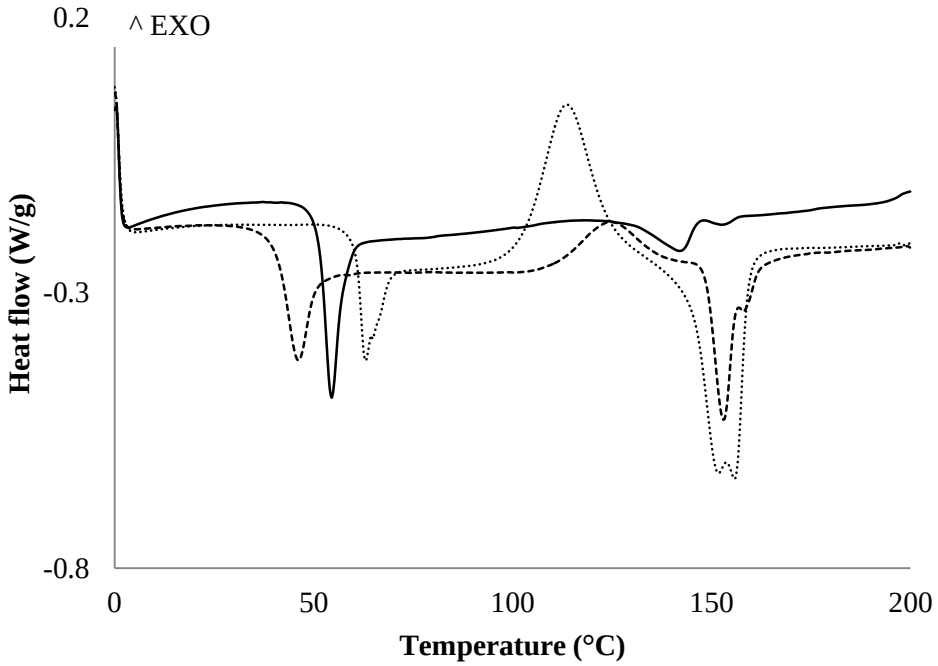

Figure 36 DSC thermogram of IND:PLLA extrudates at the ratios of 0:100 (dot line), 30:70 (black line) and 50:50 (dash line)

All DSC thermograms of IND:PLLA extrudates were shown in Figure 65 of Appendix. A T_g of PLLA EX was detected at 59.7°C. A T_m of PLLA EX was detected at 155.3°C. Recrystallization was observed in the extrudates at all ratios regardless of the type of drug. Single T_gs and T_ms of IND:PLLA EX at the ratios of 5:95, 10:90 and 20:80 were detected. At the ratios of 30:70 and 50:50, single T_gs were detected together with two separated T_m, indicating recrystallization of IND occurring in these IND:PLLA extrudates. The two separated T_m were increased as increasing the drug content.

This may be explained that at relatively high drug contents, drug molecules were rich in the polymeric matrix. Under DSC condition, the heat applied to the extrudates could induce the drug molecules to be highly mobile and hence rearrange themselves to form a crystal. However, T_c of IND cannot be detected in the DSC thermogram (black line and dash line in Figure 36) of these extrudates, possibly due to detection limit of DSC. It was also possible that recrystallization of IND may occur during recrystallization of PLLA. The recrystallization of PLLA could cause reduction in drug-polymer interaction. The drug-polymer interaction in the extrudate

was weaker than the drug-drug or polymer-polymer interactions as previously suggested by the negative deviation of the measured T_g from the theoretical T_g and results of RDF analysis which showed greater drug-drug interaction as increasing drug content.

The single T_gs were generally decreased as increasing the drug to polymer ratio, suggesting miscibility between the IND and PLLA, as predicted earlier by calculation and thermal properties of their physical blends.

Although separate T_ms were found in some extrudates with relatively high drug contents, IND:PLLA EX at all drug to polymer ratios were classified as miscible mixture because of evidences in single T_gs, together with X-ray halo pattern and transparent character of the extrudates at the ambient temperature after preparation.

Table 14 Thermal properties of PAR:PLLA extrudates determined by DSC

Ratio of PAR:PLLA	**T_g (°C)**	**T_m (°C)**
0:100	60.9 / 58.4[a]	155.8 / 154.8[a]
5:95	51.8	150.8
10:90	44.1	149.5
20:80	42.9, 56.9	149.6, 167.6
30:70	53.2	146.8, 170.3
50:50	56.2	146.7, 172.1

[a]n=2

DSC thermograms of PAR:PLLA extrudates were shown in Figure 66 of Appendix. Single T_gs and T_ms of PAR:PLLA EX at the ratios of 5:95 and 10:90 were

detected and they was decreased as increasing the drug content. At the ratio of 20:80, two separate T_gs was detected. However, single T_gs were again detected in the extrudates at the ratios of 30:70 and 50:50. They were close to the T_g of the PLLA EX; therefore, it was attributed to amorphous part of the polymer, rather than the amorphous drug. Two separated T_ms were detected in the extrudates at the ratios of 20:80, 30:70 and 50:50. The higher T_m could be due to T_m of a residue of crystalline PAR which was not dissolved in the molten PLLA during hot melt extrusion. The drug was almost immiscible with polymer and stayed as crystalline phase in the extrudates with relatively high drug contents. The lower T_m could be T_m of the blends, indicating that there was some drug dissolved into the polymer.

Accordingly, the results of T_g and T_m determination indicated that miscibility between PAR and PLLA occurred in the PAR:PLLA EX at the ratio of 5:95 and 10:90, and partial miscibility or immiscibility between the drug and polymer occurred in the PAR:PLLA EX at the ratios of 20:80, 30:70 and 50:50. This agreed with the prediction by calculation and thermal behavior of their physical blends. The results of RDF analysis also supported about the drug-polymer interaction that in the blend at the ratio of 5:95, drug-polymer interaction was higher than drug-drug interaction, and in the blends with higher drug contents, drug-polymer interaction was similar to drug-drug interaction.

All evidences, i.e. appearance, crystallinity, T_g and T_m of the extrudates, could classify the blends of IND:PLLA to be miscible at all studied ratios. They also confirmed that PAR:PLLA blends at the ratios of 5:95 and 10:90 were miscible and those at the ratios of 20:80, 30:70 and 50:50 were immiscible. The classification was similar to the prediction results of solubility parameter (δ) from MD simulation based on Greenhalgh et al.'s criteria (17) from which IND was suggested to be miscible with the polymer and PAR was suggested to be immiscible with the polymer. Although the prediction by Flory-Huggins interaction parameter (χ_{FH}) could not clearly classify miscibility of the IND:PLLA and PAR:PLLA blends, the values could suggest the effect of drug content and potential immiscibility between drug and polymer as increasing the drug content.

The trend of increased χ_{FH} values may beneficial in prediction of immiscible blends with some degree of dissolved drug in the polymer such as PAR: PLLA EX at the ratio 20:80, 30:60 and 50:50 which showed the lower T_m of the blends. For these blends, the χ_{FH} of higher than -3.3 were, therefore, found to an indicative value for immiscibility between drug and polymer.

The results of extrudates corresponded to the prediction results from HSM and DSC. They agreed that IND was miscible with PLLA at all studied ratios, while PAR was miscible with PLLA at a limited drug content. However, the maximum drug content which could be dissolved or miscible with the polymer was slightly different for the extrudate and the prediction results of DSC. All the results of the PAR:PLLA extrudate showed limited miscibility up to the ratio of 10:90, while the prediction results of DSC indicated miscibility up to the ratio of 5:95.

This may be explained that the cooling rate of heat-cool-heat cycle by DSC in prediction was different from the cooling rate of hot melt extrusion. As a result, the miscibility prediction by DSC could not accurately determine the limit of miscibility of the extrudate, but it could suggest borderline of miscibility.

3.4 Fourier transfers infrared spectroscopy

The miscibility or immiscibility between drug and polymer is involved with hydrogen bonding as mentioned *in the section 1.3*. In this section, the hydrogen bonding of drug-polymer, drug-drug or polymer-polymer molecules could be determined by Fourier transfer infrared spectroscopy (FTIR).

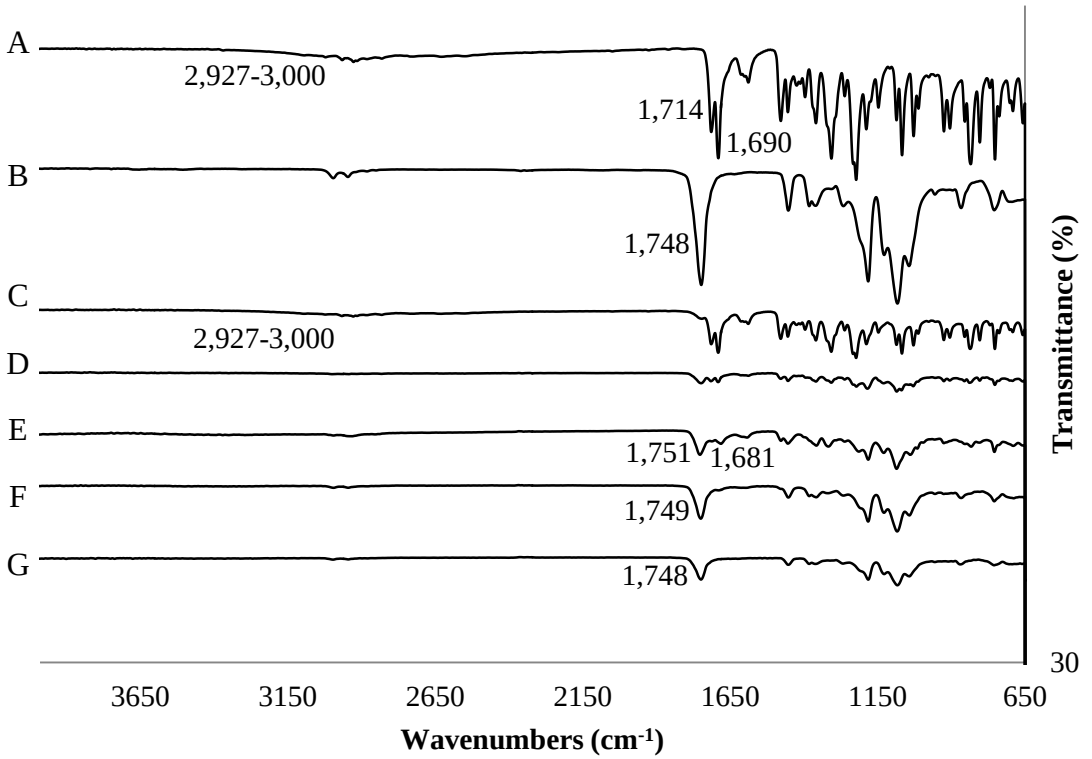

Figure 37 IR spectrum of IND:PLLA blends. IND RM (A), PLLA RM (B), IND:PLLA PM 50:50 (C), IND:PLLA PM 10:90 (D), IND:PLLA EX 50:50 (E), IND:PLLA EX 10:90 (F) and PLLA EX (G).

The functional groups of IND which can interact with other molecules by hydrogen bonding were hydroxyl (OH) in carboxylic acid (-COOH), carbonyl (C=O) in –COOH, and carbonyl (C=O) between indole and chlorobenzyl groups (81). IR absorption bands of these groups were in the range of 3,371 and 2,900-3,400 cm^{-1} for OH in -COOH, at 1,718 cm^{-1} for C=O in –COOH, and at 1,693 cm^{-1} for the other C=O. IR absorption bands of C=C aromatics was in the range of 1,625-1,575 and 1,480 cm^{-1} and C-Cl was at 1,068 cm^{-1} (97).

The functional group of PLLA which can interact with other molecules by hydrogen bonding was carbonyl (C=O) in esters (70). The IR absorption band of C=O was detected in the range of 1,757-1,758 cm^{-1}. Other bands was detected at 2,755 and 2,767 cm^{-1} for CH of methyl group ($-CH_3$). The absorption band of OH groups was approximate 3,000 cm^{-1} which can be detected obviously in the monomers and the band was decreased after polymerization (91).

In IR spectrum of IND:PLLA PM (Figure 37 (C, D)), the absorption bands were not different from the bands of IND RM and PLLA RM. Intensity of the IND bands was increased as increasing the drug content in the physical mixtures. In IR spectrum of PLLA EX (Figure 37 (G)), the band of C=O and CH of $-CH_3$ were not different from the band in PLLA RM. In IR spectrum of IND:PLLA EX (Figure 37 (E, F)), the band of $C=O_{PLLA}$ shifted from 1,748 to 1,749 cm^{-1} and 1,751 cm^{-1} at the drug to polymer ratios of 10:90 and 50:50, respectively. The band of CH_{PLLA} of $-CH_3$ in IND:PLLA EX's spectra was not different from the spectra of PLLA RM, PLLA EX and IND:PLLA PM.

The bands of OH_{IND} and $C=O_{IND}$ in -COOH group in the range of 2,927-3,000 cm^{-1} (for OH), and at 1,714 cm^{-1} (for C=O) in IND RM and IND:PLLA PM were not detected in extrudates. The band of $C=O_{IND}$ between indole and chlorobenzyl groups at 1,690 cm^{-1} in IND RM and IND:PLLA PM was shifted to 1,684 cm^{-1} in IND:PLLA EX at the ratio of 30:70, and to 1,681 cm^{-1} in IND:PLLA EX at the ratio of 50:50. The $C=C_{IND}$ of aromatics at 1,588 cm^{-1} in IND RM and IND:PLLA PM was shifted to 1,593 cm^{-1} in the extrudates. $C-Cl_{IND}$ band was difficult to detect in IR spectra of extrudates, while the $C-Cl_{IND}$ band in IND RM and IND:PLLA PM was obviously detected at 1,067 cm^{-1}.

These IR results confirmed the presence of drug-polymer interaction in the IND:PLLA extrudates. The functional groups involved with hydrogen bonding between IND and PLLA from IR spectrum were $C=O_{PLLA}$, OH_{IND} and $C=O_{IND}$ of carboxylic group, and $C=O_{IND}$ between indole and chlorobenzyl groups; and this agreed with the results from RDF analysis. The drug-polymer interaction from IR was also confirmed by the appearance IND:PLLA extrudates which was transparent, halo pattern from XRPD and single T_gs of the extrudates by DSC at all studied ratios.

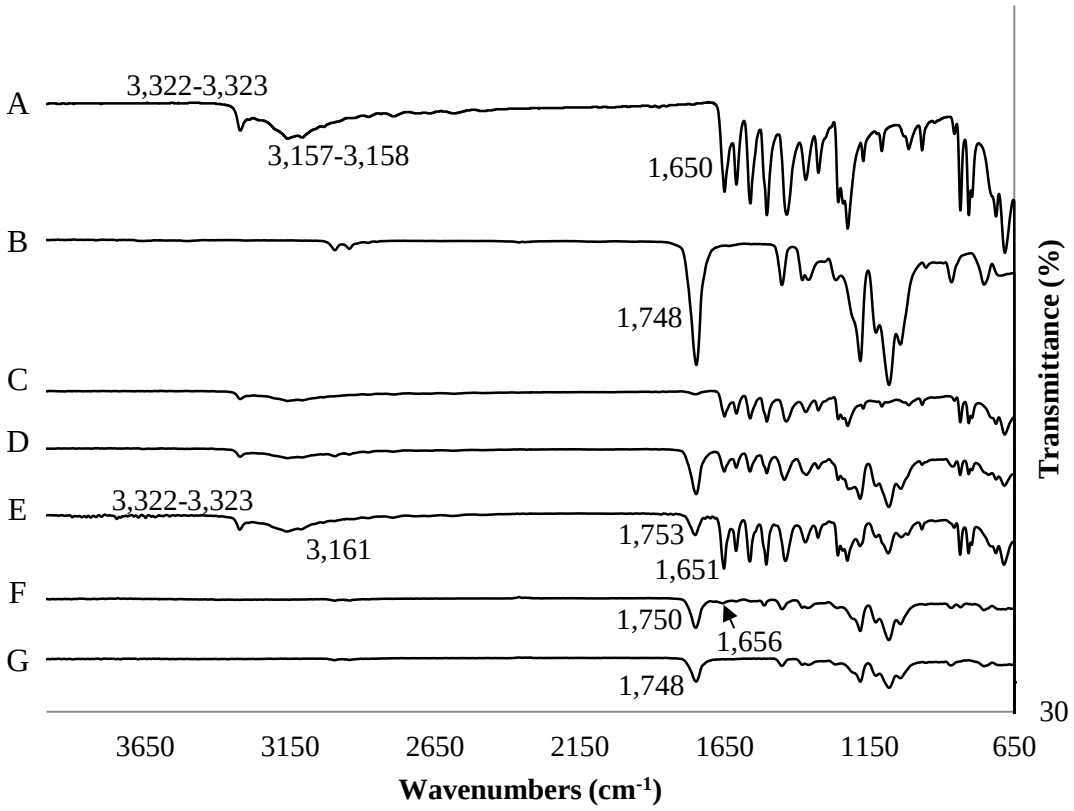

Figure 38 IR spectrum of PAR:PLLA blends. PAR RM (A), PLLA RM (B), PAR:PLLA PM 50:50 (C), PAR:PLLA PM 10:90 (D), PAR:PLLA EX 50:50 (E), PAR:PLLA EX 10:90 (F) and PLLA EX (G).

The functional groups of PAR which can interact with other molecules by hydrogen bonding were NH and C=O in amide group (–CONH), and OH in phenolic group (82). For monoclinic crystalline form (form I) of PAR, IR absorption bands of these groups were at 3,327 cm^{-1} for NH in -CONH, at 1,653 cm^{-1} for C=O in -CONH, and at 3,161 cm^{-1} for OH in phenolic group. IR absorption bands of phenyl ring was in the range of 1,371-1,610 cm^{-1} (97). The functional group of PLLA which can interact with other molecules by hydrogen bonding was C=O in esters (70). The IR absorption bands of PLLA's functional group was same as described earlier in part of IND:PLLA EX (91).

In IR spectra of PAR:PLLA PMs (Figure 38 (C, D)), the absorption bands were not different from the bands of PAR RM and PLLA RM. Intensity of the PAR bands was increased as increasing the drug content in the physical mixtures.

In IR spectrum of PLLA EX (Figure 38 (G)), the band of C=O and CH of -CH_3 were not different from the band in PLLA RM. In IR spectrum of PAR:PLLA EX (Figure 38 (E, F)), the band of $C=O_{PLLA}$ was shifted from 1,748 to 1,750 cm^{-1} in PAR:PLLA EX at the ratio of 10:90 and to 1,753 cm^{-1} in PAR:PLLA EX at the ratio of 50:50. The band of CH_{PLLA} of -CH_3 in 5:95 and 10:90 PAR:PLLA EX spectra was not different from PLLA RM and PLLA EX; and it cannot be detected in the spectrum of 20:80, 30:70 and 50:50 PAR:PLLA EX due to interference of NH and OH bands of PAR.

The band of NH_{PAR} in the range of 3,322-3,323 cm^{-1} in PAR RM and PAR:PLLA PM was not found in 5:95 and 10:90 PAR:PLLA EX. However, it was detected in 20:80, 30:70 and 50:50 PAR:PLLA EX at the same position as the PAR RM's. Also, the band of OH_{PAR} in the range of 3,157-3,158 cm^{-1} was not found in 5:95 and 10:90 PAR:PLLA EX; but it was detected in 20:80 PAR:PLLA EX at 3,162 cm^{-1}, in 30:70 PAR:PLLA EX at 3,159 cm^{-1}, and in 50:50 PAR:PLLA EX at 3,161 cm^{-1}. The band of $C=O_{PAR}$ in the range of 1,650-1,651 cm^{-1} in PAR RM and PAR:PLLA PM was not found in PAR:PLLA EX at the ratio of 5:95. However, it was detected in 10:90 PAR:PLLA EX at 1,656 cm^{-1}, in 20:80 PAR:PLLA EX at 1,653 cm^{-1}, in 30:70 PAR:PLLA EX at 1,652 cm^{-1}, and in 50:50 PAR:PLLA EX at 1,651 cm^{-1}. The band of phenyl ring of PAR in the range of 1,370-1,610 cm^{-1} in 20:80, 30:70 and 50:50 PAR:PLLA EX were same as the bands in 20:80, 30:70 and 50:50 PAR:PLLA PMs. While, this band in 5:95 and 10:90 PAR:PLLA EX was slightly different from the band in 5:95 and 10:90 PAR:PLLA PMs.

These IR results confirmed the existing drug-polymer interaction in the PAR:PLLA extrudates at the ratios of 5:95 and 10:90. The interaction was attributed to drug-polymer miscibility in the extrudates which were transparent and had halo pattern from XRPD and single T_g from DSC. Hydrogen bonding between $C=O_{PLLA}$ in PLLA and NH_{PAR} and $C=O_{PAR}$ of amide group, also OH_{PAR} in phenolic group in PAR was dominant in these extrudates. This agreed with the results from RDF analysis. In 20:80, 30:70 and 50:50 PAR:PLLA extrudates, amide group of PAR and OH_{PAR} did not much contribute to drug-polymer interaction. Opaque PAR:PLLA extrudates

were obtained because the drug content was higher than a saturated solubility in the solid polymer, resulting in precipitation as crystalline of PAR.

4. Mechanical properties of extrudates

The drugs which were miscible with polymer, i.e. IND (in the blends at all drug to polymer ratio) and PAR (in the blends with low drug content) were evaluated for the plasticizing effect for the model drugs as shown in Table 15.

Table 15 Mechanical properties of the extrudates (n=5)

	σ (MPa)	**e (%)**	***E* (MPa)**
PLLA	50.03±2.82	82.45±13.90	104.77±7.13
IND:PLLA			
5:95	49.74±0.97	67.40±10.32	104.58±11.52
10:90	49.70±1.11	55.77±6.89	113.75±2.99
20:80	49.26±0.86	49.66±4.35	116.32±3.42
30:70	47.40±0.85	45.31±8.27	119.02±7.15
50:50	12.67±0.99	18.35±5.77	140.00±13.92
PAR:PLLA			
5:95	47.20±0.99	74.51±13.85	93.46±9.70
10:90	47.03±1.88	72.48±10.85	98.65±10.30
20:80	22.16±4.75	31.54±5.35	100.17±5.33
30:70	22.05±1.01	26.79±1.97	104.07±11.97
50:50	12.42±0.72	25.23±1.93	77.43±11.82

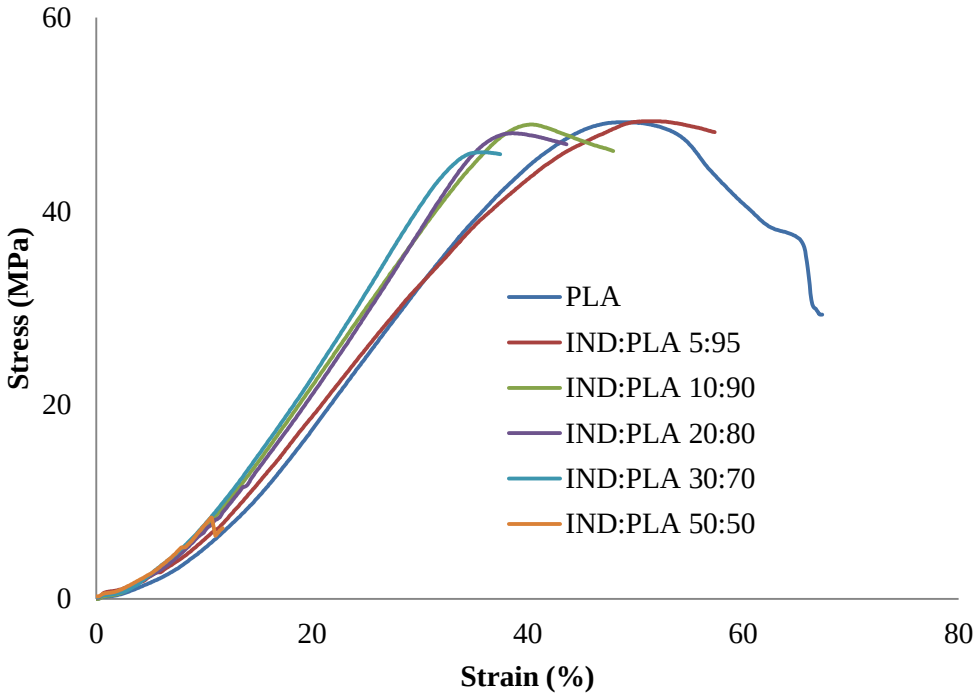

Figure 39 Stress-strain curve of IND:PLLA extrudates

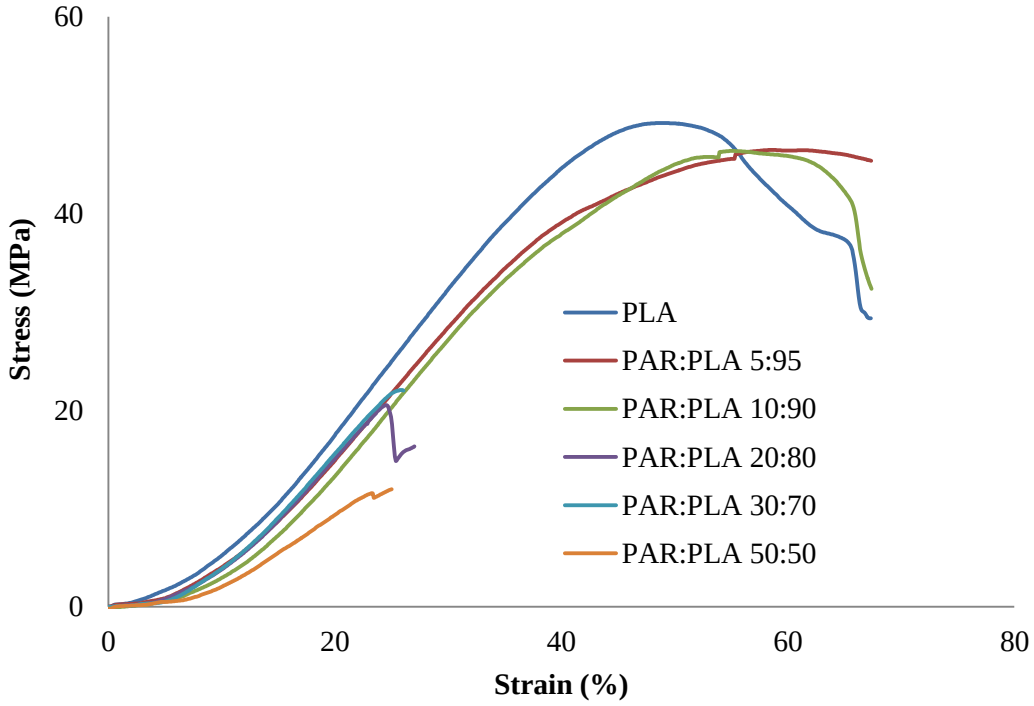

Figure 40 Stress-strain curve of PAR:PLLA extrudates

The value of tensile strength or stress (σ) represented force resistance of the extrudate which corresponded to hardness or strength of the extrudate. The value of elongation or strain (e) represented a stretching capacity of the extrudate before breaking. The value of Young's modulus (*E*) represented an elasticity of the extrudate, indicating a behavior of the extrudate under the force during elastic deformation. The elastic deformation is a type of deformation which can be reversible (60).

For IND:PLLA extrudates, σ and e values were decreased as increasing drug content, especially at the ratio of 50:50, where they were markedly decreased. But the *E* value was increased as increasing the drug to polymer ratios, especially at the ratio of 50:50 where it was obviously increased. This suggested that the force required for stretching of the extrudates with high drug content was higher than that of the extrudates with relatively low drug content. As a result, the IND:PLLA extrudates with higher drug contents were more brittle and less strong.

Although IND was classified to be miscible with PLLA according to the existence of single T_gs at all drug to polymer ratios, IND could not effectively plasticize PLLA. This was reflected in a minor decrease in the T_g of extrudates at the ratios of 5:95 up to 30:70. At the ratio of 50:50, although a marked decrease in the single T_g was observed, σ and e of this extrudate was considerably decreased and *E* was markedly increased.

Likewise, σ and e values of PAR:PLLA extrudates were decreased as increasing drug content. The values were markedly decreased at the ratios of 20:80 up to 50:50 where PAR was immiscible with PLLA in the extrudate. The *E* value was also increased as increasing the drug to polymer ratio from 5:95 to 30:70. However, markedly decrease was found at the ratio of 50:50. Similar to the IND:PLLA extrudates, the PAR:PLLA extrudates with high drug contents were more brittle and less strong. In addition, PAR could not plasticize the polymer, although it was miscible with PLLA in the extrudate at low drug contents.

CHAPTER 5
CONCLUSIONS

Miscibility between the model drugs, i.e. benzocaine, indomethacin, paracetamol and semi-crystalline polymer having L and D forms, i.e. polylactide could be predicted by calculation and experimental methods.

- Criterion of Greenhalgh et al. (17) was simply useful in miscibility classification based on the solubility parameters which were calculated by molecular dynamics simulation. However, "immiscibility" here was proved that the drug could be miscible with the polymer at a limited content such as 10:90 in the extrudate of paracetamol and polylactide. Although the value of Flory-Huggins interaction paramater (χ_{FH}), comparing with the critical parameter (χ_c) of the polymer, was less sensitive for miscibility classification, it suggested that an increase in the drug content would lead to phase separation or immiscibility as the χ_{FH} was increased towards χ_c. In addition, a relatively high value of χ_{FH} of paracetamol and poly-l-lactide or poly-d-lactide at any drug content which was close to χ_c could imply immiscibility.
- Miscibility prediction by thermal behaviors such as a decrease in the melting temperature (T_m) of the component and a presence of single glass transition temperature (T_g) between T_gs of the drug and polymer, was more indicative than the calculation method, pointing out the drug to polymer ratio where they were miscible.
- The prediction corresponded with the drug-polymer miscibility results of the extrudate. Indomethacin was miscible with polylactide up to the ratio of 50:50. While, paracetamol could be miscible with the polymer at the maximum ratio of 10:90.

The mechanical properties of the indomethacin and paracetamol extrudates in terms of tensile strength and elongation were decreased, while Young's modulus was increased, indicating an increase in brittleness, as increasing the drug content. In

other words, the extrudate was less brittle at relatively low drug content where the drug was miscible with the polymer. However, there was no noticeable relationship between miscibility in the extrudate and the mechanical properties. Also, indomethacin and paracetamol could not plasticize polylactide.

Benzocaine was excluded from the mechanical test because it could not be hot melt extruded at the processing temperature.

Radial distribution function (RDF) could explain miscibility between drug and the polymer, in particular L-form. It showed that hydrogen bonding between drug-polymer, drug-drug and polymer-polymer was found in the blends. Density of drug-polymer interaction was higher than that of drug-drug or polymer-polymer in the miscible blends with the low drug contents, such as the blends of indomethacin and poly-l-lactide at 5:95, 10:90 and 20:80, also the blends of paracetamol and poly-l-lactide at 5:95. As increasing drug content, density of drug-drug interaction was greater than drug-polymer interaction, inducing crystallization of the drug. This could explain the existence of two separated T_m of separated phases in the extrudate at the high drug contents. The results agreed with the shift in the IR spectra of the functional groups' taken into RDF calculation.

It is noted that the outcome of this study was based on the maximum drug to polymer ratio at 50:50. Correlation of the predictive miscibility between the drug and D-form of polylactide and the miscibility in the extrudate was rarely established. This because the polymer used in hot melt extrusion was rich in L-form. In addition, extension of molecular dynamics simulation time is required to obtain more information to explain the unstable phenomena found in the drug and D-form of polylactide blends.

REFERENCES

1. Vasanthavada M, Tong WQ, Serajuddin ATM. Development of solid dispersion for poorly water-soluble drugs. In: Liu R, editor. Water-insoluble drug formulation. 2 ed. New York: Taylor & Francis Group; 2008. p. 500-529.
2. Tran PL, Tran TD, Park JB, Lee BJ. Controlled release systems containing solid dispersions: strategies and mechanisms. Pharmaceutical Research. 2011;28(10):2353-2378.
3. Labarre D. Introduction: why study polymers for the health sciences? In: Labarre D, Ponchel G, Vauthier C, editors. Biomedical and Pharmaceutical Polymers. 1 ed. London: Pharmaceutical Press; 2011. p. 92-148.
4. Dhawan S, Varma M, Sinha VR. High molecular weight poly(ethylene oxide)–based drug delivery systems part I: hydrogels and hydrophilic matrix systems [Online]. Pharmaceutical Technology; 2005 [2015, 2 July]. Available from: http://images.alfresco.advanstar.com/alfresco_images/pharma/2014/08/22/51527393-3f8e-49b8-bb69-772daba5dc0a/article-160393.pdf.
5. Sarika Madan, Madan S. Hot melt extrusion and its pharmaceutical applications. Asian Journal of Pharmaceutical Sciences. 2012;7(2):123-133.
6. Serajuddin ATM. Solid dispersion of poorly water-soluble drugs: Early promises, subsequent problems, and recent breakthroughs. Journal of Pharmaceutical Sciences. 1999;88(10):1058-1066.
7. Shah S, Repka MA. Melt extrusion in drug delivery: three decades of progress. In: Repka MA, Langley N, DiNunzio J, editors. Melt Extrusion. New York: Springer-Verlag 2013. p. 3-46.
8. Dhawan S, Dhawan K, Varma M, Sinha VR. Applications of poly(ethylene oxide) in drug delivery systems part II [Online]. Pharmaceutical Technology; 2005 [2015, 2 July]. Available from: http://images.alfresco.advanstar.com/alfresco_images/pharma/2014/08/22/678845a2-b24c-4c47-bc3a-e711da795690/article-178636.pdf.

9. Pooponpun S. The mechanical and adhesion properties of film coats of cellulose derivatives containing some selected solid additives [Master's thesis]. Bangkok: Mahidol University; 2005.
10. Snejdrova E, Dittrich M. Pharmaceutical applications of plasticized polymers. In: Luqman M, editor. Recent Advances in Plasticizers. Rijeka: InTech; 2012. p. 69-90.
11. Jacobsen S, Fritz HG. Plasticizing polylactide—the effect of different plasticizers on the mechanical properties. Polymer Engineering & Science. 1999;39(7):1303-1310.
12. Sungsanit K, Kao N, Bhattacharya SN. Properties of linear poly(lactic acid)/polyethylene glycol blends. Polymer Engineering & Science. 2012;52(1):108-116.
13. Qussi B, Suess WG. The influence of different plasticizers and polymers on the mechanical and thermal properties, porosity and drug permeability of free shellac films. Drug Development and Industrial Pharmacy. 2006;32(4):403-412.
14. Zivanovic S, Li J, Davidson PM, Kit K. Physical, mechanical, and antibacterial properties of chitosan/PEO blend films. Biomacromolecules. 2007;8(5):1505-1510.
15. Maekawa M, Pearce R, Marchessault RH, Manley RSJ. Miscibility and tensile properties of poly (β-hydroxybutyrate)–cellulose propionate blends. Polymer. 1999;40(6):1501-1505.
16. Forster A, Hempenstall J, Tucker I, Rades T. Selection of excipients for melt extrusion with two poorly water-soluble drugs by solubility parameter calculation and thermal analysis. International Journal of Pharmaceutics. 2001;226:147-161.
17. Greenhalgh DJ, Williams AC, Timmins P, York P. Solubility parameters as predictors of miscibility in solid dispersions. Journal of Pharmaceutical Sciences. 1999;88(11):1183-1190.
18. Gupta J, Nunes C, Vyas S, Jonnalagadda S. Prediction of solubility parameters and miscibility of pharmaceutical compounds by molecular dynamics simulations. The Journal of Physical Chemistry. 2011;115:2014-2023.

19. Maus M, Wagner KG, Kornherr A, Zifferere G. Molecular dynamics simulations for drug dosage form development: thermal and solubility characteristics for hot melt extrusion. Molecular simulation. 2008;34:1197-1207.
20. Wu C, McGinity JW. Non-traditional plasticization of polymeric films. International Journal of Pharmaceutics. 1999;177(1):15-27.
21. Repka MA, Gerding TG, Repka SL, McGinity JW. Influence of plasticizers and drugs on the physical-mechanical properties of hydroxypropylcellulose films prepared by hot melt extrusion. Drug Development and Industrial Pharmacy. 1999;25(5):625-633.
22. Win LC, Riegelman S. Pharmaceutical applications of solid dispersion systems. Journal of Pharmaceutical Sciences. 1971;60(9):1281-1302.
23. Singh S, Singh Baghel R, Yadav L. A review on solid dispersion. International Journal of Pharmacy & Life Sciences. 2011;2(9):1078-1095.
24. Jorg B, Markus M. Melt-extruded molecular dispersions. In: Ghebre-Selassie I, Martin C, editors. Pharmaceutical Extrusion Technology. Drugs and the Pharmaceutical Sciences. New York: CRC Press; 2003. p. 222-238.
25. Breitenbach J. Melt extrusion: from process to drug delivery technology. European Journal of Pharmaceutics and Biopharmaceutics. 2002;54(2):107-117.
26. Repka MA, Shah S, Lu J, Maddineni S, Morott J, Patwardhan K, et al. Melt extrusion: process to product. Expert Opinion on Drug Delivery. 2012;9(1):105-125.
27. Shah S, Maddineni S, Lu J, Repka MA. Melt extrusion with poorly soluble drugs. International Journal of Pharmaceutics. 2013;453(1):233-252.
28. Shah A, Gupta M, editors. Comparison of the flow in co-rotating and counter-rotating twins screw extruders. ANTEC 2004; 2004; Chicago: Brookfield, Conn.
29. DiNunzio JC, Miller DA. Formulation development of amorphous solid dispersions prepared by melt extrusion. In: Repka MA, Langley N, DiNunzio J, editors. Melt Extrusion. New York: Springer-Verlag; 2013. p. 161-204.

30. Martin C. Twin screw extrusion for pharmaceutical processes. In: Michael A. Repka, Nigel Langley, DiNunzio J, editors. Melt Extrusion. New York: Springer-Verlag; 2013. p. 47-79.
31. Nakamichi K, Nakano T, Yasuura H, Izumi S, Kawashima Y. The role of the kneading paddle and the effects of screw revolution speed and water content on the preparation of solid dispersions using a twin-screw extruder. International Journal of Pharmaceutics. 2002;241(2):203-211.
32. David DJ, Misra A. Cohesive properties and solubility parameter concepts. In: David DJ, Misra A, editors. Relating Materials Properties to Structure with MATPROP Software. New York: CRC Press; 2001. p. 287-304.
33. Krevelen DWV, Nijenhuis KT. Cohesive properties and solubility. In: Van Krevelen DW, Nijenhuis KT, editors. Properties of Polymers. 4 ed. Amsterdam: Elsevier; 2009. p. 189-227.
34. Allan BFM. Handbook of solubility parameters and other cohesion parameters 2ed. London: CRC Press; 1991.
35. Bicerano J. Cohesive energy and solubility parameter. In: Bicerano J, editor. Prediction of Polymer Properties. Plastics Engineering. 3 ed. New York: CRC Press; 2002.
36. Choi P, Kavassalis TA, Rudin A. Estimation of Hansen solubility parameters for (hydroxyethyl) and (hydroxypropyl) cellulose through molecular simulation. Industrial & Engineering Chemistry Research. 1994;33(12):3154-3159.
37. Patel S, Lavasanifar A, Choi P. Application of molecular dynamics simulation to predict the compatability between water-insoluble drugs and self-associating poly(ethylene oxide)-b-poly(ε-caprolactone) block copolymers. Biomacromolecules. 2008;9:3014–3023.
38. Timko RJ, Lordi NG. Thermal analysis studies of glass dispersion systems. Drug Development and Industrial Pharmacy. 1984;10(3):425-451.
39. Arenaza IMd, Meaurio E, Coto B, Sarasua J-R. Molecular dynamics modelling for the analysis and prediction of miscibility in polylactide/polyvinilphenol blends. Polymer. 2010;51:4431-4438.

40. Fu Y, Liao L, Yang L, Lan Y, Mei L, Liu Y, et al. Molecular dynamics and dissipative particle dynamics simulations for prediction of miscibility in polyethylene terephthalate/polylactide blends. Molecular simulation. 2012:1-8.
41. Huynh L, Grant J, Leroux J-C, Delmas P, Allen C. Predicting the solubility of the anti-cancer agent docetaxel in small molecule excipients using computational Methods. Pharmaceutical Research. 2008;25(1):147-157.
42. Rubinstein M, Colby RH. Thermodynamics of mixing. In: Rubinstein M, Colby RH, editors. Polymer Physics. 1 ed. New York: Oxford University Press; 2003.
43. Andersen B. Investigations on environmental stress cracking resistance of LDPE/EVA blends [Doctoral thesis]. Germany: University of Halle Wittenberg; 2004.
44. Robeson LM. Fundamentals of polymer blends. In: Robeson LM, editor. Polymer Blends A Comprehensive Review. München: Carl Hanser Verlag; 2007. p. 11-23.
45. Moolman FS, Meunier M, Labuschagne PW, Truter PA. Compatibility of polyvinyl alcohol and poly(methyl vinyl ether-co-maleic acid) blends estimated by molecular dynamics. Polymer. 2005;46(16):6192-6200.
46. Tian Y, Booth J, Meehan E, Jones DS, Li S, Andrews GP. Construction of drug–polymer thermodynamic phase diagrams using Flory–Huggins interaction theory: identifying the relevance of temperature and drug weight fraction to phase separation within solid dispersions. MOLECULAR PHARMACEUTICS. 2012;10(1):236-248.
47. Rakkapao N. Structure and properties of chitosan-based nanocomposite and blend: for drug controlled release and solid polymer electrolyte applications [Doctoral thesis]. Nakhon Ratchasima: Suranaree University of Technology; 2010.
48. Hansen CM. Solubility parameters - an introduction. In: Hansen CM, editor. Hansen Solubility Parameters. 2 ed. New York: CRC Press; 2007. p. 1-26.
49. Zhao Y, Inbar P, Chokshi HP, Malick AW, Choi DS. Prediction of the thermal phase diagram of amorphous solid dispersions by flory–huggins theory. Journal of Pharmaceutical Sciences. 2011;100(8):3196-3207.

50. Marsac P, Shamblin S, Taylor L. Theoretical and practical approaches for prediction of drug–polymer miscibility and solubility. Pharmaceutical Research. 2006;23(10):2417-2426.
51. Fermeglia M, Pricl S. Multiscale molecular modelling of dispersion of nanoparticles in polymer systems of industrial interest IUTAM symposium on modelling nanomaterials and nanosystems. Dordrecht: Springer Netherlands; 2009. 261-270 p.
52. Hinchliffe A. Molecular modelling for beginners. West Sussex: John Wiley & Sons Ltd.; 2003.
53. Molecular modeling and simulation [Online]. [2013, 10 February]. Available from: http://www.weizmann.ac.il/sb/Pages/Levy/group_meet/Molecular_dynamics_simulation.pdf.
54. Lindahl E. Molecular dynamics simulations. In: Kukol A, editor. Molecular Modeling of Proteins. Methods Molecular Biology™. 443. Clifton: Humana Press; 2008. p. 3-23.
55. Allen MP. Introduction to molecular dynamics simulation [Online]. 2004 [2015, 2 July]. Available from: http://wwwabi.snv.jussieu.fr/jompo/Public/PSF/IntroductionMolecularDynamics.pdf.
56. Guvench O, MacKerell A. Comparison of protein force fields for molecular dynamics simulations. In: Kukol A, editor. Molecular Modeling of Proteins. Methods Molecular Biology™. 443. Clifton: Humana Press; 2008. p. 63-88.
57. Cohen NC. Guidebook on molecular modeling in drug design. San Diego: Academic Press; 1996.
58. Sun H. COMPASS: an ab initio force-field optimized for condensed-phase applications overview with details on alkane and benzene compounds. The Journal of Physical Chemistry B. 1998;102(38):7338-7364.
59. Forcefield-based simulations [Online]. Structural Biology Computational Laboratory at School of Environmental and Biological Sciences of Rutgers University; 1997 [2013, 10 February]. Available from: http://benedick.rutgers.edu/software-manuals/forcefield.pdf.

60. Pelleg J. Mechanical testing of materials. Mechanical Properties of Materials. Solid Mechanics and Its Applications. 190. Dordrecht: Springer Netherlands; 2013. p. 1-84.
61. Roylance D. Uniaxial mechanical response. In: Roylance D, editor. Mechanical Properties of Materials. Massachusetts: MIT; 2008.
62. Baird JA, Van Eerdenbrugh B, Taylor LS. A classification system to assess the crystallization tendency of organic molecules from undercooled melts. Journal of Pharmaceutical Sciences. 2010;99(9):3787-3806.
63. Peña MA, Reíllo A, Escalera B, Bustamante P. Solubility parameter of drugs for predicting the solubility profile type within a wide polarity range in solvent mixtures. International Journal of Pharmaceutics. 2006;321(1–2):155-161.
64. Ahumada EA, Delgado DR, Martínez F. Solubility of acetaminophen in polyethylene glycol400 + water mixtures according to the extended Hildebrand. Revista Colombiana de Química. 2012;41:433-477.
65. Dr. C. Mauli Agrawal, Gabriele G. Niederauer, Athanasiou KA. Fabrication and characterization of PLA-PGA orthopedic implants. Tissue Engineering. 1995;1(3):241-252.
66. Nair LS, Laurencin CT. Biodegradable polymers as biomaterials. Progress in Polymer Science. 2007;32(8–9):762-798.
67. Engelberg I, Kohn J. Physico-mechanical properties of degradable polymers used in medical applications: A comparative study. Biomaterials. 1991;12(3):292-304.
68. David EH, Patrick G, Jim L, Jed R. Polylactic acid technology. In: Mohanty AK, Misra M, Drzal LT, editors. Natural Fibers, Biopolymers, and Biocomposites. New York: CRC Press; 2005.
69. Rowe RC, Sheskey PJ, Quinn ME. Handbook of Pharmaceutical Excipients. 6 ed. London: Pharmaceutical Press; 2009.
70. Lin Y, Zhang KY, Dong ZM, Dong LS, Li YS. Study of hydrogen-bonded blend of polylactide with biodegradable hyperbranched poly(ester amide). Macromolecules. 2007;40(17):6257-6267.
71. SureMed. TIGR matrix surgical mesh [Online]. [2015, 18 May]. Available from: http://suremed.co.th/product.html.

72. Covidien. Caprosyn sugure [Online]. 2015 [2015, 18 May]. Available from: http://www.covidien.com/imageServer.aspx?contentID=14349&contenttype=application/pdf.
73. Covidien. Polysorb sugure [Online]. 2015 [2015, 18 May]. Available from: http://www.covidien.com/imageServer.aspx?contentID=14357&contenttype=application/pdf.
74. Russias J, Saiz E, Nalla RK, Gryn K, Ritchie RO, Tomsia AP. Fabrication and mechanical properties of PLA/HA composites: A study of in vitro degradation. Materials Science and Engineering: C. 2006;26(8):1289-1295.
75. Qin Y, Yuan M, Li L, Li W, Xue J. Formulation and evaluation of in situ forming PLA implant containing tinidazole for the treatment of periodontitis. Journal of Biomedical Materials Research Part B: Applied Biomaterials. 2012;100B(8):2197-2202.
76. Mc Conville C, Major I, Friend DR, Clark MR, Woolfson AD, Malcolm RK. Development of polylactide and polyethylene vinyl acetate blends for the manufacture of vaginal rings. Journal of Biomedical Materials Research Part B: Applied Biomaterials. 2012;100B(4):891-895.
77. Patomchaiviwat V, Paeratakul O, Kulvanich P. Formation of inhalable Rifampicin–poly(l-lactide) microparticles by supercritical anti-solvent process. AAPS PharmSciTech. 2008;9(4):1119-1129.
78. Melo N, Grillo R, Guilherme V, Araujo D, Paula E, Rosa A, et al. Poly(lactide-co-glycolide) nanocapsules containing Benzocaine: influence of the composition of the oily nucleus on physico-chemical properties and anesthetic activity. Pharmaceutical Research. 2011;28(8):1984-1994.
79. Aguado E, Leon I, Cocinero EJ, Lesarri A, Fernandez JA, Castano F. Molecular recognition in the gas phase: benzocaine-phenol as a model of anaesthetic-receptor interaction. Physical Chemistry Chemical Physics. 2009;11(48):11608-11616.
80. Fulias A, Vlase G, Grigorie C, Ledeţi I, Albu P, Bilanin M, et al. Thermal behaviour studies of procaine and benzocaine. Journal of Thermal Analysis and Calorimetry. 2013;113(1):265-271.

81. Xiang TX, Anderson BD. Molecular dynamics simulation of amorphous Indomethacin. MOLECULAR PHARMACEUTICS. 2013;10(1):102-114.
82. Johnson MR, Prager M, Grimm H, Neumann MA, Kearley GJ, Wilson CC. Methyl group dynamics in paracetamol and acetanilide: probing the static properties of intermolecular hydrogen bonds formed by peptide groups. Chemical Physics. 1999;244(1):49-66.
83. Pubchem substance [Online]. U.S. National Library of Medicine; [2015, 09 Febuary]. Available from: http://www.ncbi.nlm.nih.gov/pcsubstance.
84. Alger M. Polymer science dictionary. 2 ed. London: Chapman & Hall; 1997.
85. Wiranidchapong C, Tucker IG, Rades. T, Kulvanich P. Miscibility and interactions between 17β-estradiol and Eudragit®RS in solid dispersion. Journal of Pharmaceutical Sciences. 2008;97(11):4879-4888.
86. Xiang TX, Anderson BD. Molecular dynamics simulation of amorphous indomethacin–poly(vinylpyrrolidone) glasses: Solubility and hydrogen bonding interactions. Journal of Pharmaceutical Sciences. 2013;102(3):876-891.
87. Szatyłowicz H. Structural aspects of the intermolecular hydrogen bond strength: H-bonded complexes of aniline, phenol and pyridine derivatives. Journal of Physical Organic Chemistry. 2008;21(10):897-914.
88. Biggs WD, McColl IR, Moon JR. Atomic structure and interatomic bonding. In: J.M. Illston, Domone PLJ, editors. Construction Materials. New York: Spon Press; 2001. p. 1-6.
89. Pipatpanukul C. Study of polylactide/poly(ethylene glycol)/montmorillonite nanocomposite [Master's thesis]: Suranaree University of Technology; 2010.
90. Tabi T, Sajo IE, Szabo F, Luyt AS, Kovacs JG. Crystalline structure of annealed polylactic acid and its relation to processing. Express Polymer Letters. 2010;4(10):659-668.
91. Astrid J, Rincon L. Synthesis and characterization of poly(lactic acid) for use in biomedical field [Online]. [2015, 2 July]. Available from: http://www.aidic.it/icheap10/webpapers/310Lasprilla.pdf.

92. Kopinke FD, Remmler M, Mackenzie K, Möder M, Wachsen O. Thermal decomposition of biodegradable polyesters—II. Poly(lactic acid). Polymer Degradation and Stability. 1996;53(3):329-342.
93. Janssens S, De Zeure A, Paudel A, Van Humbeeck J, Rombaut P, Van den Mooter G. Influence of preparation methods on solid state supersaturation of amorphous solid dispersions: a case study with itraconazole and Eudragit E100. Pharmaceutical Research. 2010;27(5):775-785.
94. Sacchetti M. Thermodynamic analysis of DSC data for acetaminophen polymorphs. Journal of Thermal Analysis and Calorimetry. 2000;63(2):345-350.
95. Otsuka M, Kato F, Matsuda Y, Ozaki Y. Comparative determination of polymorphs of indomethacin in powders and tablets by chemometrical near-infrared spectroscopy and X-ray powder diffractometry. AAPS PharmSciTech. 2003;4(2):58-69.
96. Nichols G, Frampton CS. Physicochemical characterization of the orthorhombic polymorph of paracetamol crystallized from solution. Journal of Pharmaceutical Sciences. 1998;87(6):684-693.
97. Zhang GC, Lin HL, Lin SY. Thermal analysis and FTIR spectral curve-fitting investigation of formation mechanism and stability of indomethacin-saccharin cocrystals via solid-state grinding process. Journal of Pharmaceutical and Biomedical Analysis. 2012;66(0):162-169.

APPENDIX

1. Miscibility prediction by calculation

Molecular dynamics (MD) simulation

Determination of the number of configurations required for MD simulation

Table A-16 Density and solubility parameter of three different configurations of BZC from MD simulation

Starting configuration (initial energy (kcal/mol))	**Density (g/cm^3)**	δ_t	δ_d **$MPa^{0.5}$**	δ_e
1st (-645.01)	1.10	22.74	20.28	10.29
2nd (-602.39)	1.09	22.48	20.12	10.02
3rd (-596.81)	1.10	22.54	20.12	10.15
Average	**1.10**	**22.59**	**20.17**	**10.16**
SD	**0.00**	**0.14**	**0.09**	**0.14**

Among three different starting configurations, differences in calculated values of density and solubility parameter of benzocaine (BZC) were small, reflected by small standard deviation (SD) as shown in Table A-16. Therefore, the first starting configuration with a minimal energy was chosen for MD simulation.

Determination of the number of repeating units of polymer required for MD simulation

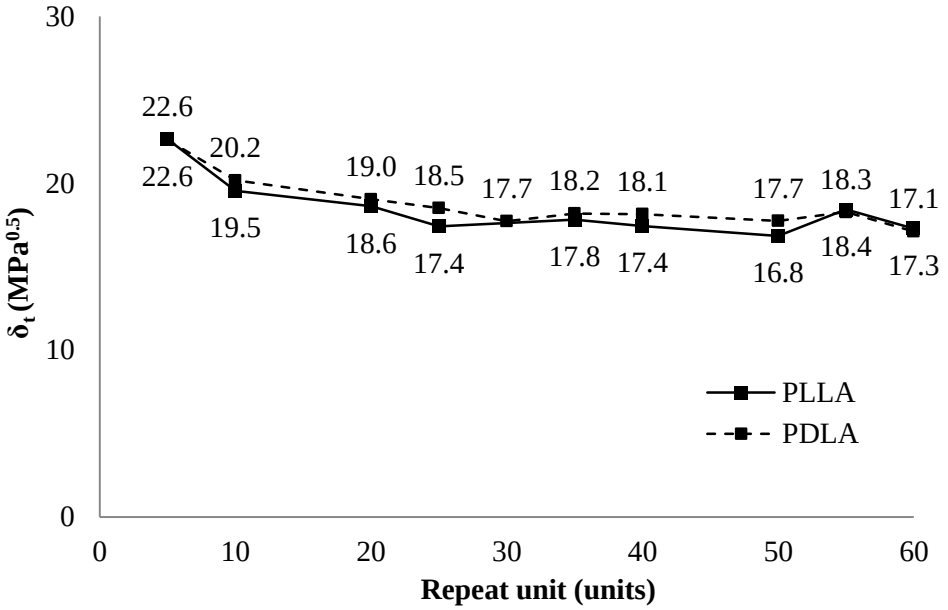

Figure 41 Total solubility parameter and repeat units of polymer chain (n=1)

Relation between total solubility parameter (δ_t) values and repeating units (chain length) of the studied polymers, i.e. poly l-lactide (PLLA) and poly d-lactide (PDLA), is shown in Figure 41. The δ_t value was decreased when the repeating units of polymers was increased. After the number of repeating units of PLLA and PDLA were 25 and 35 units, respectively, the values of δ_t began to be constant. As a result, 25 repeating units of PLLA and 35 repeating units of PDLA were used in MD simulation.

Determination of the number of configurations of drug-polymer blend required for MD simulation

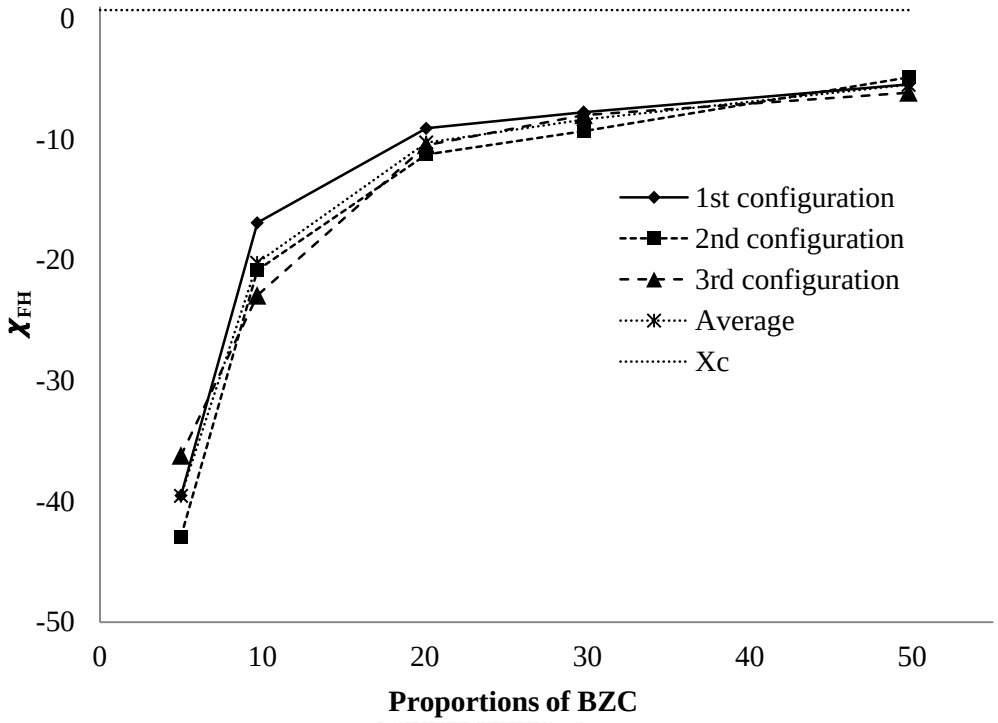

Figure 42 Relationship between Flory-Huggins interaction parameter and proportions of BZC in the BZC:PLLA blend (n=3)

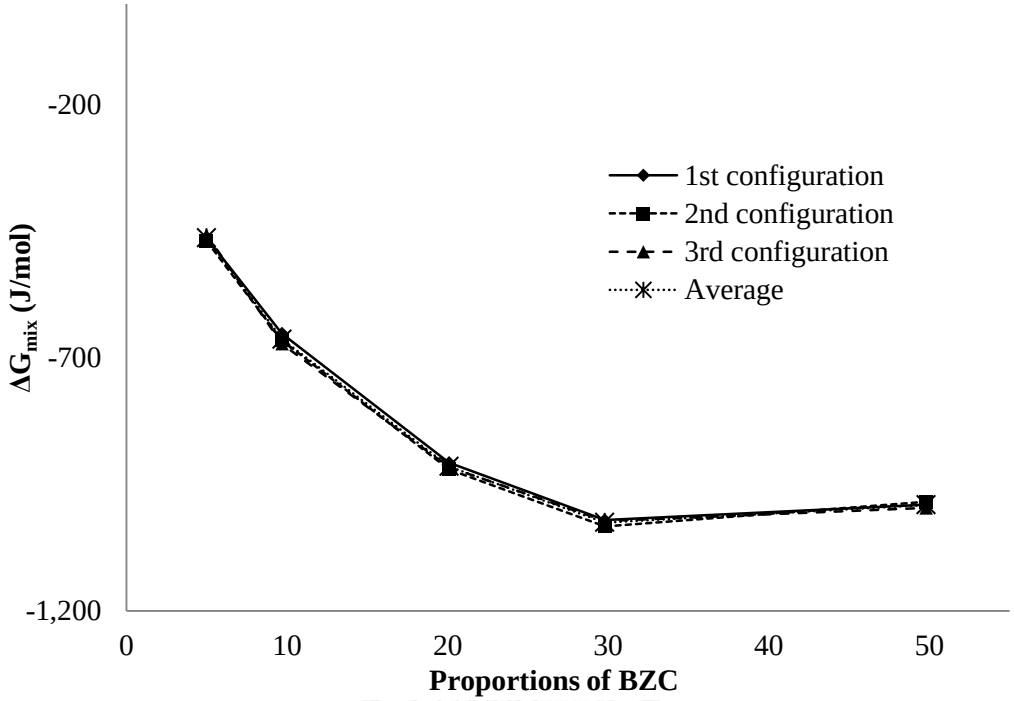

Figure 43 Retationship between Gibbs free energy of mixing and proportions of BZC in the BZC:PLLA blend (n=3)

The plot between BZC:PLLA ratios and Flory-Huggins interaction parameter (χ_{FH}) and the plot between BZC:PLLA ratios and Gibbs free energy of mixing (ΔG_{mix}) showed similar trend for the different staring configurations. Thus, one starting configuration which had the lowest energy was employed in MD simulation of the blends.

MD simulation of drug and polymer blends

Table A-17 Density, cohesive energy density and total solubility parameter of BZC:PLLA blends (n=3)

Ratio BZC:PLLA	**Configuration**	**Density (g/cm^3)**	**CED (J/cm^3)**	**CED_d (J/cm^3)**	**CED_e (J/cm^3)**	**δ_t $(J/cm^3)^{0.5}$**
0:100	-	1.130	302.989	244.782	58.207	17.406
5:95	1st	1.188	386.332	317.060	69.272	19.655
	2nd	1.187	392.614	320.215	72.399	19.814
	3rd	1.181	380.251	312.217	68.034	19.500
	Average	**1.185**	**386.399**	**316.497**	**69.902**	**19.656**
	SD	**0.004**	**6.182**	**4.028**	**2.250**	**0.157**
10:90	1st	1.181	381.334	312.838	68.496	19.543
	2nd	1.173	394.619	320.501	74.118	19.893
	3rd	1.183	401.810	326.522	75.287	20.045
	Average	**1.179**	**392.588**	**319.954**	**72.634**	**19.813**
	SD	**0.005**	**10.388**	**6.859**	**3.631**	**0.257**
20:80	1st	1.176	401.817	330.068	71.750	20.045
	2nd	1.183	415.246	338.573	76.672	20.425
	3rd	1.172	410.447	334.452	75.995	20.260
	Average	**1.177**	**409.170**	**334.364**	**74.806**	**20.227**
	SD	**0.006**	**6.805**	**4.254**	**2.668**	**0.191**

Table A-17 (continue) Density, cohesive energy density and total solubility parameter of BZC:PLLA blends (n=3)

Ratio BZC:PLLA	**Configuration**	**Density (g/cm^3)**	**CED (J/cm^3)**	**CED_d (J/cm^3)**	**CED_e (J/cm^3)**	**δ_t $(J/cm^3)^{0.5}$**
30:70	1st	1.173	428.084	348.959	79.124	20.690
	2nd	1.179	440.723	358.450	82.273	21.033
	3rd	1.166	430.003	348.876	81.127	20.736
	Average	**1.172**	**432.936**	**352.095**	**80.842**	**20.806**
	SD	**0.007**	**6.811**	**5.504**	**1.594**	**0.186**
50:50	1st	1.148	459.009	364.899	94.110	21.406
	2nd	1.148	453.578	366.316	87.262	21.302
	3rd	1.152	465.593	373.493	92.100	21.577
	Average	**1.149**	**459.393**	**368.236**	**91.157**	**21.433**
	SD	**0.002**	**6.017**	**4.607**	**3.520**	**0.139**
100:0	-	1.097	510.093	406.838	103.255	22.586

Table A-18 Density, cohesive energy density and total solubility parameter of BZC:PDLA blends (n=1)

Ratio BZC:PDLA	Density (g/cm^3)	CED (J/cm^3)	CED_d (J/cm^3)	CED_e (J/cm^3)	δ_t $(J/cm^3)^{0.5}$
0:100	1.180	330.790	281.655	49.135	18.187
5:95	1.185	378.596	313.609	64.987	19.457
10:90	1.185	385.645	323.484	62.161	19.638
20:80	1.165	380.827	317.339	63.488	19.515
30:70	1.178	428.885	355.144	73.741	20.709
50:50	1.149	453.541	368.618	84.923	21.296
100:0	1.097	510.093	406.838	103.255	22.586

Table A-19 Density, cohesive energy density and total solubility parameter of IND:PLLA blends (n=1)

Ratio IND:PLLA	Density (g/cm^3)	CED (J/cm^3)	CED_d (J/cm^3)	CED_e (J/cm^3)	δ_t $(J/cm^3)^{0.5}$
0:100	1.130	302.989	244.782	58.207	17.406
5:95	1.189	382.936	309.582	73.354	19.568
10:90	1.206	399.362	325.241	74.121	19.984
20:80	1.210	410.188	332.854	77.334	20.253
30:70	1.220	425.140	340.605	84.535	20.619
50:50	1.221	445.696	352.244	93.452	21.111
100:0	1.288	537.738	421.925	115.813	23.189

Table A-20 Density, cohesive energy density and total solubility parameter of IND:PDLA blends (n=1)

Ratio IND:PDLA	Density (g/cm^3)	CED (J/cm^3)	CED_d (J/cm^3)	CED_e (J/cm^3)	δ_t $(J/cm^3)^{0.5}$
0:100	1.180	330.790	281.655	49.135	18.187
5:95	1.187	375.628	312.849	62.779	19.568
10:90	1.201	383.285	321.329	61.956	19.984
20:80	1.196	398.344	328.176	70.168	20.253
30:70	1.206	415.865	335.730	80.135	20.619
50:50	1.240	446.754	359.717	87.038	21.111
100:0	1.288	537.738	421.925	115.813	23.189

Table A-21 Density, cohesive energy density and total solubility parameter of PAR:PLLA blends (n=1)

Ratio PAR:PLLA	Density (g/cm^3)	CED (J/cm^3)	CED_d (J/cm^3)	CED_e (J/cm^3)	δ_t $(J/cm^3)^{0.5}$
0:100	1.130	302.989	244.782	58.207	17.406
5:95	1.190	332.660	264.796	67.864	18.239
10:90	1.200	418.991	320.919	98.072	20.469
20:80	1.194	480.803	349.644	131.159	21.323
30:70	1.208	533.571	357.474	176.096	23.099
50:50	1.213	620.949	384.864	236.085	24.919
100:0	1.208	838.787	434.401	404.385	28.962

Table A-22 Density, cohesive energy density and total solubility parameter of PAR:PDLA blends (n=1)

Ratio PAR:PDLA	**Density (g/cm^3)**	**CED (J/cm^3)**	**CED_d (J/cm^3)**	**CED_e (J/cm^3)**	**δ_t $(J/cm^3)^{0.5}$**
0:100	1.180	330.790	281.655	49.135	18.187
5:95	1.185	388.783	313.866	74.917	19.717
10:90	1.194	423.599	331.517	92.082	20.581
20:80	1.197	459.484	333.129	126.355	21.435
30:70	1.203	515.194	357.875	157.319	22.698
50:50	1.206	601.372	375.717	225.655	24.523
100:0	1.208	838.787	434.401	404.385	28.962

Radial distribution function analysis

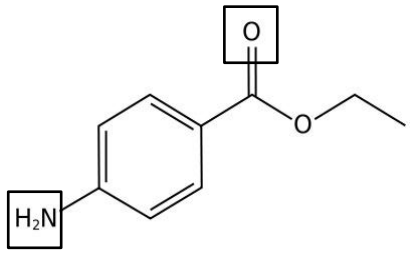

(A) BZC structure

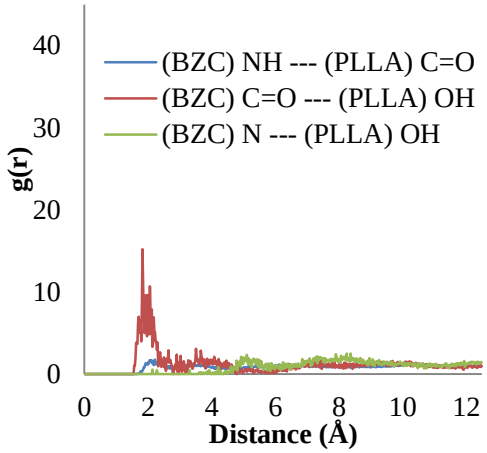

(B) 5:95

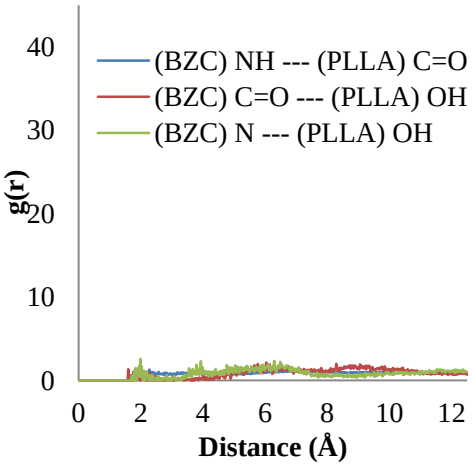

(C) 10:90

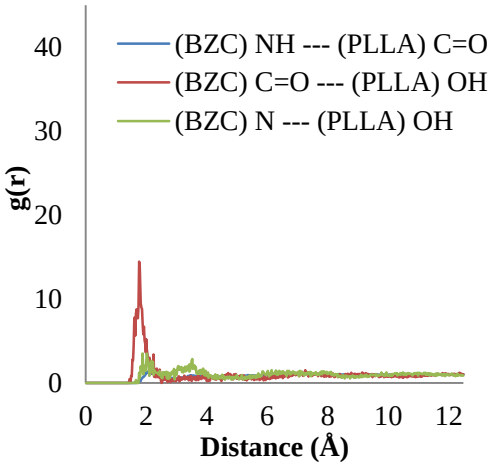

(D) 20:80

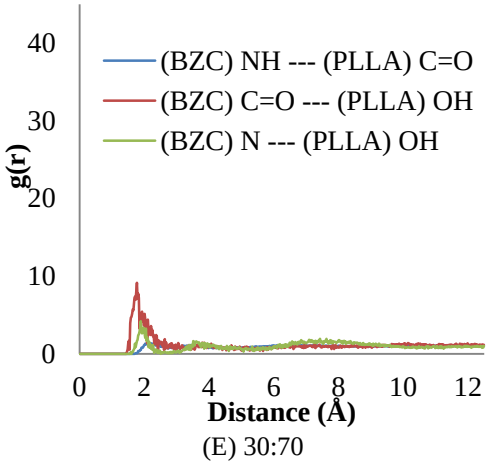

(E) 30:70

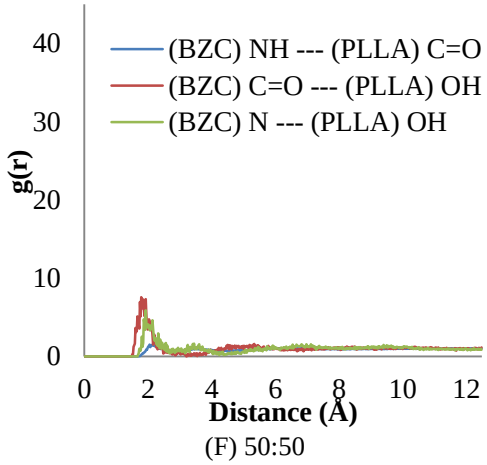

(F) 50:50

Figure 44 BZC-PLLA intermolecular interaction in BZC:PLLA blends by RDF analysis

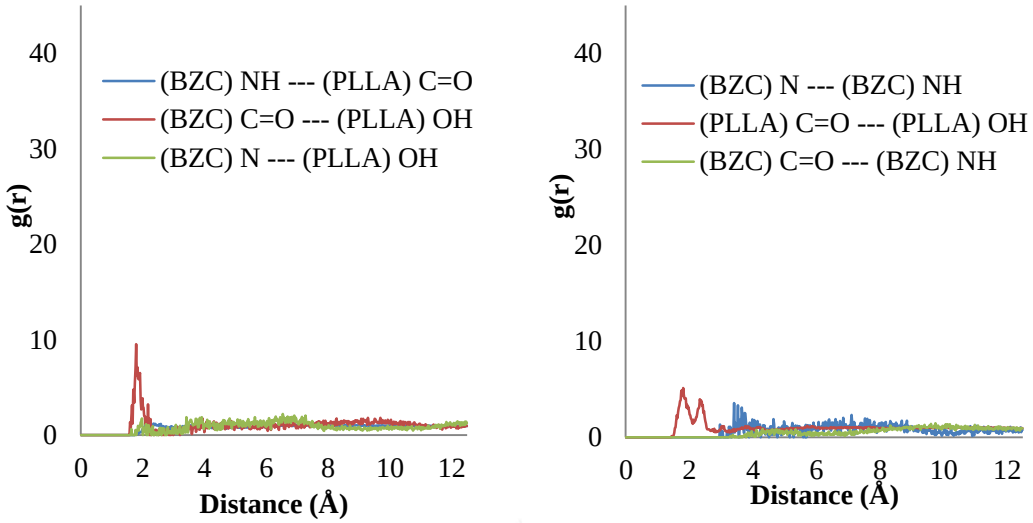

(A) BZC-PLLA interaction (B) BZC-BZC and PLLA-PLLA interactions

Figure 45 RDF analysis of BZC:PLLA blend at the ratio of 10:90 in 400-800 ps of the simulation under NVT ensemble.

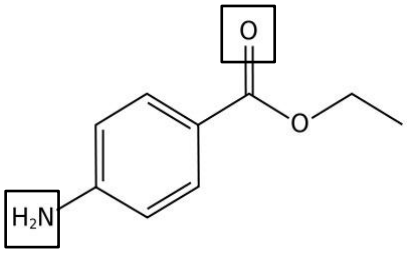

(A) BZC structure

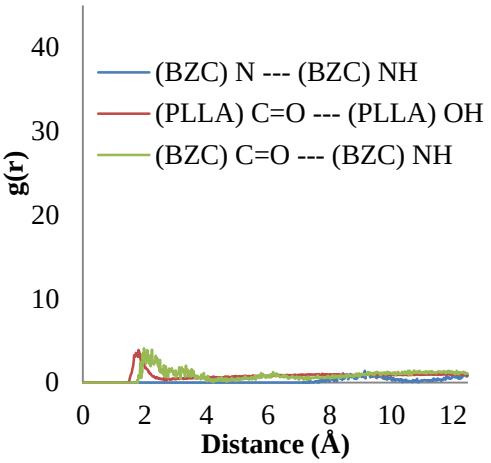

(B) 5:95

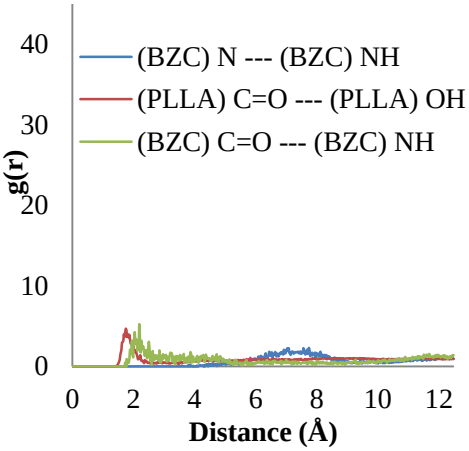

(C) 10:90

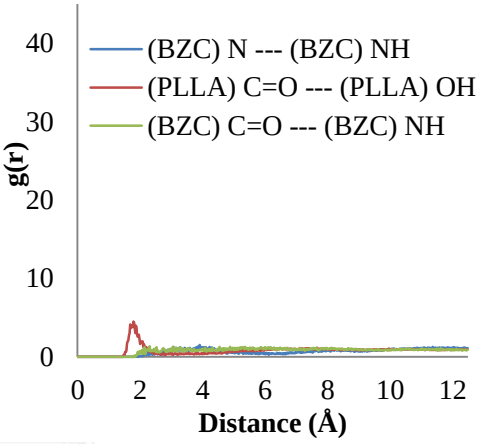

(D) 20:80

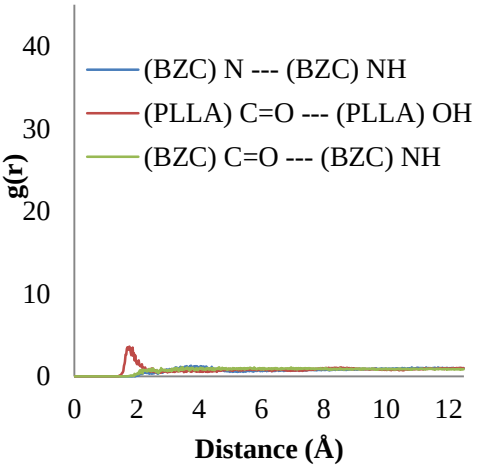

(E) 30:70

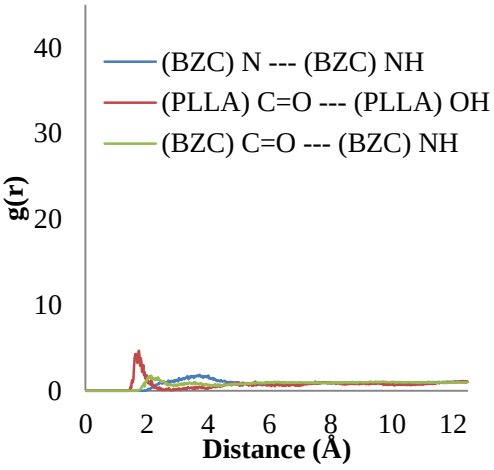

(F) 50:50

Figure 46 BZC-BZC and PLLA-PLLA intermolecular interactions in BZC:PLLA blends by RDF analysis

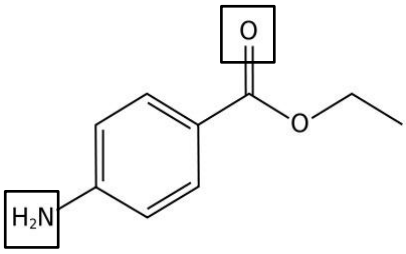

(A) BZC structure

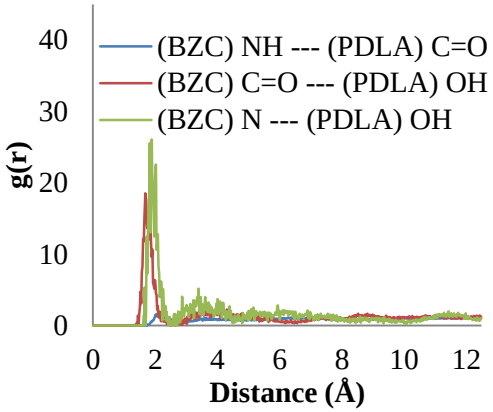

(B) 5:95

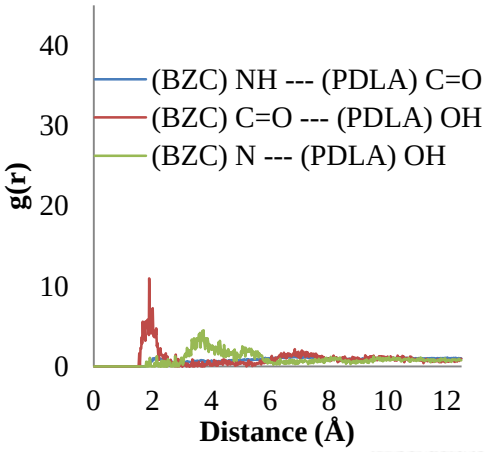

(C) 10:90

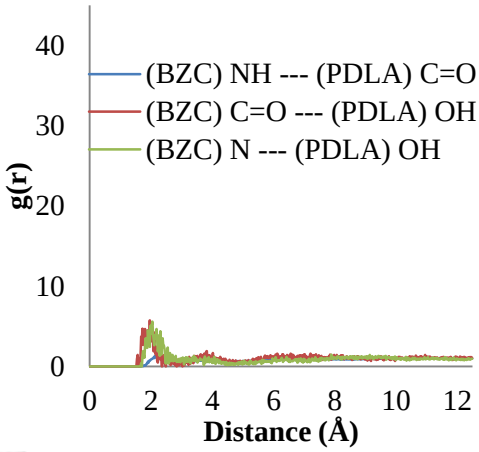

(D) 20:80

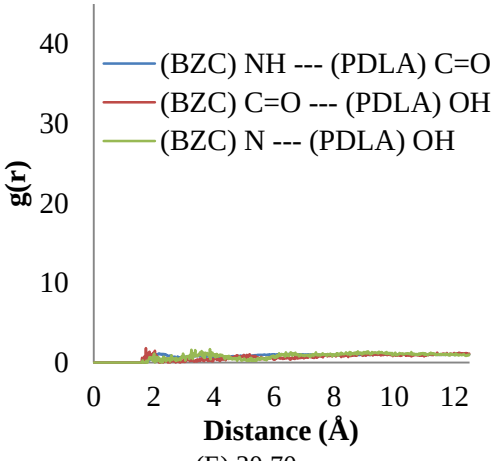

(E) 30:70

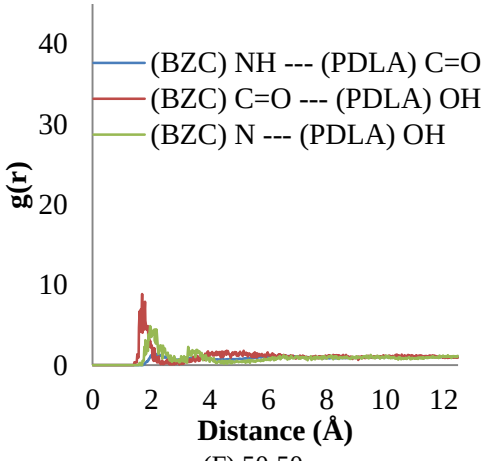

(F) 50:50

Figure 47 BZC-PDLA intermolecular interaction in BZC:PDLA blends by RDF analysis

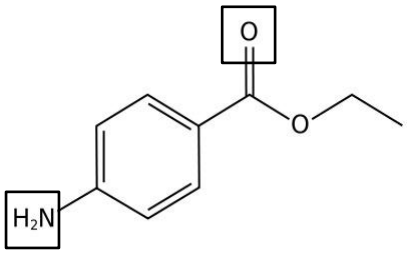

(A) BZC structure

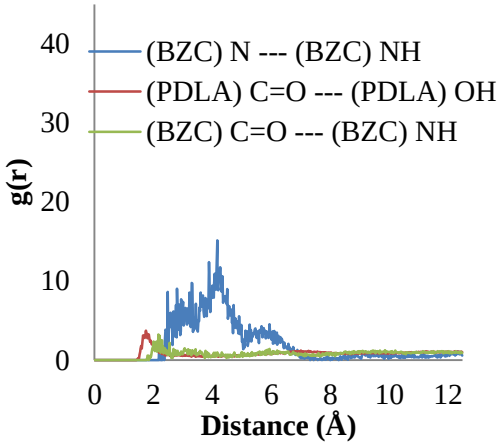

(B) 5:95

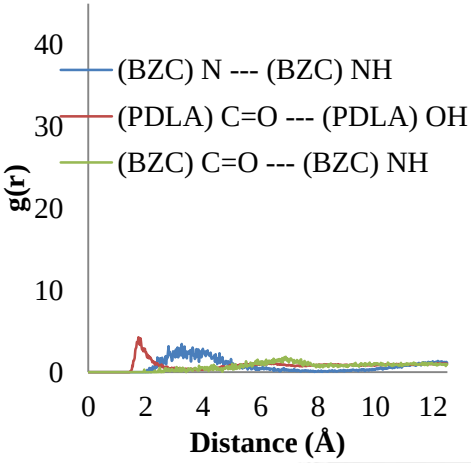

(C) 10:90

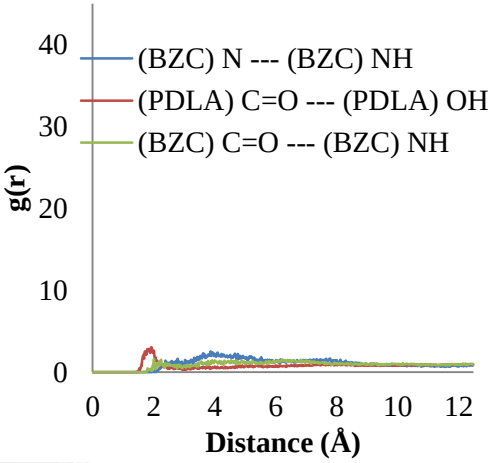

(D) 20:80

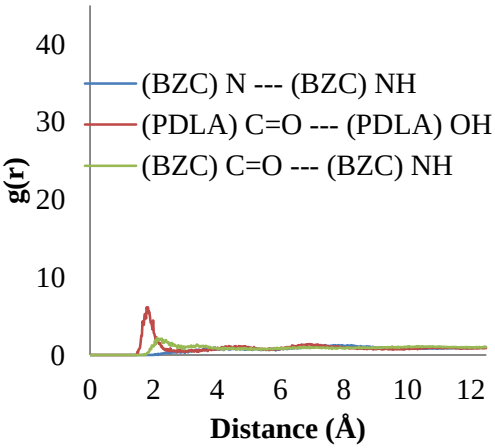

(E) 30:70

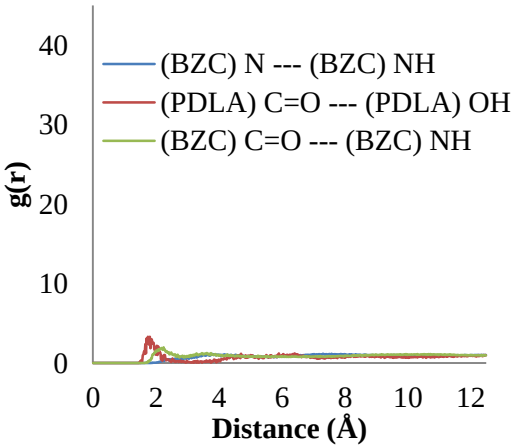

(F) 50:50

Figure 48 BZC-BZC and PDLA-PDLA intermolecular interactions in BZC:PDLA blends by RDF analysis

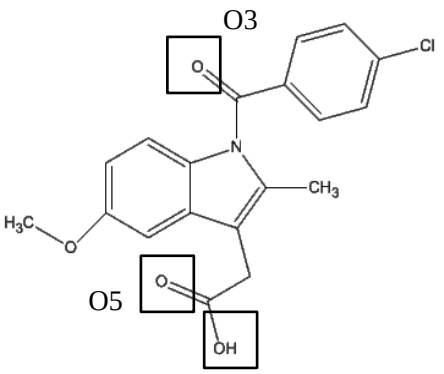

(A) IND structure

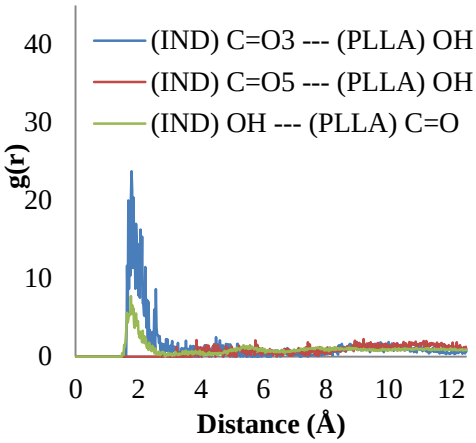

(B) 5:95

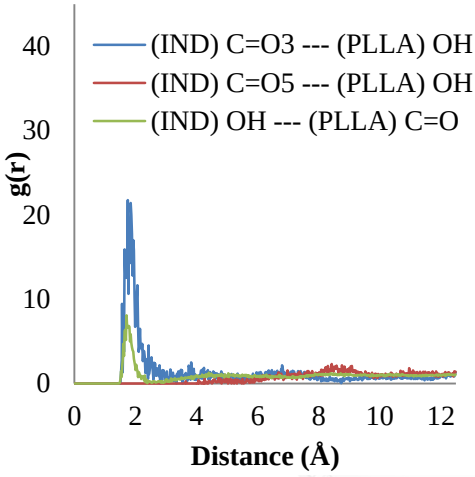

(C) 10:90

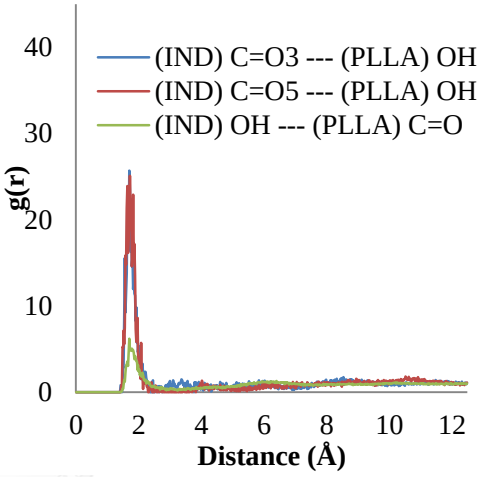

(D) 20:80

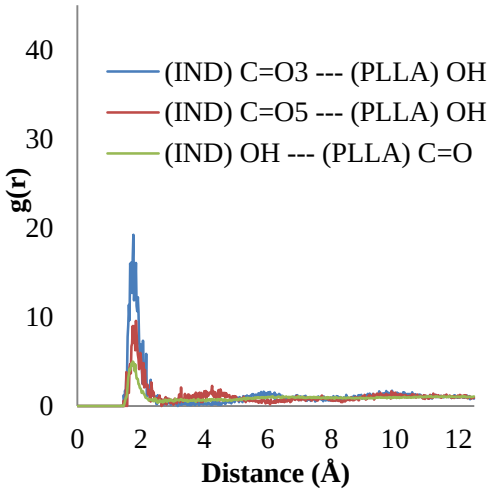

(E) 30:70

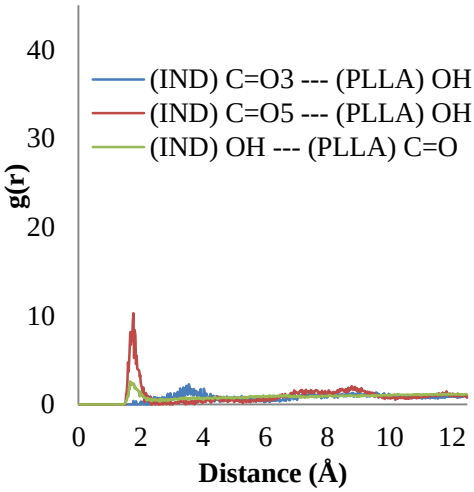

(F) 50:50

Figure 49 IND-PLLA intermolecular interaction in IND:PLLA blends by RDF analysis

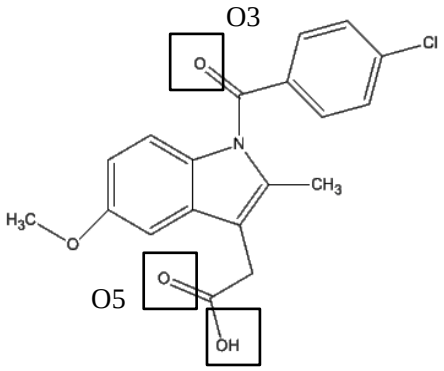

(A) IND structure

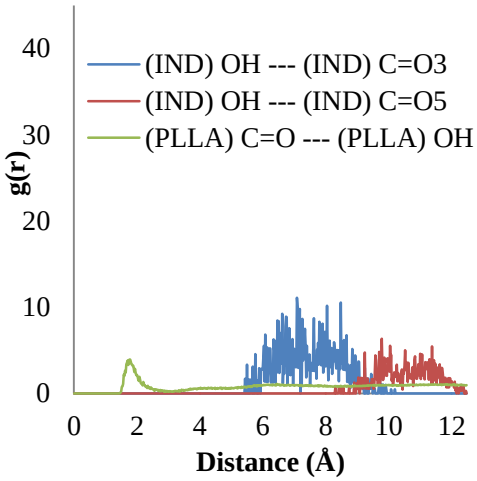

(B) 5:95

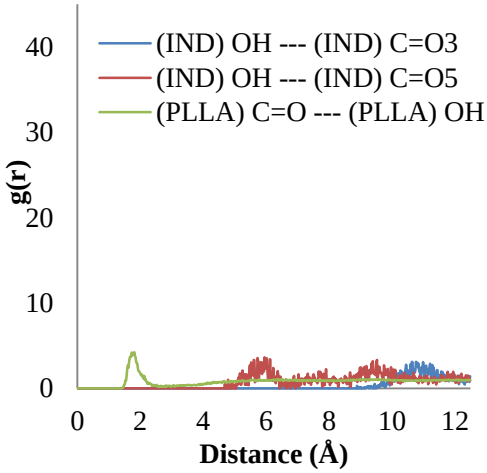

(C) 10:90

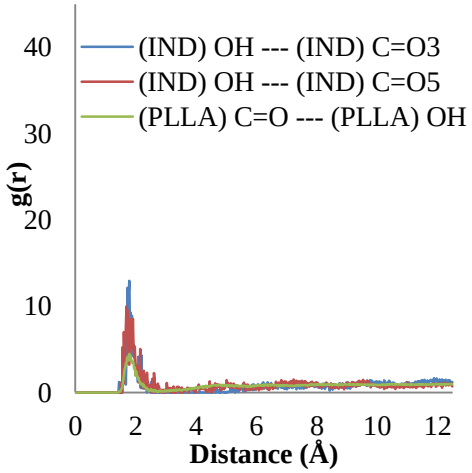

(D) 20:80

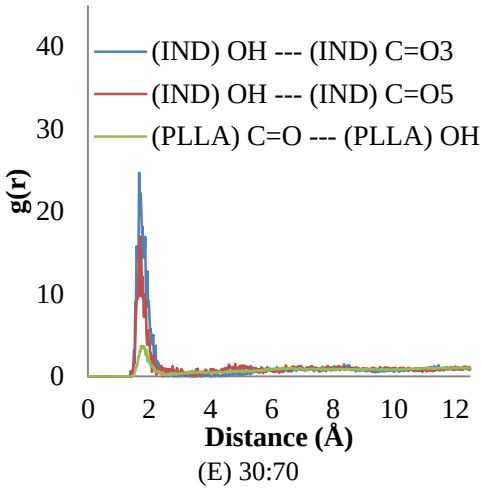

(E) 30:70

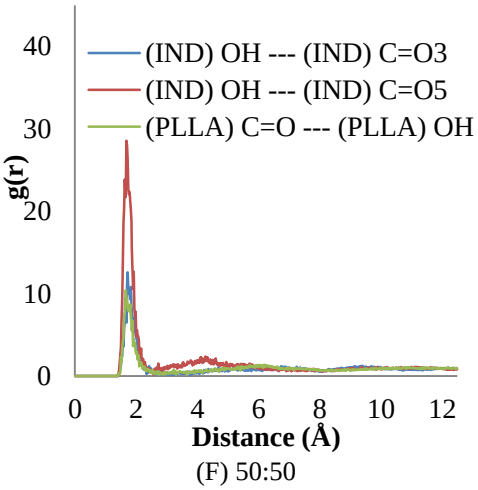

(F) 50:50

Figure 50 IND-IND and PLLA-PLLA intermolecular interactions in IND:PLLA blends by RDF analysis

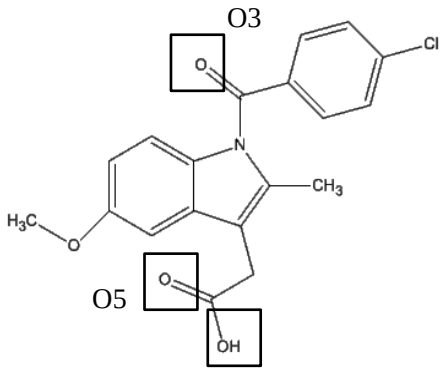

(A) IND structure

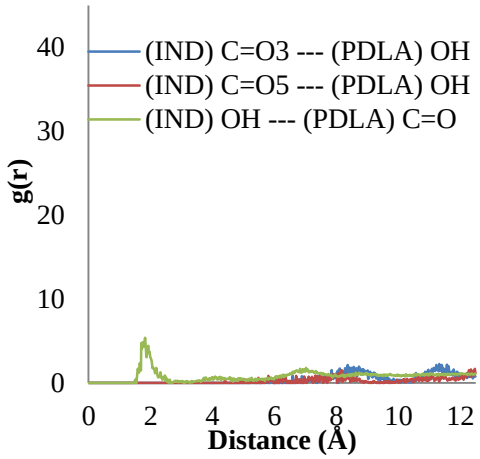

(A) 5:95

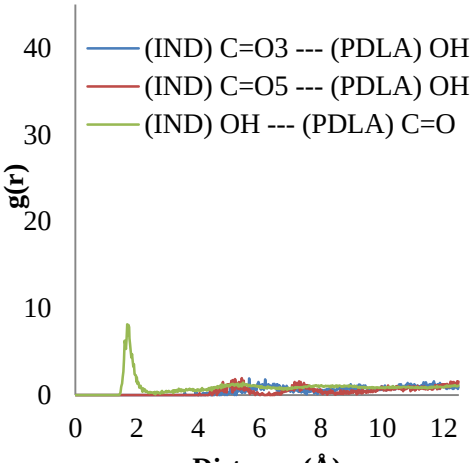

(B) 10:90

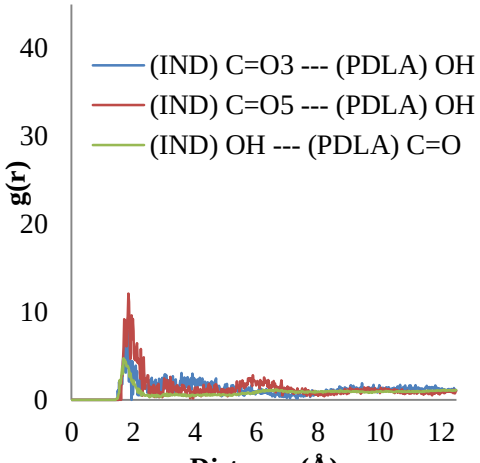

(C) 20:80

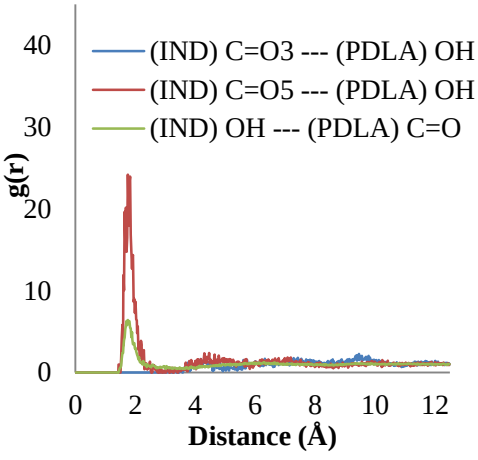

(D) 30:70

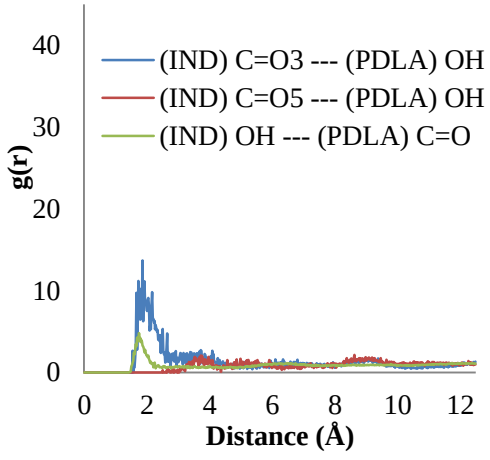

(E) 50:50

Figure 51 IND-PDLA intermolecular interaction in IND:PDLA blends by RDF analysis

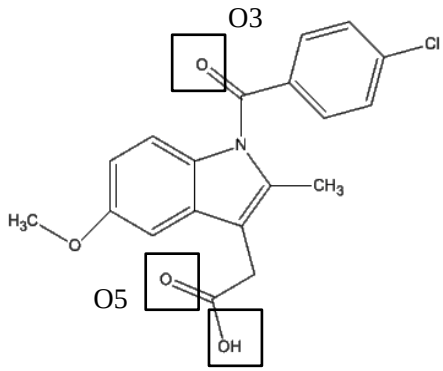

(A) IND structure

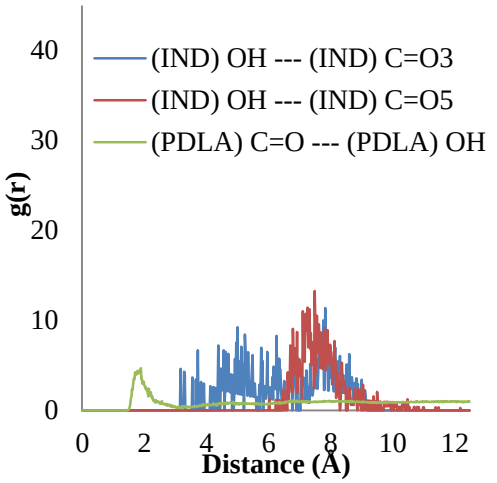

(B) 5:95

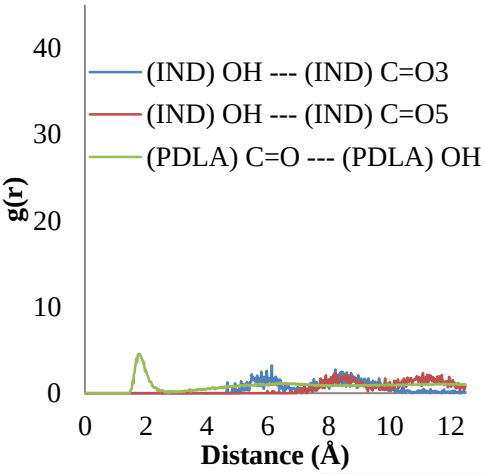

(C) 10:90

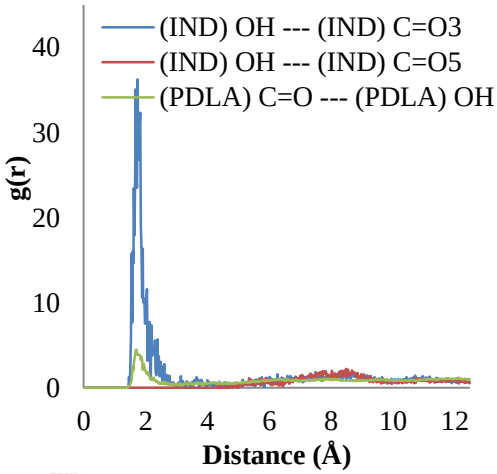

(D) 20:80

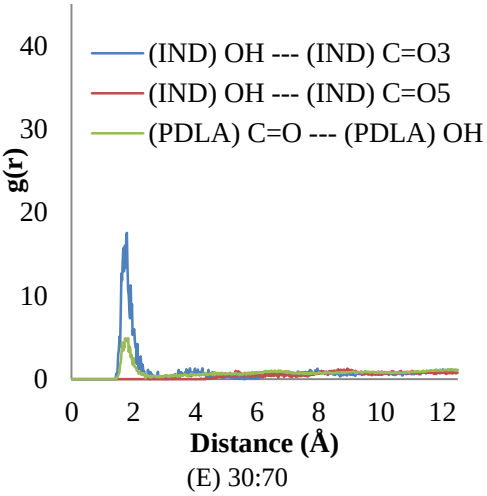

(E) 30:70

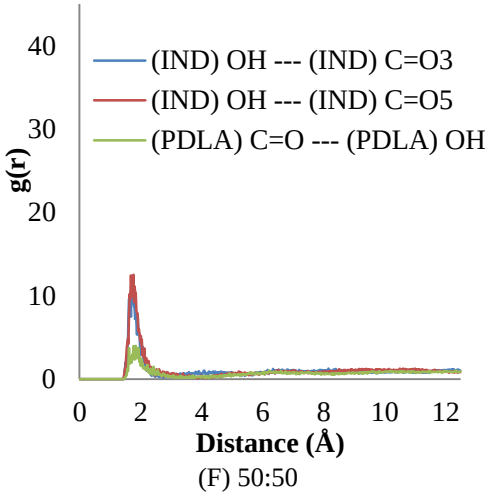

(F) 50:50

Figure 52 IND-IND and PDLA-PDLA intermolecular interactions in IND:PDLA blends by RDF analysis

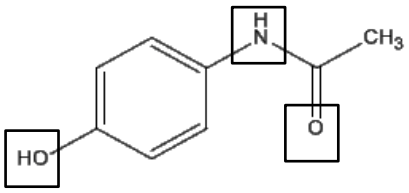

(A) PAR structure

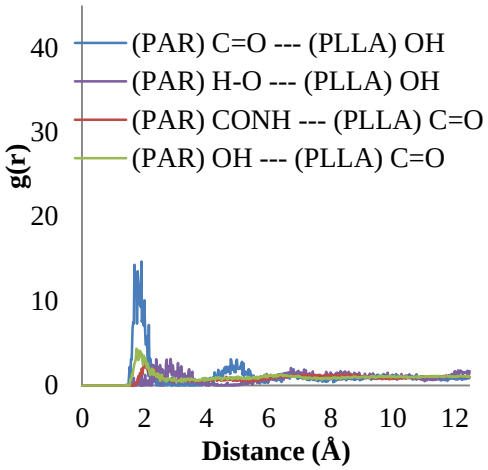

(B) 5:95

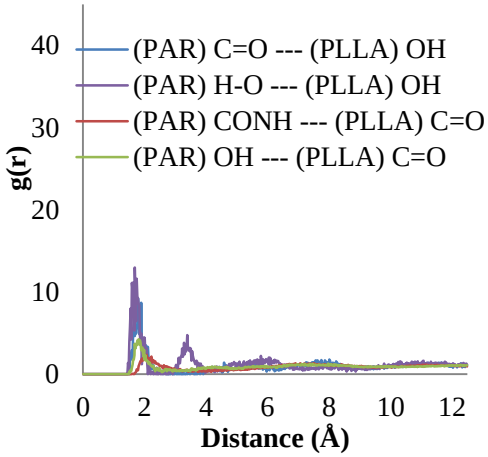

(C) 10:90

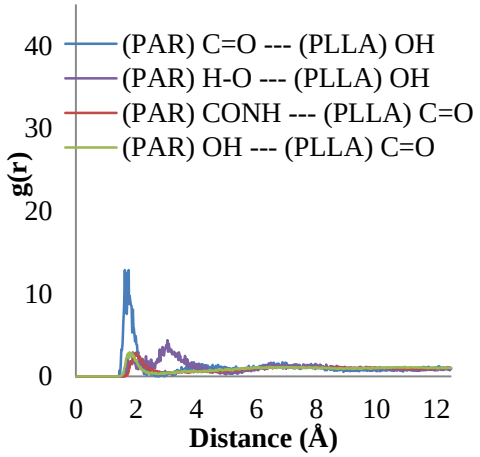

(D) 20:80

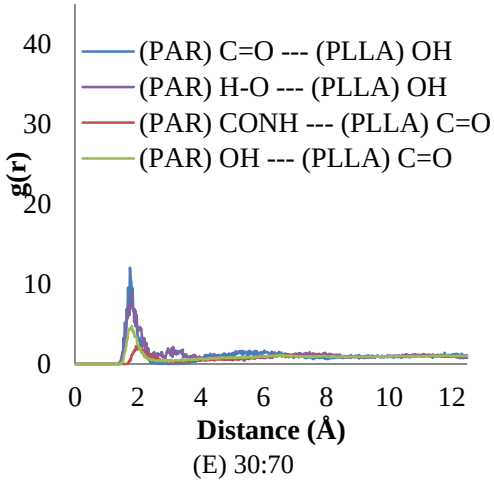

(E) 30:70

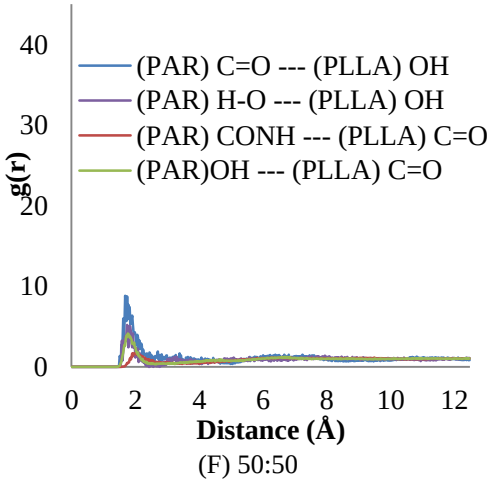

(F) 50:50

Figure 53 PAR-PLLA intermolecular interaction in PAR:PLLA blends by RDF analysis

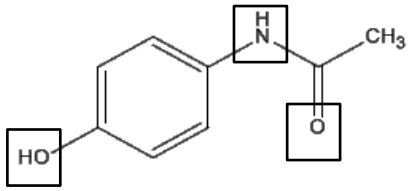

(A) PAR structure

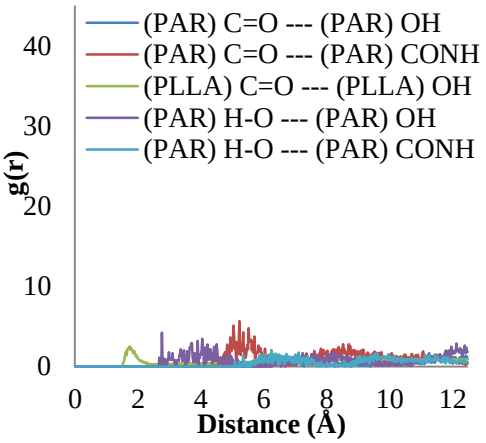

(B) 5:95

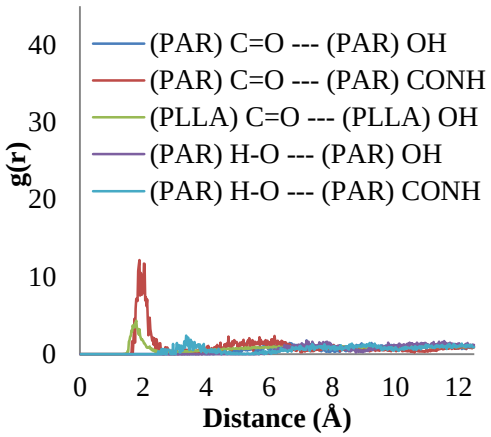

(C) 10:90

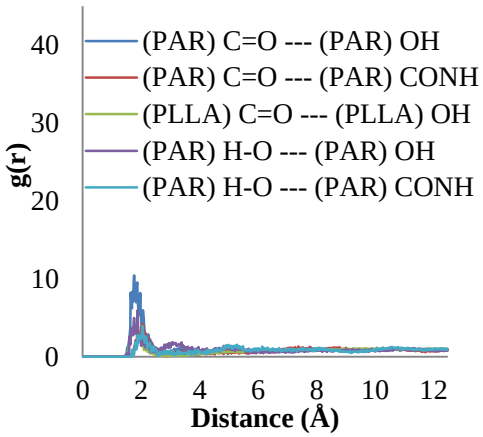

(D) 20:80

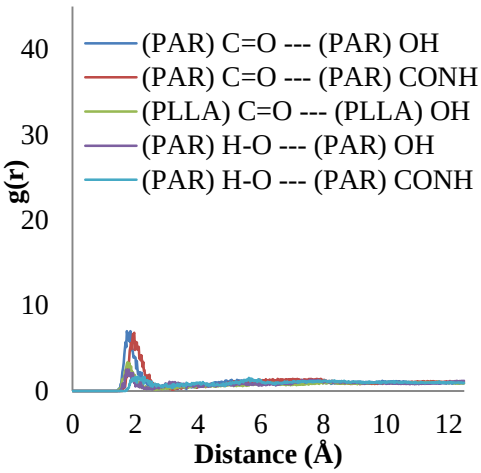

(E) 30:70

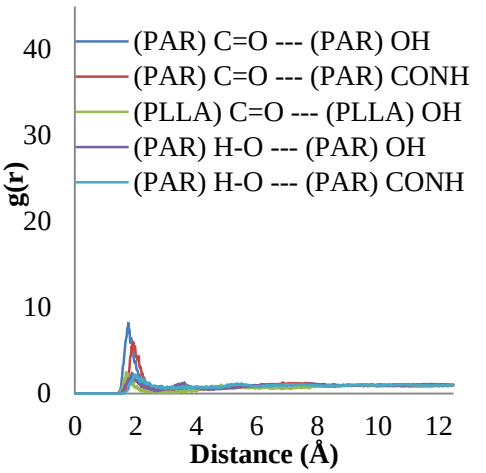

(F) 50:50

Figure 54 PAR-PAR and PLLA-PLLA intermolecular interactions in PAR:PLLA blends by RDF analysis

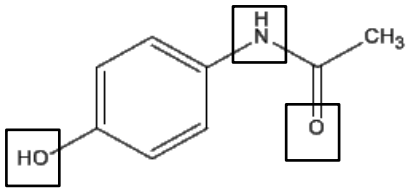

(A) PAR structure

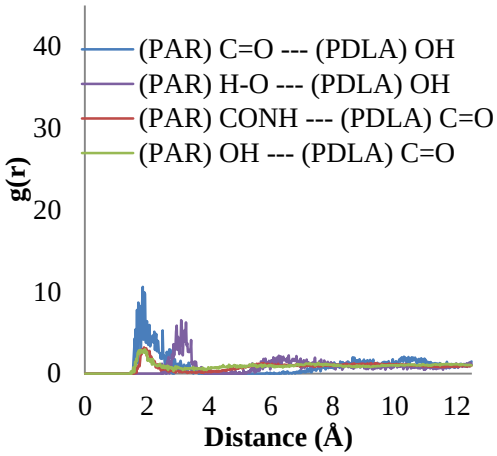

(B) 5:95

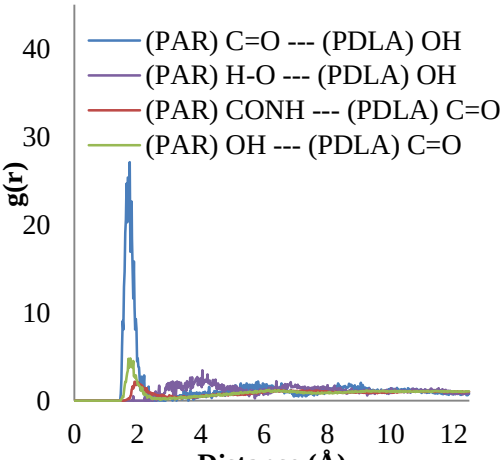

(C) 10:90

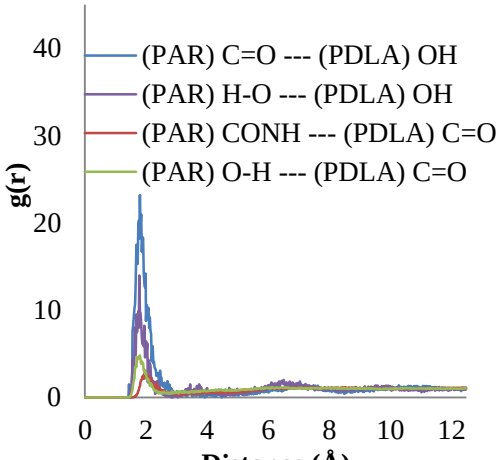

(D) 20:80

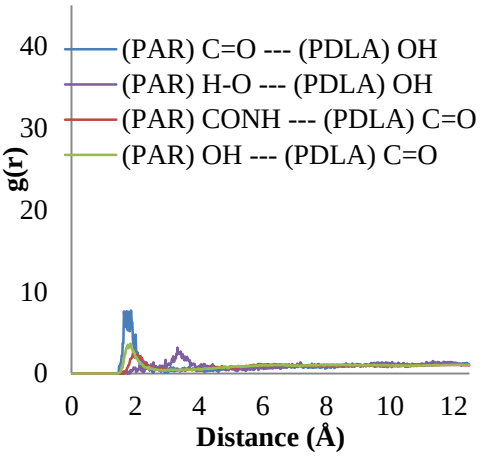

(E) 30:70

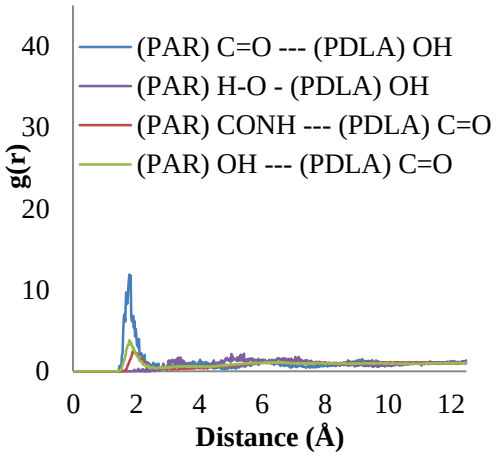

(F) 50:50

Figure 55 PAR-PDLA intermolecular interaction in PAR:PDLA blends by RDF analysis

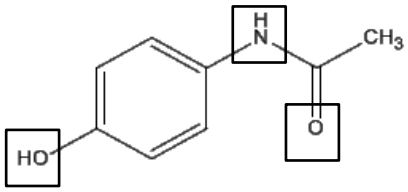

(A) PAR structure

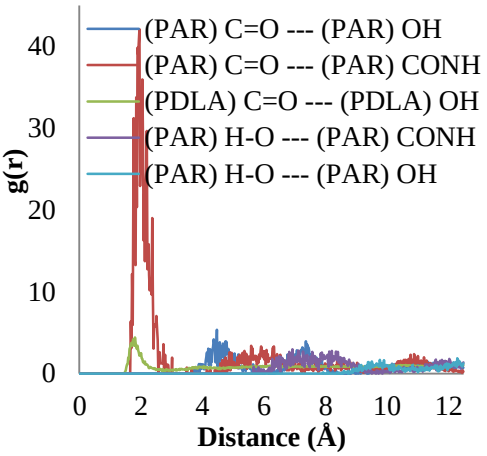

(B) 5:95

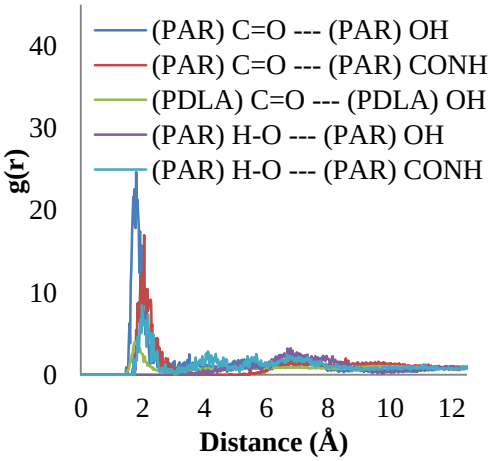

(C) 10:90

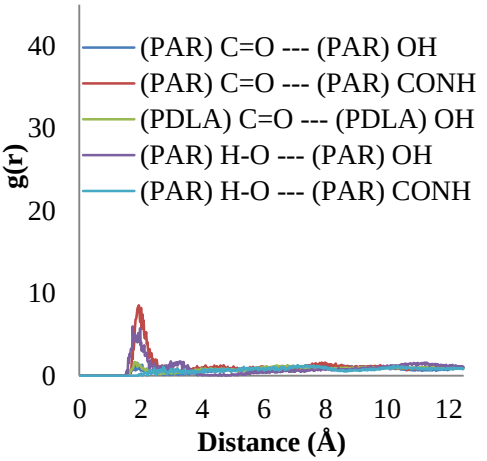

(D) 20:80

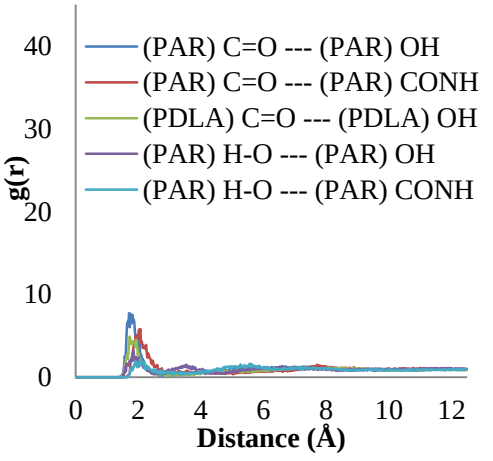

(E) 30:70

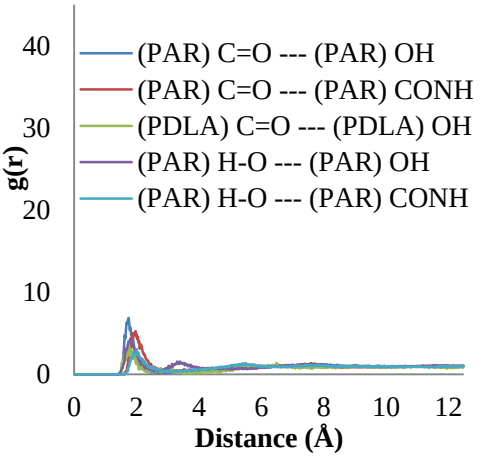

(F) 50:50

Figure 56 PAR-PAR and PDLA-PDLA intermolecular interactions in PAR:PDLA blends by RDF analysis

2. Miscibility prediction by experiments

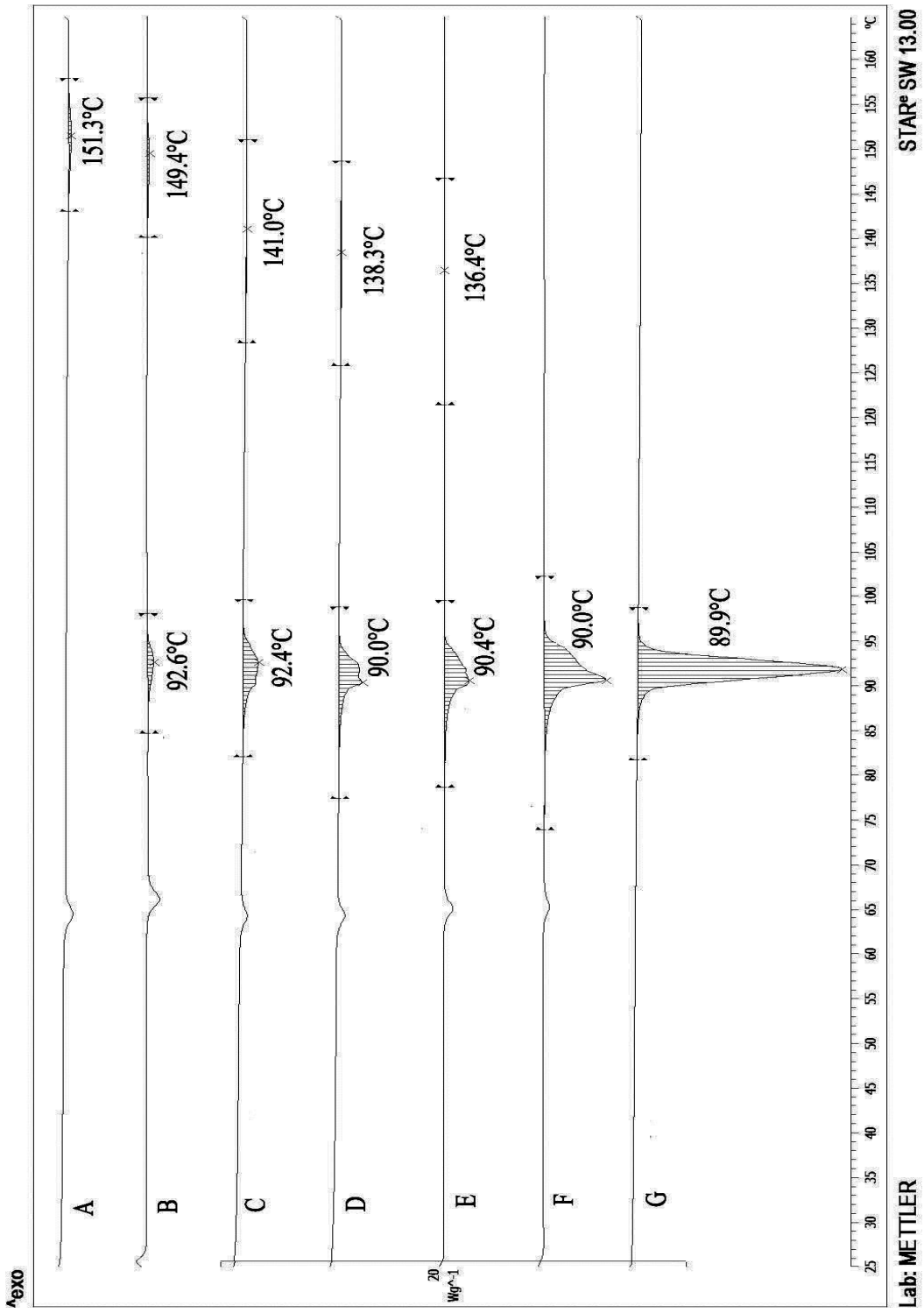

Figure 57 DSC thermogram of BZC:PLLA blends during heating of heat-cool-heat cycle: BZC:PLLA ratio of 0:100 (A), 5:95 (B), 10:90 (C), 20:80 (D), 30:70 (E), 50:50 (F) and 100:0 (G).

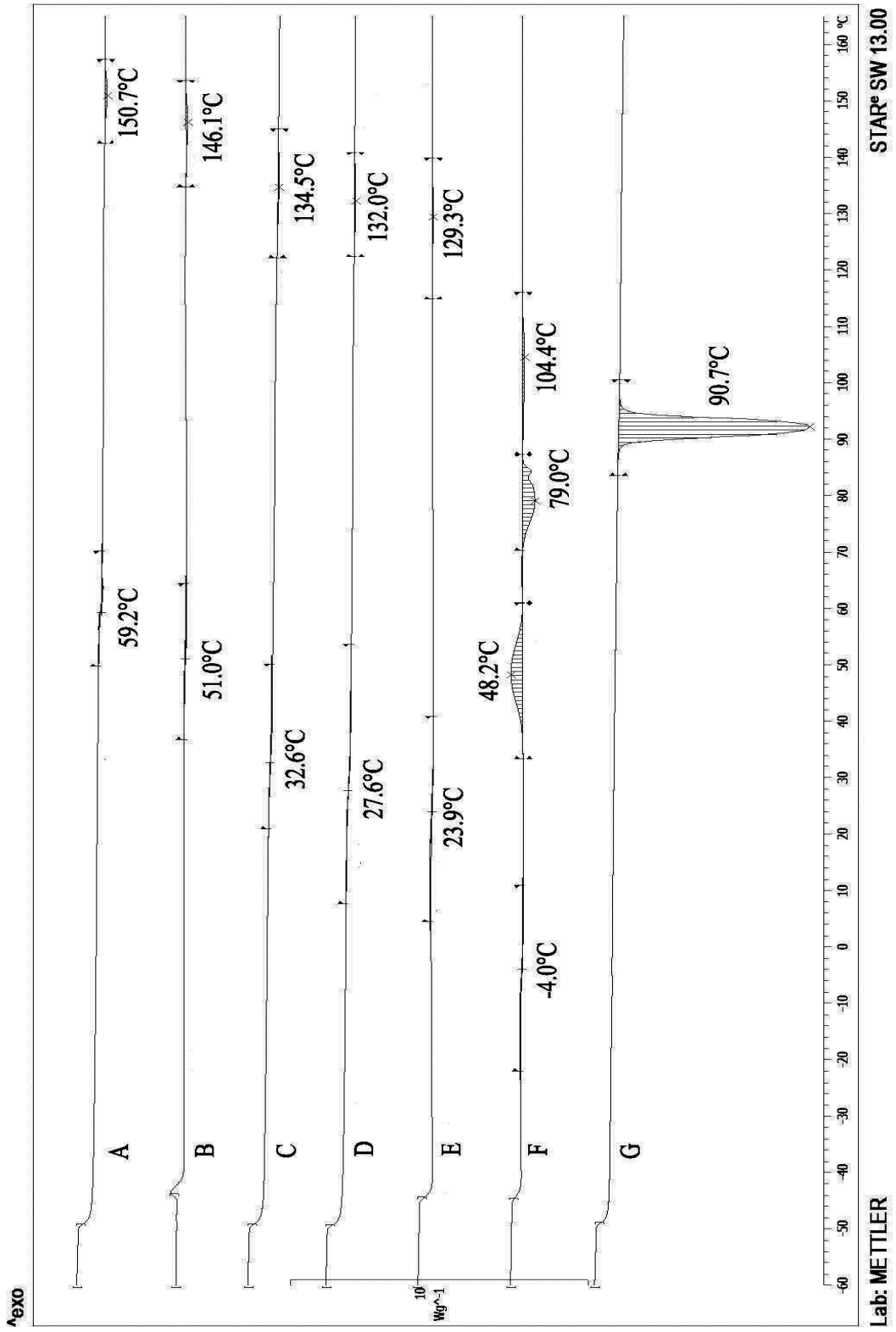

Figure 58 DSC thermogram of BZC:PLLA blends during reheating of heat-cool-heat cycle: BZC:PLLA ratio of 0:100 (A), 5:95 (B), 10:90 (C), 20:80 (D), 30:70 (E), 50:50 (F) and 100:0 (G).

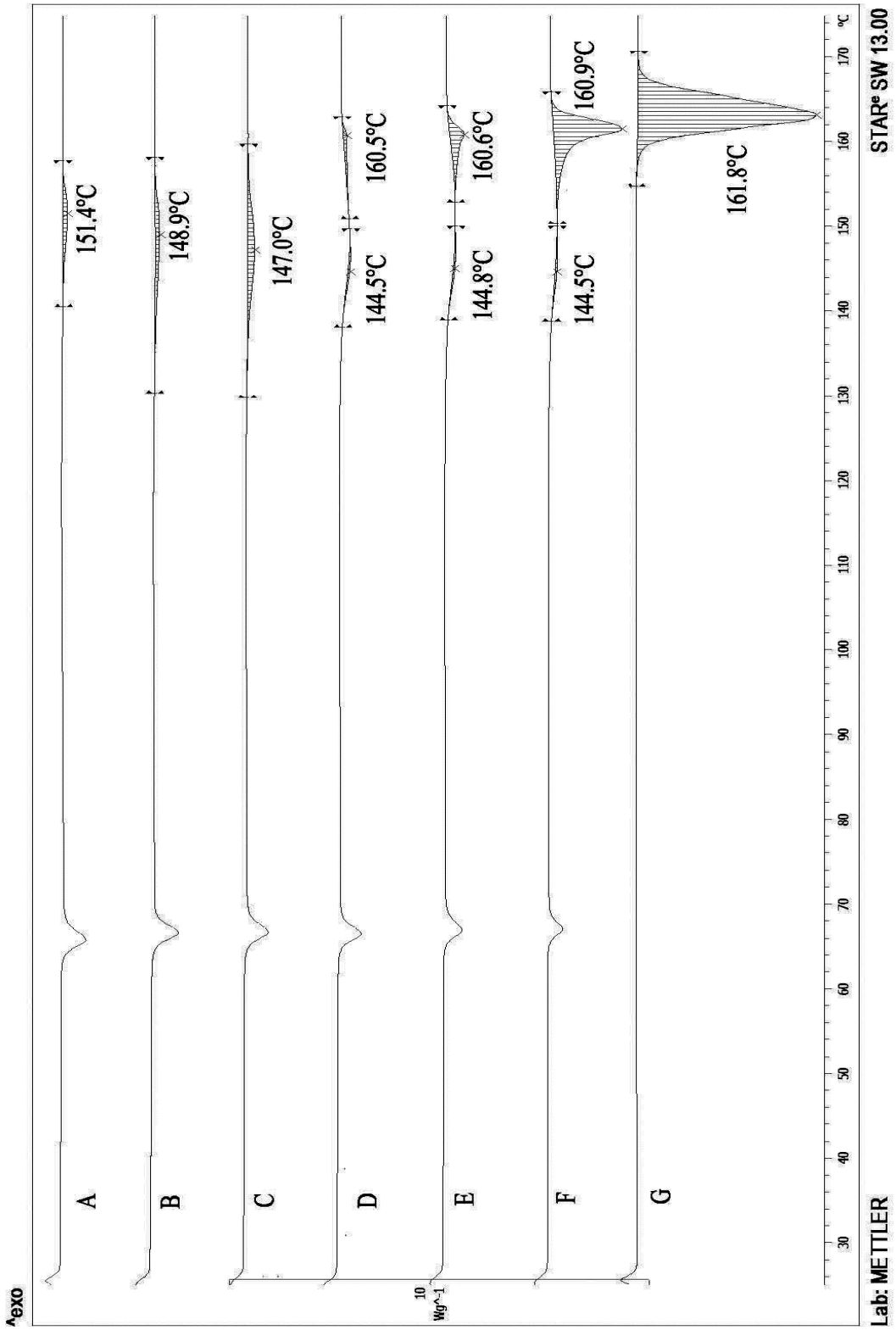

Figure 59 DSC thermogram of IND:PLLA blends during heating of heat-cool-heat cycle: IND:PLLA ratio of 0:100 (A), 5:95 (B), 10:90 (C), 20:80 (D), 30:70 (E), 50:50 (F) and 100:0 (G).

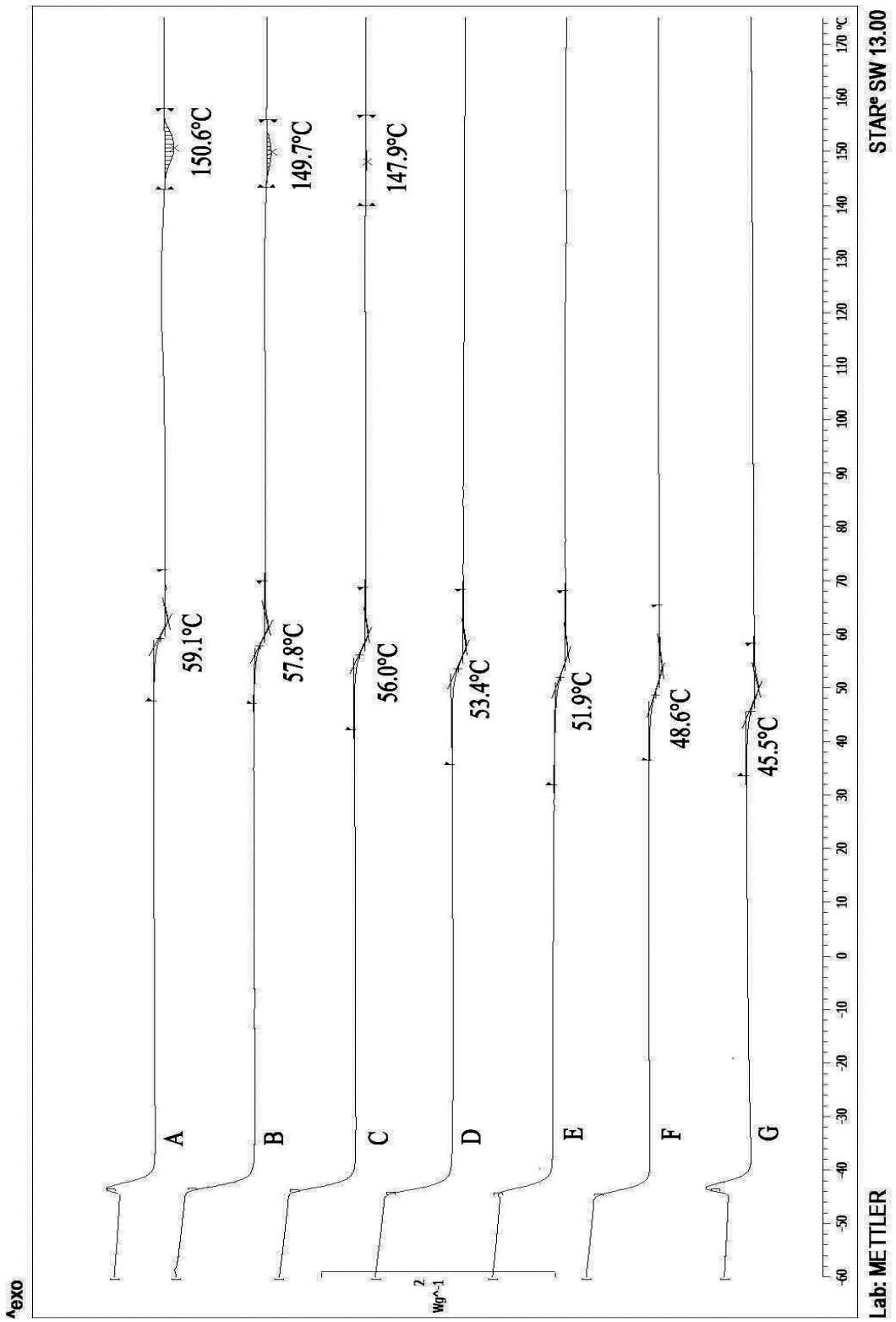

Figure 60 DSC thermogram of IND:PLLA blends during reheating of heat-cool-heat cycle: IND:PLLA ratio of 0:100 (A), 5:95 (B), 10:90 (C), 20:80 (D), 30:70 (E), 50:50 (F) and 100:0 (G).

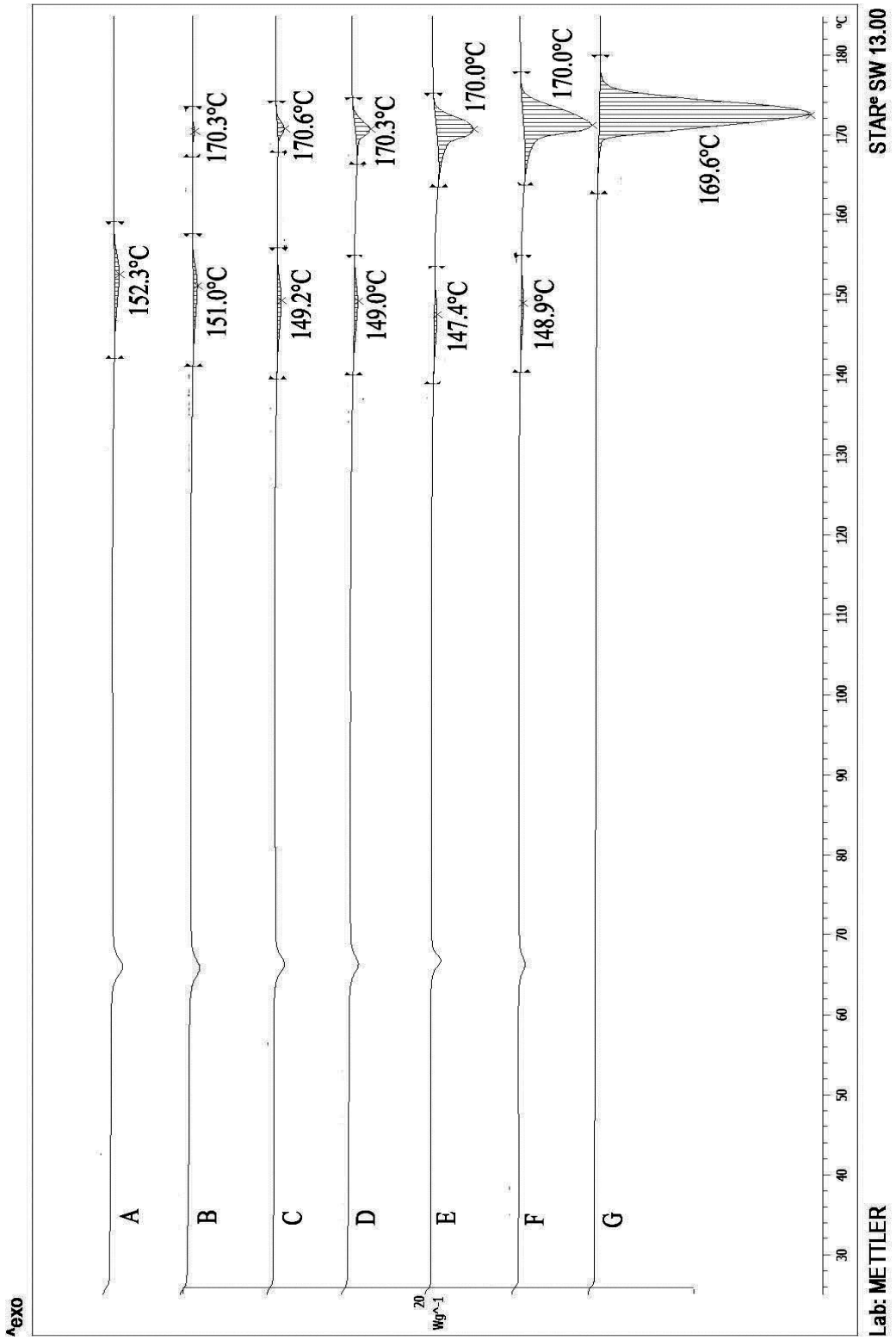

Figure 61 DSC thermogram of PAR:PLLA blends during heating of heat-cool-heat cycle: PAR:PLLA ratio of 0:100 (A), 5:95 (B), 10:90 (C), 20:80 (D), 30:70 (E), 50:50 (F) and 100:0 (G).

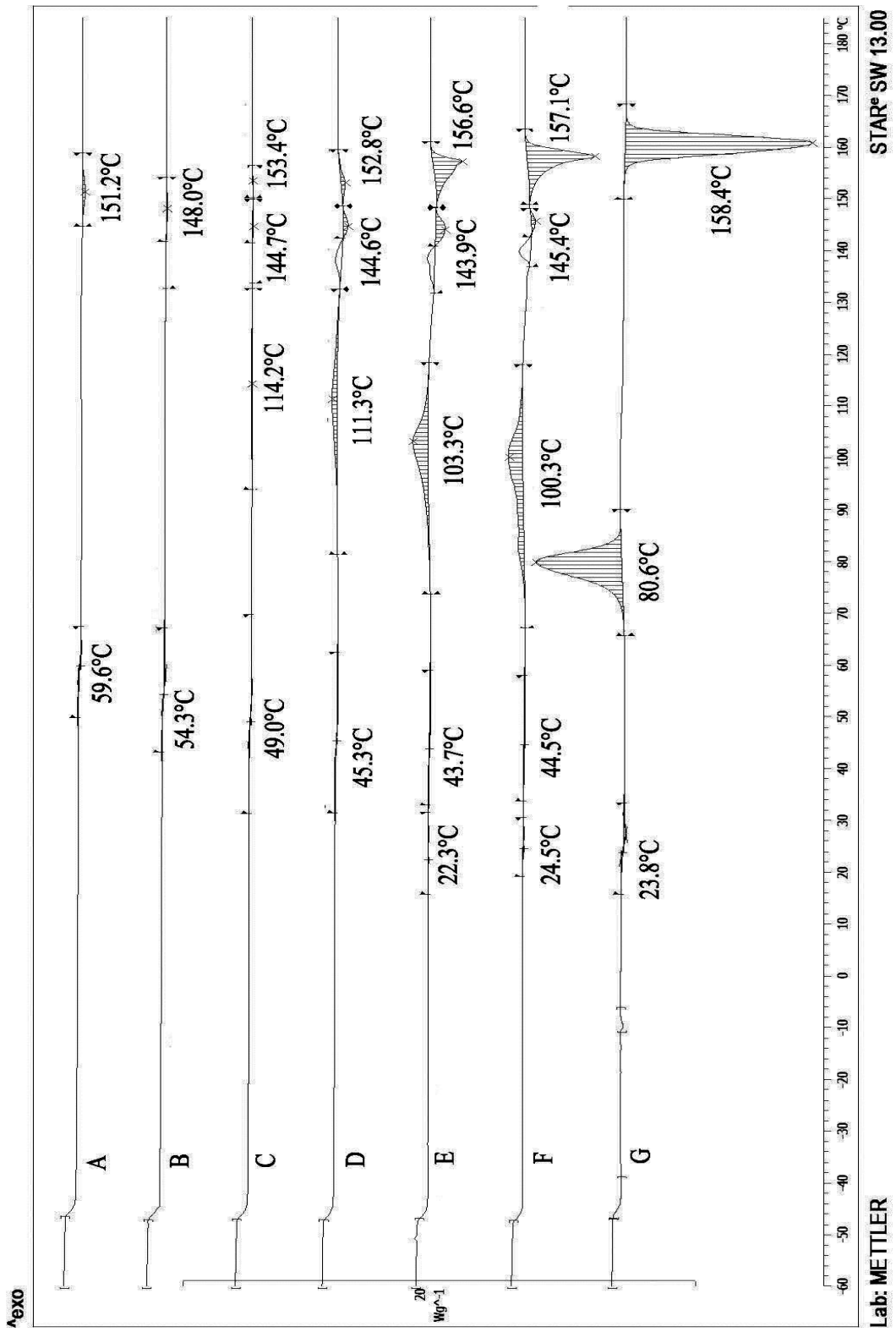

Figure 62 DSC thermogram of PAR:PLLA blends during reheating of heat-cool-heat cycle: PAR:PLLA ratio of 0:100 (A), 5:95 (B), 10:90 (C), 20:80 (D), 30:70 (E), 50:50 (F) and 100:0 (G).

3. Miscibility evaluation between drug and polymer in extrudates

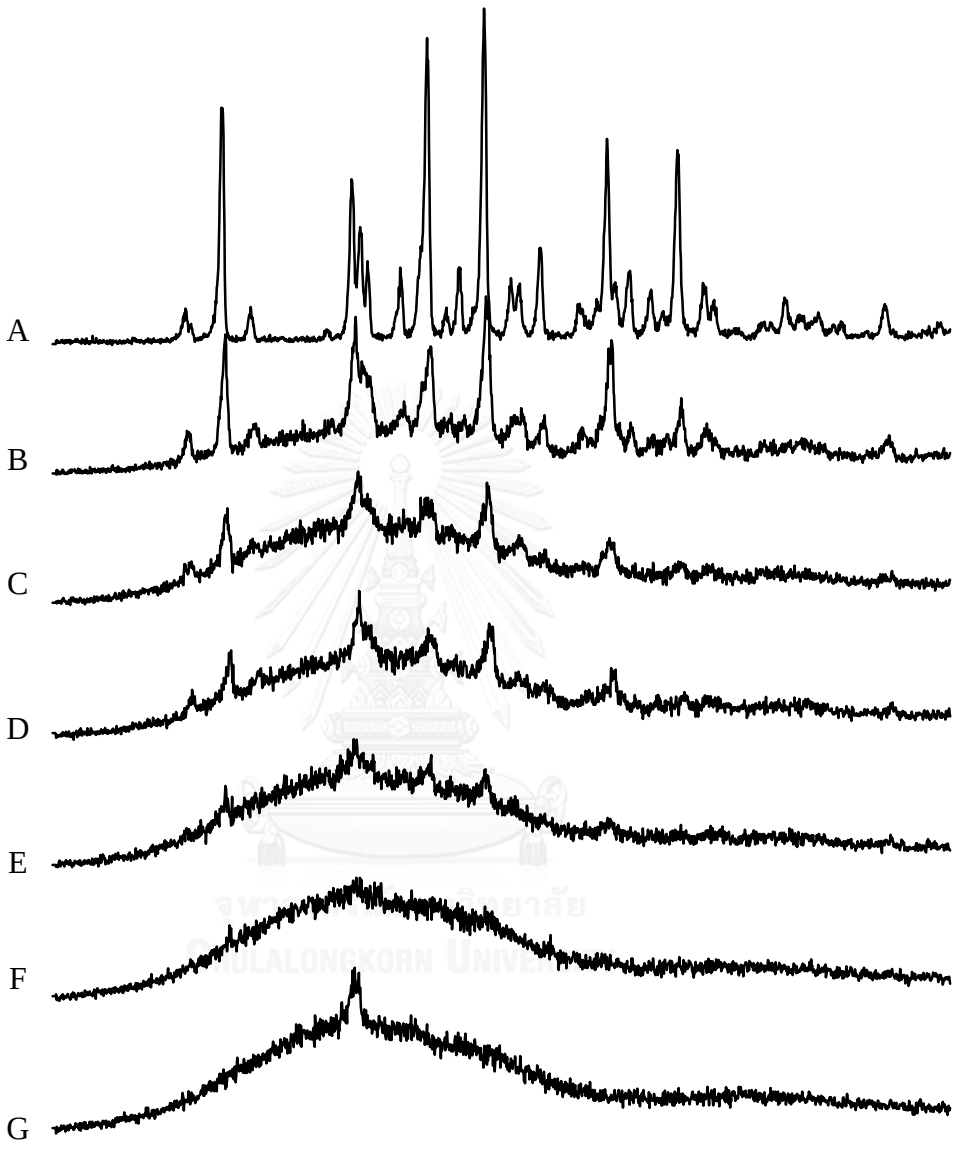

Figure 63 Crystallinity of IND:PLLA physical mixtures by XRPD. IND RM (A), IND:PLLA PM 50:50 (B), IND:PLLA PM 30:70 (C), IND:PLLA PM 20:80 (D), IND:PLLA PM 10:90 (E), IND:PLLA PM 5:95 (F) and PLLA RM (G).

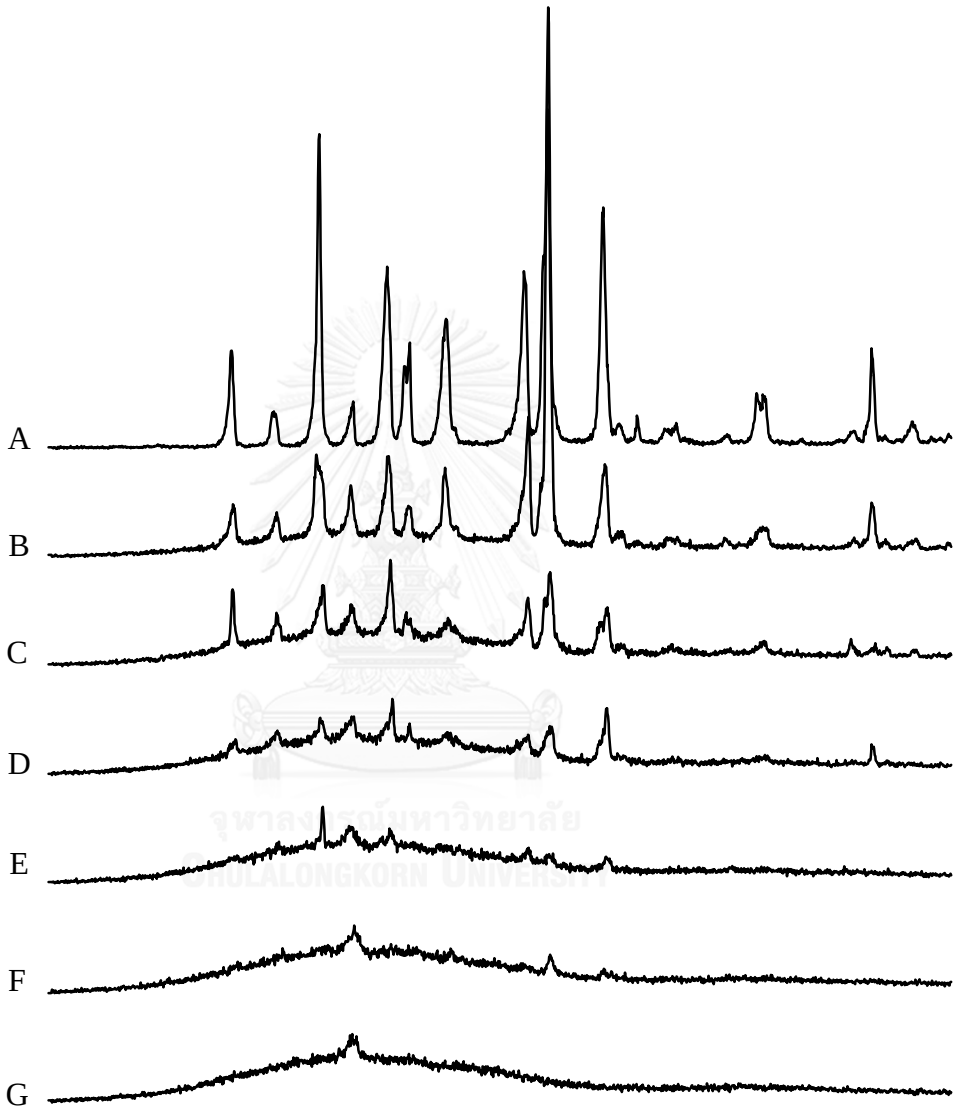

Figure 64 Crystallinity of PAR:PLLA physical mixtures by XRPD: PAR RM (A), PAR:PLLA PM 50:50 (B), PAR:PLLA PM 30:70 (C), PAR:PLLA PM 20:80 (D), PAR:PLLA PM 10:90 (E), PAR:PLLA PM 5:95 (F) and PLLA RM (G).

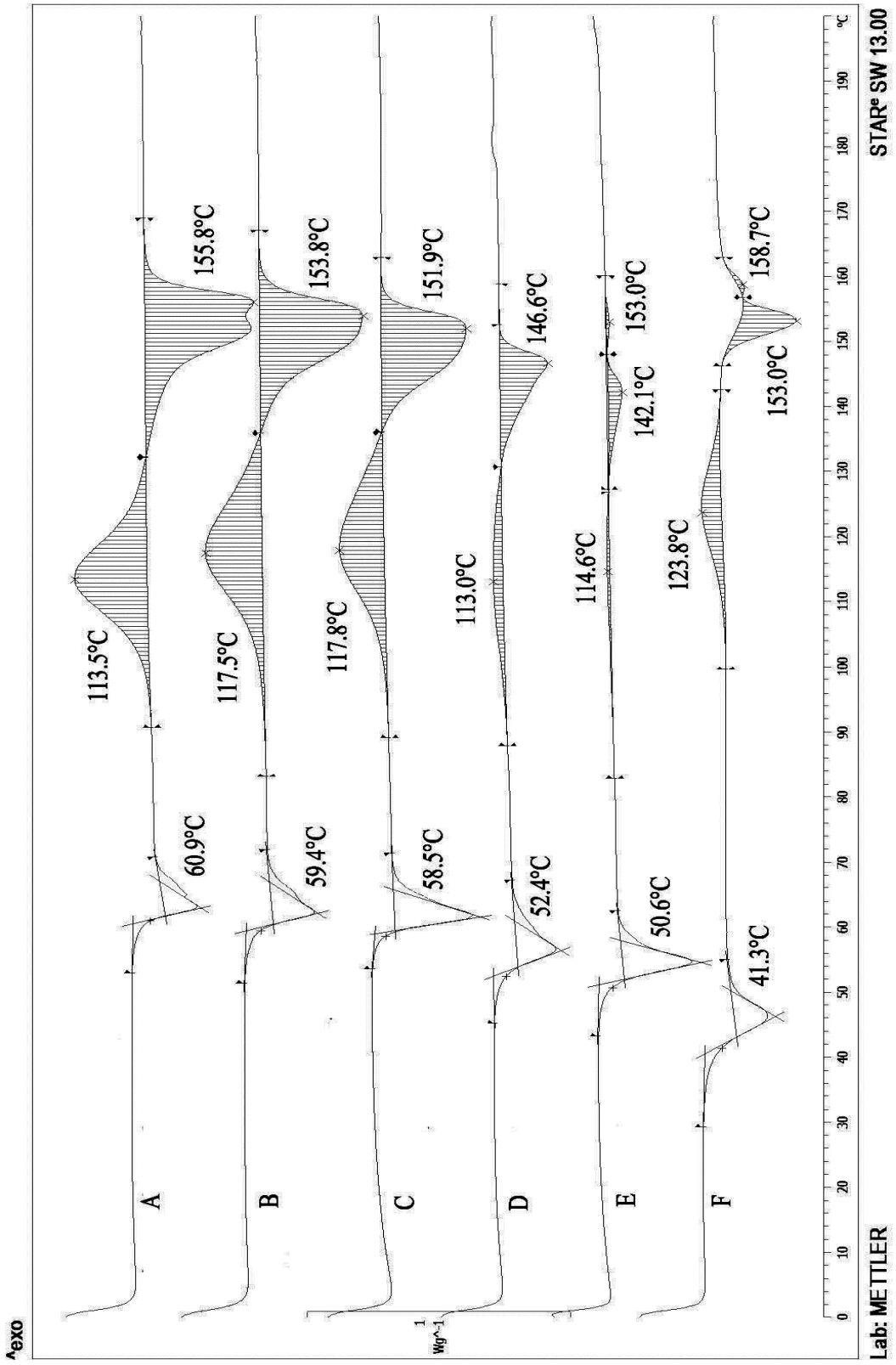

Figure 65 DSC thermogram of IND:PLLA extrudates: IND:PLLA ratio of 0:100 (A), 5:95 (B), 10:90 (C), 20:80 (D), 30:70 (E) and 50:50 (F).

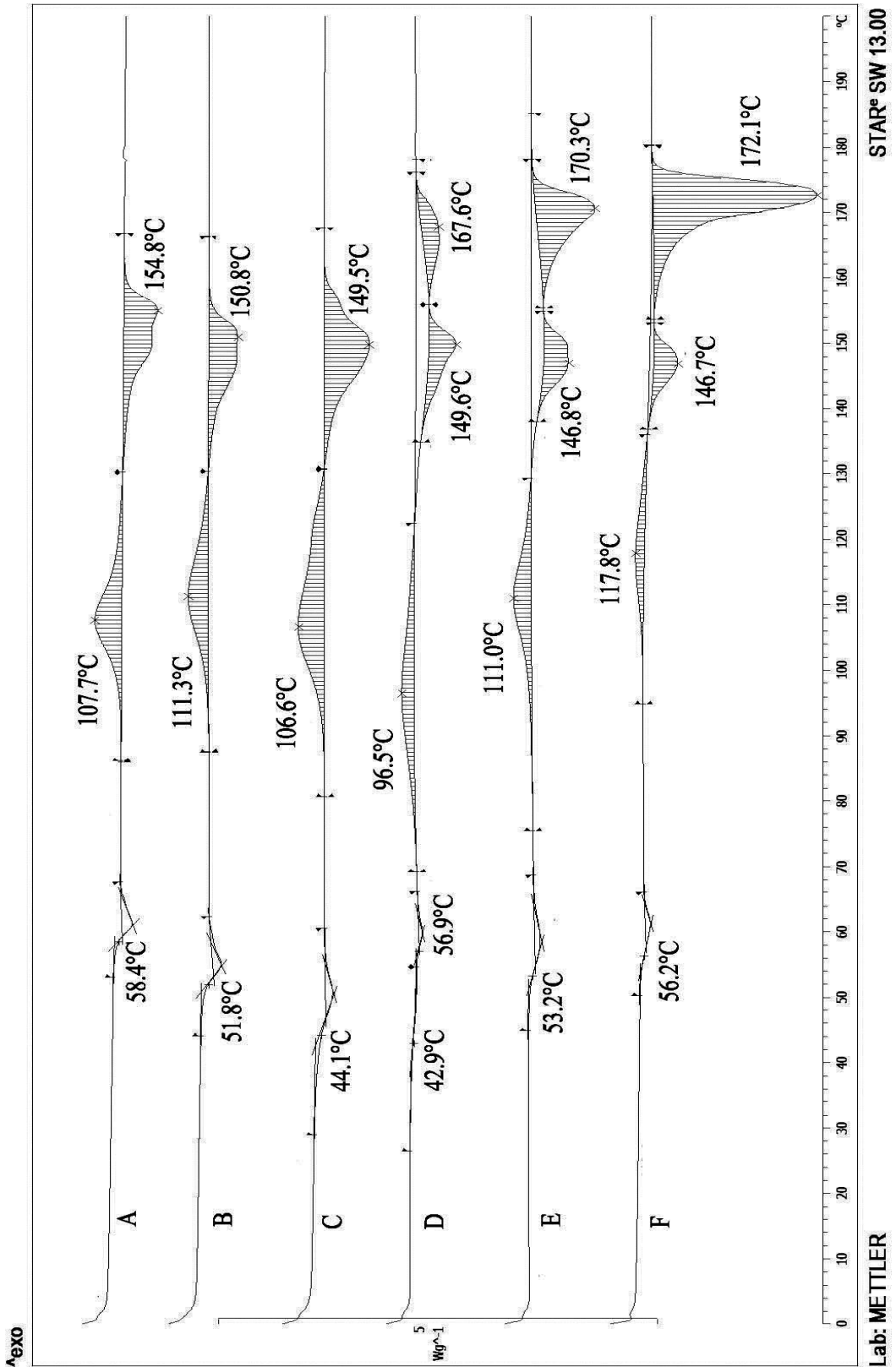

Figure 66 DSC thermogram of PAR:PLLA extrudates: PAR:PLLA ratio of 0:100 (A), 5:95 (B), 10:90 (C), 20:80 (D), 30:70 (E) and 50:50 (F).

VITA

Education

In 2009, I took the bachelor's degree in Pharmacy, Chulalongkorn University, Thailand. The major was Manufacturing Pharmacy and the senior project was "Development of controlled release diltiazem hydrochloride pellets", supervised by Dr. Jittima Chatchawalsaisin.

Awards

In 2014, I was offered Chula-Chiba University Pharmaceutical Student Exchange Program for 40 days.

In 2009, my team was offered Industrial and Research Projects for Undergraduate Students (IRPUS) scholarship from the Thailand Research Fund for the senior project supporting.

Experiences

From 2009 to 2011, I worked at Greater Pharma Co., Ltd., Thailand in quality assurance and quality control department.

Presentations

In 2014, I presented the research "Miscibility study of benzocaine and poly l-lactide using solubility parameter calculation and thermal analysis" in 30th Annual Research Conference in Pharmaceutical Sciences.